A Study on the Dynamic Characterization of a Tunable Magneto-Rheological Fluid-Elastic Mount in Squeeze Mode Vibration

By
Khaled Adjerid

Thesis submitted to the faculty of the Virginia Polytechnic Institute and State University in partial fulfillment of the requirements for the degree of

Master of Science
In
Mechanical Engineering

Mehdi Ahmadian (Chair)

Daniel J. Inman

Steve C. Southward

June 9th, 2011
Blacksburg, Virginia

Keywords: mount, isolator, elastomer, magneto-rheological fluid, tunable isolator,

A Study on the Dynamic Characterization of a Tunable Magneto-Rheological Fluid-Elastic Mounts in Squeeze Mode Vibration

Khaled Adjerid

ABSTRACT

This research undertakes the task of static and dynamic characterization for a squeeze mode Magneto-Rheological (MR) Fluid-Elastic mount. MR fluid's variable viscosity rate is advantageously used to develop a mount capable of mitigating input vibrations of varying magnitudes and frequencies depending on electromagnetic flux. Various mechanical components are synthesized into a dynamic testing rig in order to extract vibrational characteristics of the mount and to compare it with existing mount technologies.

This project focuses on a mount design that was proposed and improved upon by previous researchers at the Center for Vehicle Systems and Safety (CVeSS). Using a previously designed electromagnet and test rig, the MR mounts are characterized using a quasi-static test. From this test we extract the stiffness and damping characteristics of the MR mount. A set of upper and lower limit baseline mounts made with rubber and steel inserts are also tested simultaneously with the MR mount. Their isolation improvements are compared with conventional passive mounts.

After acquiring the stiffness and damping characteristics of the mount, a model is used to simulate a response to input vibrations in the frequency domain. A dynamic test is run on both the baseline testers as well as the MR mount. Having the frequency-magnitude response allows us to determine a usable resonance range and magnitude of vibration mitigation. The results of this study indicate that the mounts tested here are an effective means of suppressing start-up vibrations within mechanical systems and show promise for further development and application. Future studies of these systems can include tests of MR metal-elastic mount designs for durability as well as parametric studies based on MR fluid type and other factors.

Dedicated to my grandfather,

Allel 'Al-Taleb' Adjerid

"Despite his lack of education, he was the smartest man that I have ever met"

And for my beloved parents

Farida Morsli and Slimane Adjerid

Acknowledgements

In the name of Allah, the most gracious, the most merciful I begin.

First, I would like to thank Dr. Mehdi Ahmadian. His guidance, support, charisma and belief in me were the main driving forces throughout my career as a Masters student. Through his vast knowledge and experience, he was able to offer wisdom and insight in my academic, professional and personal lives. For his unrelenting dedication, I am appreciative and greatly indebted. Furthermore, I would like to thank my committee members for their contribution. Both Dr. Inman and Dr. Southward were former teachers of mine and the knowledge they imparted on me has had a profound effect on my development as a student and as an engineer. Dr. Inman was a keystone to my understanding of both introductory and advanced vibrations. Dr. Southward was a dedicated educator who showed the utmost respect and concern for me as a student and for that I am grateful. I would also like to express gratitude to VT's Physics Department and to CVeSS for funding me and this research respectively

Next, I would like to thank the CVeSS family as a whole. Specifically, I would like to start by thanking Michael Craft for all of his help with my project and his patience with me as I developed the skills that are necessary to become a good researcher. Next, I would like to thank Dr. Corina Sandu for first introducing me to CVeSS in 2007 as an undergraduate researcher. I would like to also thanks my friends and colleagues Dr. Ali-Reza Farjoud, Dr. Nima Mahmoodi, and (future Dr.) Clement Nagode for their help throughout my project. Dr. Farjoud provided extensive knowledge on MR technology and Dr. Nagode always provided critical input. I would also like to thank my lab mates Dr. Parham Shahidi, Dr. Reza Soltan, Chris Liam and (future Dr.) Andrew Peterson for being there for encouragement and moral support. Lastly, I'd like to thank Sue Teel for being amazing!

I would like to thank my Khalil, Alperen N. Ketene who was with me from that first day of engineering classes in 2005 until our last days here at Virginia Tech. Thank you for putting up with me and for being my supporter even when no one else was there for me. I would also like to thank Syed Shamim, Nandan Shah, Forrest Shroyer, Ziyad Shalaby, Arshad Ali, Tamer Desouky and Imad Sheikh for being like brothers to me throughout my undergraduate and graduate experience.

Last but not least, none of this would have been possible without the undying and unending love and support of my family. My father, Dr. Slimane Adjerid, who always pushed me to be the best, my mother, Farida Adjerid, who supported me through good and bad, my favorite sister, Dr. Nassiba Adjerid, for being there for me whenever I needed her, my older brother, Dr. Idris Adjerid, for keeping me in check, and my baby brother, Ilyes Adjerid for always making me smile.

And I end by thanking the most high, Allah subhanah, for giving me the intellect and ability to pursue my education.

Contents

List of Tables

List of Figures

Chapter 1| Introduction

This first chapter serves as a brief overview and guide to the remainder of the thesis. It begins by providing a background section featuring the history of vibration isolation and vibration absorbers and their uses in current applications. It then turns the discussion to magneto-rheological fluids and their potential uses in tunable vibration absorbers. Next, a section is presented that lists the deliverable objectives of this research study and the driving factors that inspired the pursuit of these goals. The approach section discusses the method by which the objectives are achieved. An outline section lays out the organization of the chapters in this document. And finally, a contributions section highlights what contributions this work will be making to the field of tuned vibration absorber development.

1.1|Background

Since moving machines were first invented, the suppression of unwanted vibrations has been a lingering problem. Whether it is found in state of the art manufacturing equipment, supersonic aircraft or the most commonly driven car on the road, there always exist input vibrations. These vibrations, though seemingly harmless, can lead to machine misalignment, operator fatigue and could significantly reduce the quality and ultimately the usable lifetime of the equipment. Therefore, certain devices have been extensively developed and their usefulness has been studied. Of these devices, are vibration-isolating mounting platforms, simply known as mounts. Initially, these platforms were made of an elastomer that could be tuned for a range of frequencies [1]. However as technology evolved, the mounts also evolved into fluid filled hydraulic elastomeric mounts capable of isolating a vastly greater bandwidth of frequencies. However, due to the nature of these passive mounts, they are generally unable to account for start-up modes from a rotating motor or vehicle engine because they are designed to conquer vibrations that occur at the devices' operating ranges, which generally falls between 10 - 100hz. Additionally, the threshold for human perception of vibrations is between 1- 10 Hz making suppression in this range all the more important because humans can perceive these frequencies the most [2].

The second category of mounts that were mentioned, the fluid filled or hydraulic mounts, can provide better performance at natural frequencies and resonance modes [1]. Included in those

frequencies are those that an engine or equipment would encounter at both start-up as well as normal operating speeds. To further improve on the concept, there have been studies on hydraulic mounts featuring smart materials. [3]. Of these materials are Magneto-Rheological (MR) Fluids. MR-Fluids were first invented in the early 1940's by Jacob Rabinow [4] and are now some of the best known and most widely researched smart fluids in tunable suspensions [5]. MR-Fluids consist of micron-sized Ferro-magnetic particles dispersed in a non-magnetic oil-based carrier fluid, generally mineral or synthetic oil, water or glycol [6]. Because of this, the fluid acts as a normal free flowing suspension fluid when not magnetized. However, its rheological behavior changes when a magnetic field is applied [7]. This is advantageous because the mix of Ferro-magnetic particles and carrier fluid, can easily switch from Newtonian-like fluid behavior to the behavior of a stiff semi-solid by applying a magnetic field of 0.1-0.4 Tesla [6]. Because of their versatile nature, MR fluids are currently being used in a variety of other applications including controllable dampers, rotary brakes [8] and even in prosthetic devices [9] and earthquake suppression in buildings [10].

Mounts and electromagnetic mount assemblies that feature MR Fluids have been designed and tested before, such as in the studies conducted by Wang et al. and York et al., both detailed in the background chapter of this document. However, the driving point behind this study is to continue the research first initiated by BM Southern. In that study, the main purpose listed was to design a slender elastomeric MR-Fluid mount with an efficient and low profile magnetic activation system [11]. That study however, only went as far as developing the mounts and determining their characteristics. In order to validate, determine the efficiency and dynamic range, as well as to determine overall usability of the mount configuration, a set of dynamic tests were completed. The results from which will be detailed in this study.

1.2 |Objectives

The primary objectives of this research study are to:

1. Better understand the dynamic characteristics of a special class of hydraulic mounts that use MR fluid
2. Determine the factors that influence dynamic isolation properties of the MR mounts
3. Conduct experiments that allow us to quantify the dynamic isolation improvements of the MR mounts
4. Provide recommendations for future studies that that can help with the practical implementation of the MR mounts

1.3 |Approach

In order to complete the objectives above, we chose the approach of building a test set-up, testing for viability, iterating and re-testing various configurations with the mount designs. Specifically, we will perform the following:

- Evaluate the desired deliverables of the experiment
- Design a custom test set up that is conducive to quasi-static and dynamic testing of the selected MR mounts
- Conduct experimental tests using the custom testing set-up to determine dynamic properties of the MR mounts
- Analyze and evaluate results
- Draw conclusions

1.4 |Outline

The next chapter, Chapter 2, gives a brief overview of MR fluid and its history and current application. It then gives a comparison of existing Tuned Vibration Absorbers (TVA's) that are passive with the ones that feature the MR fluid technology. Chapter 3 presents the design of the experiment conducted in this research study. It specifically covers the test set-up, the form of data acquisition and finally the validation of these systems. In Chapter 4, the results of the dynamic test are presented in extensive detail. It then shows the mathematical model developed and compares it to the results attained. Finally, Chapter 5 presents the concluding remarks as well as potential research possibilities for future work with this design.

1.5|Contributions

The main motivations of this research are to contribute to the existing technologies and to build upon the successes of the research of others within the field of TVA and MR fluid-elastomeric device development. The main contributions of this research include providing a better understanding of the dynamic isolation properties of a special class of MR mount that can be used for a variety of industrial applications. Also a part of the contributions of this research will be to quantify the amount of dynamic isolation that is observed through these mounts and to compare it with conventional passive mounts of the same configuration. This is the first study of its kind for this design of squeeze mode MR mounts.

Chapter 2 |Background and Literature Review

This chapter provides the scientific and engineering background information necessary to understand the reasoning behind the steps taken in the design and execution of this study. This chapter begins by providing a history of MR technology, from its origins to its many available forms today. Next a section is presented on previous work in fluid mounts and MR mounts, including the predecessors to the ones designed in this study. Lastly, a brief discussion on useful dynamics and vibrations analysis techniques is presented.

2.1 |MR Fluid History and Background

2.1.1 MR fluid history and physical composition

Jacob Rabinow was credited with being the first to invent MR fluids in 1948 [4]. He observed that certain materials would thicken and become solid when exposed to a magnetic field. Rabinow eventually patented his findings in "Magnetic Fluid Force and Torque Transmitting Device" [12]. Since then, the technology has evolved immensely. Despite the evolutions, the basic make up of MR fluids has pretty much remained the same. MR fluids are generally made up of three components: ferromagnetic particles, a carrier fluid, and a stabilizer.

The ferromagnetic particles are generally made of Iron or Iron-based magnetosoft materials. [13, 14, 15]. More specifically, these particles are typically of carbonyl iron and are usually spherical in shape. However, Iron alloy particles, including iron-nickel and iron-cobalt alloys, are found to perform much better than the original carbonyl iron. The particles sizes are preferred to be between 1 and 10 μm although successful usage of particles as small as 0.1 μm and as large as 100 μm has been reported [13]. These alloys tend to cost much more than the iron carbonyl and thus are not as commonly used. These particles are limited to between 20% and 40% to allow the fluid to retain its flowing fluid-like properties [16, 17].

Secondly, there exists a carrier fluid in which these ferromagnetic particles are suspended. This carrier fluid acts as a continuous isolating medium and is generally made of silicon oil, kerosene, mineral oil, or a mixture of water and glycol [14, 18, and 8]. The selection criteria that the fluid must meet are simple. It should have a low initial viscosity, good anti-corrosion properties and a wide range of temperature stability. A viscosity of $0.01 \sim 1.0\ PaS$ at an ambient temperature of $40°C$ is ideal for correct operation [14].

Lastly, in this mixture of particles and carrier fluid, a stabilizer is added. The stability of the fluid determines the lifetime and the durability of it. And thus, the stabilizer is another important part of the overall make up. [14].

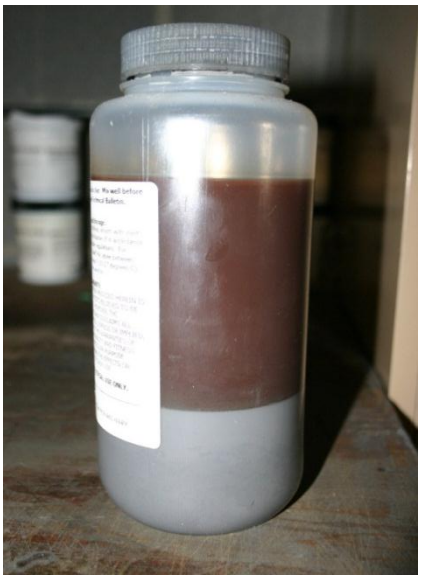

Figure 2-1: A container of Lord Corp MRF-122 that has separated into carrier fluid and material sediment.

Although this study focuses only on devices that use MR fluids, it is important to note that almost concurrently with the discovery of MR fluid by Rabinow, Winslow had discovered electro-rheological (ER) fluids [19, 20]. ER fluids are electrically polarizable particles suspended in an oil that is electrically insulating along with cornstarch, silica, barium titanate or other semiconductors [21]. These fluids have properties that are similar to MR fluids. However, the viscosity or ER fluids changes when an electric field was applied to the material.

2.1.2 Magnetorheology

In the off state, MR fluid acts like any other fluid. Essentially, it is comparable to a higher viscosity version of the carrier fluid due to the added density of the suspended particles, ($0.01 \sim 1.0\ PaS$ at low shear rates) [14]. The viscosity has the ability to change ~ 105 times, within 10 ms in some cases, upon magnetic field application. Additionally, when the field is removed, the effects are completely reversed [22, 16, 17]. When the field is present, the fluid acts as a toothpaste-like Bingham plastic flowing material [57].The change in properties of the

fluid is studied and characterized through a series of yield stress tests through various magnetic field intensities at high velocity and high shear rates [23].

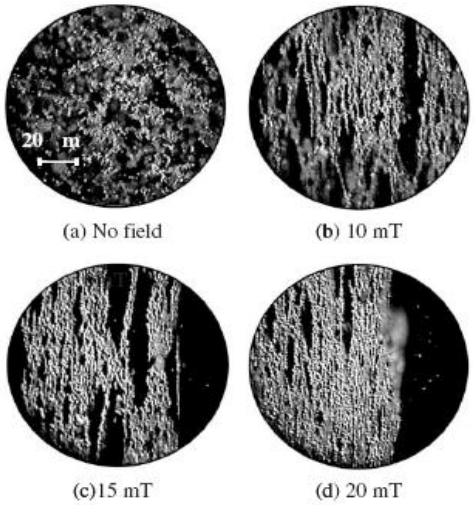

Figure 2-2: Polarization and alignment of ferrous iron in MR fluid, adapted from Ahn et al. [24].

This change in viscosity, and subsequently yield stress, is due to the ferromagnetic particles forming chains in the fluid when a magnetic field is present [7, 25]. As can be seen in figure 2-2 above, as the magnetic field is applied with increasing magnitude, the chains become more and more evident [24]. The strength of these chains is also dependent on the intensity of the magnetic field. These chains can only be broken when the necessary amount of shear stress is present; this value is known as the yield stress of the magnetic chain structures [7].

2.1.3 MR Fluid Modes of operation

MR fluids can be operated in 3 modes: Valve mode, Direct Shear mode, and Squeeze mode. The most popular mode of operation for MR fluids is currently Valve mode, also known as pressure driven mode by Lord Materials Division. The basic premise behind valve mode operation is that the fluid's controllable viscosity determines how quickly the fluid passes through a damper or valve. The flow is directed perpendicularly between two magnetic pole plates [26]. This can be seen in figure 2-3 below showing the flow of the fluid through the chains of suspended material. The amount of magnetic field varies the viscosity, thus dictating the amount of energy dissipated by a shock absorber employing MR fluid.

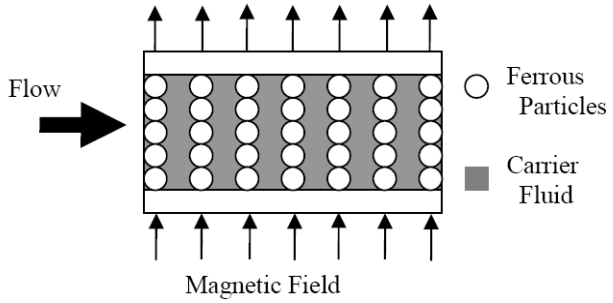

Figure 2-3: MR fluid in valve mode with an applied magnetic field, adapted from [27]**.**

The next, more well-known, operation mode for MR fluid is in direct shear mode. In this mode, the relative motion between the magnetic pole plates perpendicular to the magnetic field flow is hindered by the particle chains' tendency to remain together. Without a magnetic field, the two pole plates act with the normal amount of resistance that a fluid with the MR's inactive fluid viscosity would provide. However, when the magnetic field is applied, the chains appear in the fluid thus adding an increased shear force. This is shown below in figure 2-4.

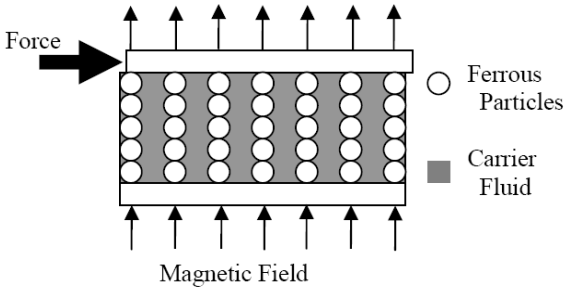

Figure 2-4: MR fluid in shear mode with an applied magnetic field, adapted from [27].

Lastly, the most relevant mode to this study is the squeeze mode operation. The squeeze mode utilizes the analogy of a buckling columnar structure. In this mode, the lateral force applied is parallel to the magnetic field lines [27, 28]. This mode is used primarily for operational modes that require high stiffness and low displacements. The MR fluid may also be embedded in a cavity within another material that provides passive stiffness and damping characteristics when the fluid is not activated. When activated, the axial force applied is resisted by the chains of suspended material and the fluid offers variable axial compressive strength [28]. The figure below shows the squeeze mode before and after application of axial force. Note the resistance of the particle chains.

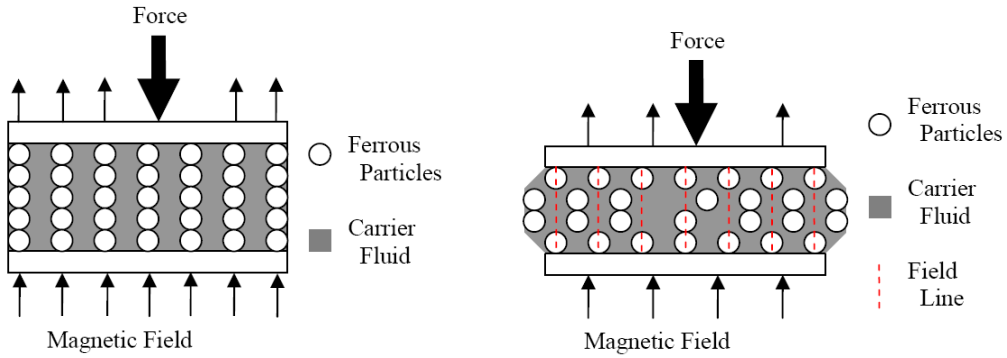

(a) (b)

Figure 2-5: MR fluid (a) in squeeze mode setup prior to axial force with an applied magnetic field, and (b) squeeze mode operation with axial force and applied magnetic field, adapted from [27].

As the force is applied and the chains begin to compress, the chains begin to aggregate as is shown in figure 2-6 below adapted from Goncalves et al. [29]. This aggregation adds a certain amount of compressive strength when loaded but does not present itself when loading is inexistent. This tends to cause hysteresis in the unloading portion of a loading cycle as was discovered by York et al. as well as BM Southern [11, 30].

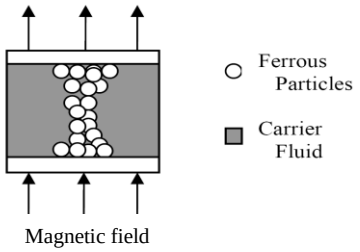

Figure 2-6: Ferrous particle aggregation in squeeze mode operation after experiencing a compressive load, adapted from [29].

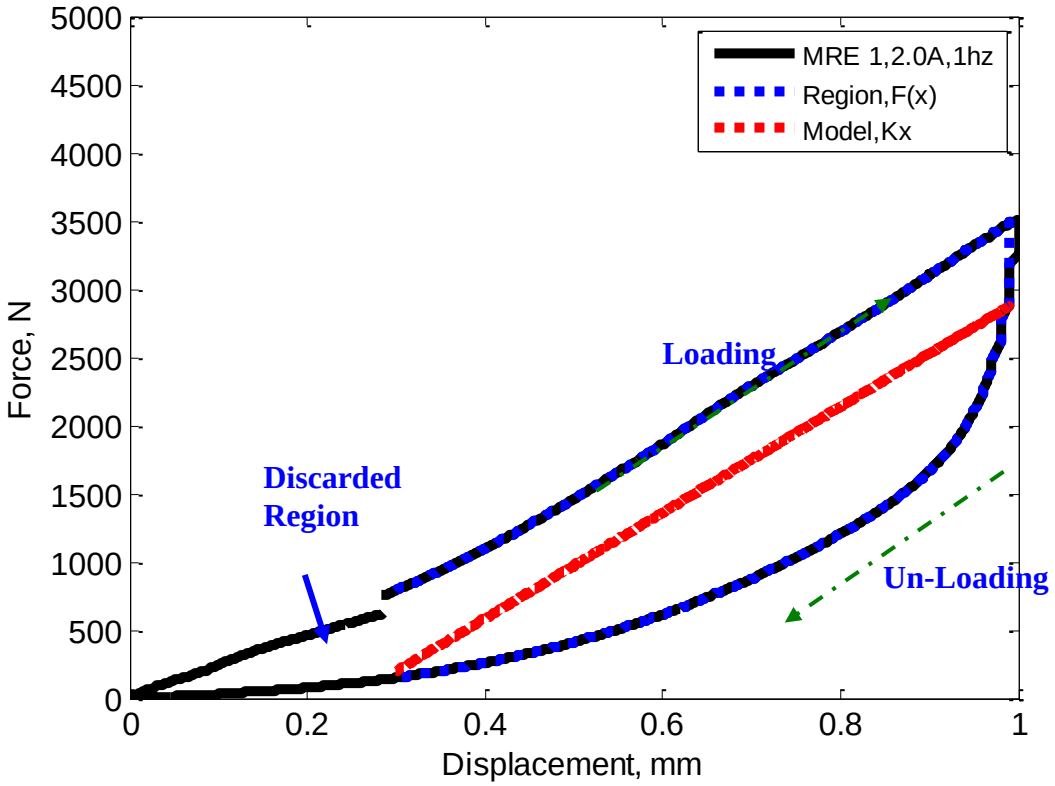

Figure 2-7: Force-displacement plot example with hysteretic content [11].

2.1.4 The Advantages of MR Fluids

The use of MR fluids is advantageous in many different respects. Firstly, the reaction time of the particles upon the application of a magnetic field is in the milli-seconds. However, in order to fully utilize this aspect, one must have an electromagnet that will react quicker than the fluid itself [7]. Next, the material is controllable and very compliant. As long as it is stable, the material will invariably return the same result, repeatedly. The material's change in viscosity is also completely reversible with no sign of artifacts or material memory [14]. The magnetic field required is in the mTesla range, and the power required to apply that amount is minimal [7]. Another advantage is the fluid's stability through a range of temperatures. This robustness to change in temperature as well as its lack of history dependency was tested and confirmed through various research studies. Tests on temperature robustness were conducted by Weiss and Ducloss, tests on magnitude of magnetic field vs. power supply were conducted by Tang and Conrad and tests on history dependency as well as the stability of the carrier were conducted by Ashour, Rogers et al. [31, 32, 14].

Table 2-1: General properties of MR Fluids, adapted from [7].

Specification	Remark
High Dynamic Yield Strength	Instantaneous generation of from 0 to 90 Pa yield stress for precise real-time control
Wide Operating Temperature Range	-40° to 150° with less than 10% variation in maximum dynamic stress
Millisecond Response Time	Ideal for use in applications requiring continuously variable, high-precision control
Non-Abrasiveness	Additives in MR fluids reduce abrasiveness, enabling devices to achieve required life expectancies
Low Sedimentation Level	The formulation of MR fluids solves sedimentation and stratification problems found in other MR fluids
Current Density	Can energize with permanent magnets
Specific Gravity	2-4
Ancillary Materials	Iron/Steel
Color	Black/Grey

2.1.5 MR Fluid Device Applications

Because of its versatile nature and many modes of operation, there exist many applications of MR Fluids. Although, many of these applications can be found in the automotive industry, there are also many applications outside of the automotive realm that benefit from MR technology. These applications include adjustable dampers, rotary clutches and brakes, seismic vibration mitigation devices and even prosthetic devices [8,9,10]. MR fluids are now gaining notoriety as many automotive manufactures are offering MR fluid operated semi-active suspension systems such as Chevrolet's Magnetic Selective Ride Control (MSRC) available on the Corvette, Camaro and Cadillac CTS-V [33]. Future roles that MR fluids may be pivotal in include power transmission systems, aeronautical servo systems, structure vibration control, optical grinding, MEMS, and robotic systems [34-39].

2.2 |Passive and Active mount history

2.2.1 Passive Mounts: Fluid-Elastic Mounts

This section describes a few examples of recent developments in passive mounts. Of these mounts, only the fluid filled or hydraulic mounts are described in detail in this section to show the contrast between a passive fluid filled mount and an active or semi-active mount. A hydraulic mount, as is seen below in figure 2-9, consists of two chambers and a decoupler. Fluid inside of the mount travels from one chamber to the other and encounters resistance from having to find a flow path through the inertial track. Additionally, a pressure differential causes the decoupler to move depending on whether the mount is experiencing compression or extension. The amplitude of the motion also affects the extent of movement and deflection that the coupler will experience [41]. Christophereson et al. rationalized the mathematical model for this simple hydraulic mount and the force being transmitted [42].

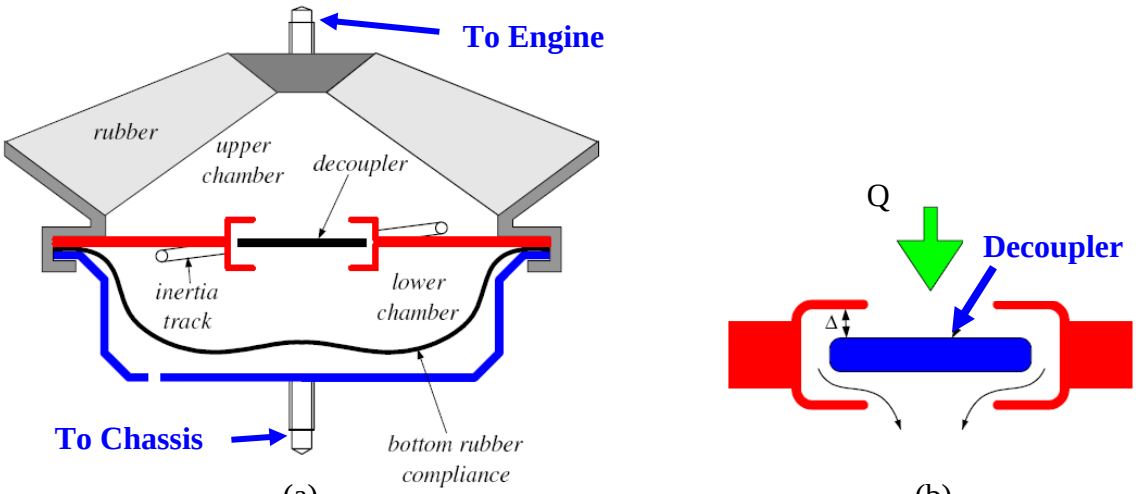

Figure 2-8: Two chamber passive hydraulic fluid mount with decoupler, adapted from [42].

Unfortunately however, as was described in earlier sections, passive mounts are rarely able to attenuate all of the input vibrations in a system. Rather, they are tuned for the operating point of the system and do not account for startup modes. Passive hydraulic mounts however, pose a secondary issue in that the fluid in the chamber must be monitored and may require costly re-tuning at some point in its operating life [43]. Regardless, they still provide excellent vibration isolation for many applications.

2.2.2 Active Mounts: MR Fluid-Elastic Mounts

The last and most important type of active mount are a combination MR Fluid-Elastomeric mount. The mounts investigated and characterized in this study are of this type. MR Fluid-Elastic Mounts are defined as mounts with an elastomeric casing as well a fluid cavity to accommodate MR Fluid. Thus far, not many designs exist, but a few of the ones that do are detailed in this section. Wang et al. showed much promise with their initial design. This design places a fluid-elastic mount in between an upper magnetic pole and a lower magnetic shield. With this setup, the mount is operated in the squeeze mode, showing a 75% increase in output force while magnetized; the mount is shown in figure 2-10 below [44].

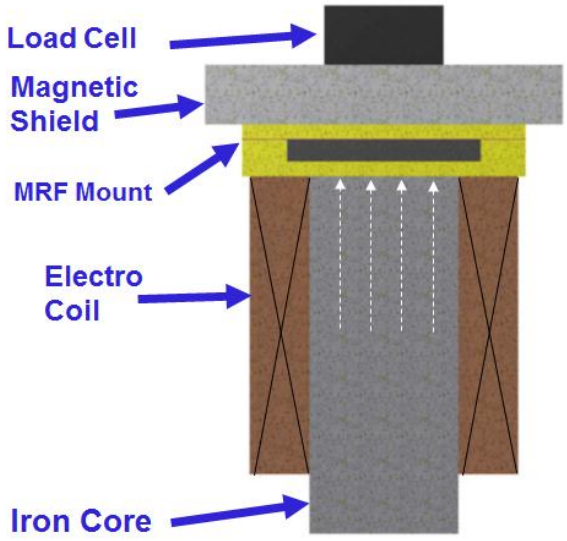

Figure 2-9: Original mount and electromagnet design as proposed by Wang et al. , adapted from [44].

The magnetic set-up by York et al. builds on the design by Wang et al. but requires that the poles be placed directly above the fluid cavity. Although this would drastically increase the effectiveness of the mount, it also requires a large magnetic field generator and bulky packaging [30].

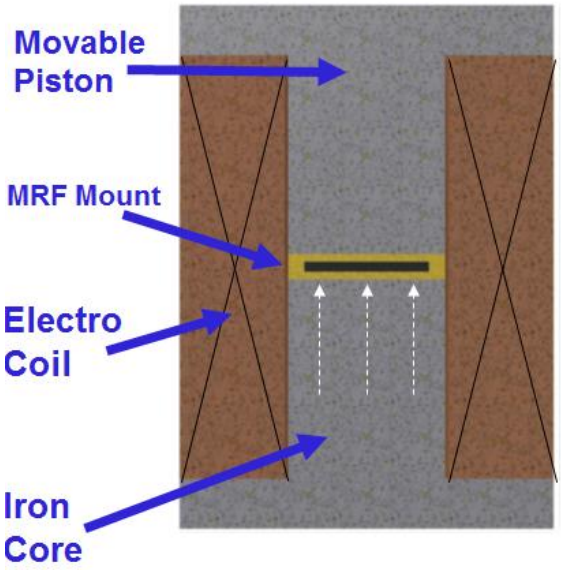

Figure 2-10: Mount and electromagnet design by York et al. , adapted from[30].

Lastly, BM Southern built upon both the design of the elastomeric casing design by Wang et al. as well as the electromagnetic enclosure by York et al. [30 ,44]. By adding upper and lower pole plates, the improved design channels the magnetic flux through the center of the mount and the directly into the MR fluid cavity using a funneled upper and lower pole plate configuration. The flux path was analyzed using Finite Element Magnetic Modeling (FEMM) Software to determine the flux path and density. This was all done while making the packaging less than half the height and making the diameter slightly smaller. This new design is called an MR Metal-elastic mount [11].

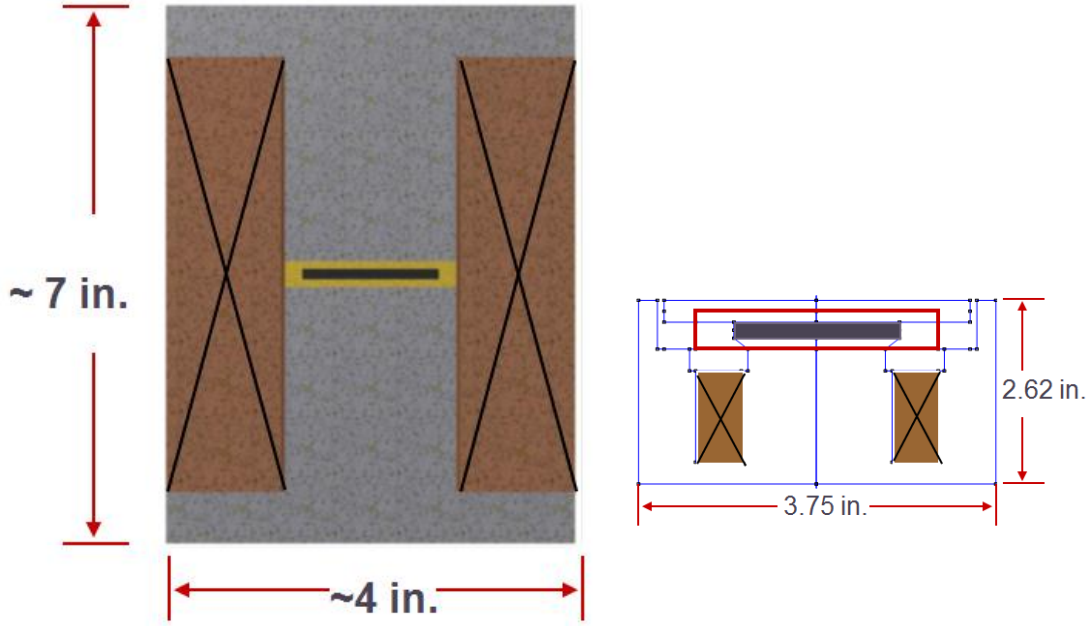

Figure 2-11: Comparison of previous design (left) with improved design used for this study (right) , adapted from [30, 11].

The results of that research study, utilizing the modified lower profile design, showed that at the maximum magnetic field, the mount experienced up to 78% stiffness increase and up to 500% damping increase, while only using a maximum of 2 amps of current [11]. This makes it a great candidate for further dynamic characterization and for possible implementation in industrial applications.

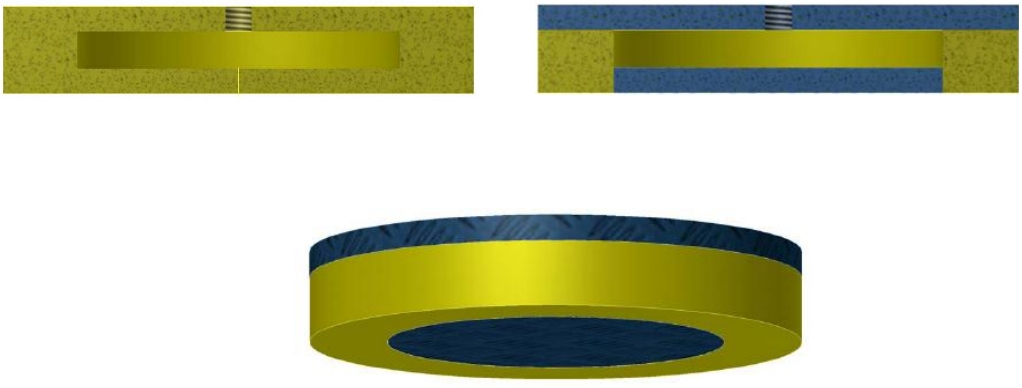

Figure 2-12: Elastic Casing sectional view (top left) , Elastic Casing with magnetic-pole plate inserts sectional view (top right), and isometric view of metal-elastic casing (bottom), adapted from [11].

2.2.3 Active mounts: Other MR Mounts

Many active MR mounts have been designed that act like hydraulic mounts or dampers. Employing pistons or chambers, they operate in squeeze mode but pose as a sort of hybrid design. Those designed by Ahn et al., Vahdati, and Choi et al. show different methods of providing stiffness and damping through various methods of fluid chamber exchange as well as magnetic field actuation [24,46, 45]. Ahn et al. show a magnetic core with a chamber of MR fluid that is compressed by a piston [24]. Vahdati describes a small inertial track for the MR reservoir to travel through from upper to lower chamber [46].

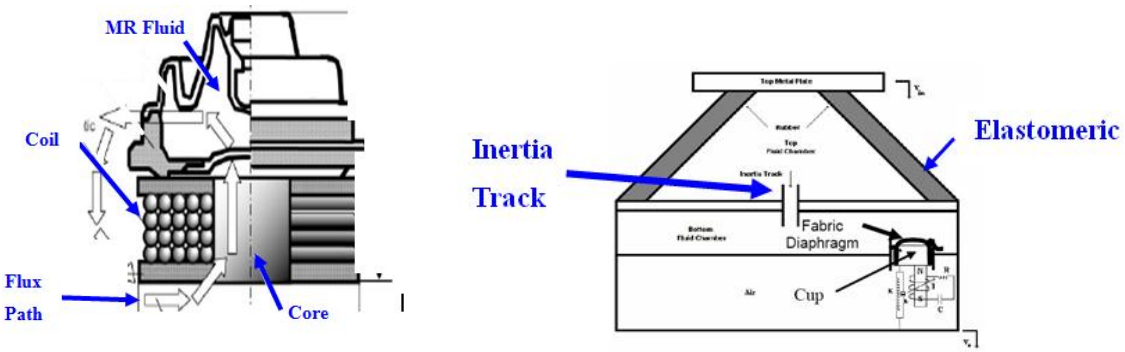

(a) (b)

Figure 2-13: Single chamber MR fluid mount (a), adapted from Ahn et al. [24] and Single pumper semi-active mount (b) proposed by Vahdati, adapted from [46].

Lastly, Choi et al. present a design that features a piston travelling through a reservoir of MR fluid experiencing different levels of resistance with varying magnetic field densities [45] .

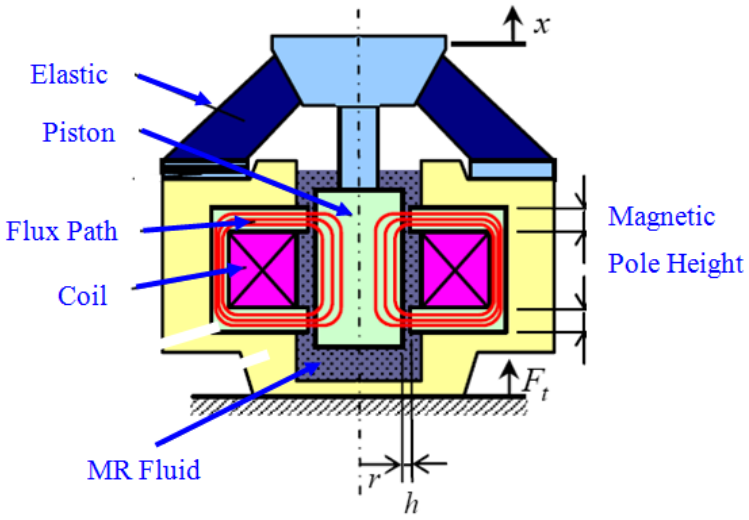

Figure 2-14: MR fluid mount by Choi et al., adapted from [45].

There also exist mount similar in operation to the fluid elastic and metal elastic mounts described above. However, instead of packaging the mount and the electromagnet separately, they share designs with the hydraulic MR mounts in that they are encapsulated in one package, but still operate in the squeeze mode [47]. All of these encapsulated designs do not feature easy MR fluid interchangeability.

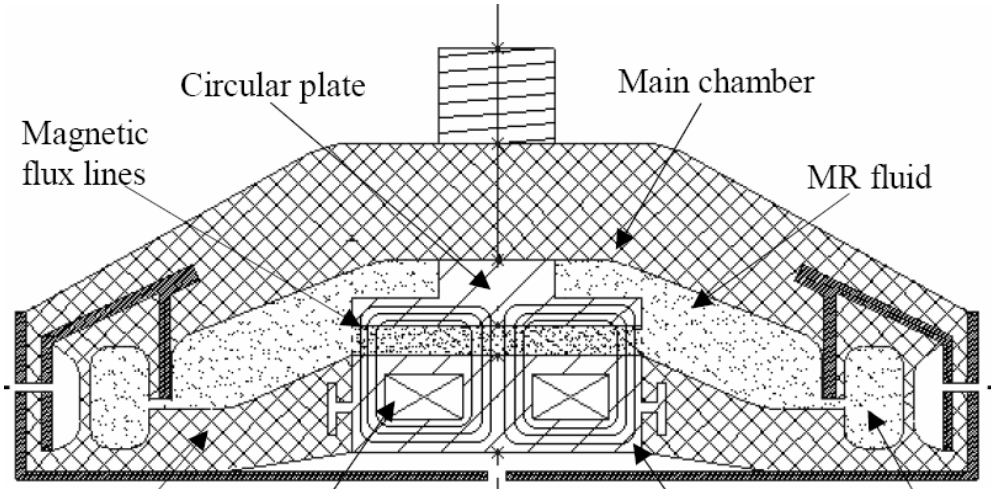

Figure 2-15: Squeeze flow mode MR fluid mount by Nguyen et al., adapted from [47].

2.3 |Principles of Vibrational Systems

2.3.1 Basic Model for squeeze-mode mounts

In order to understand the basis behind this study and the format of the test setup, some basic principles of dynamics and vibrations needed to be reviewed and understood. The problem presented in this study is a simple base excited single degree of freedom (SDOF) system problem and can be modeled as a second order differential equation.

$$\sum F = -k(x-y) - c(\dot{x}-\dot{y}) = m\dot{x} \tag{2.1}$$

$$m\ddot{x} + c\dot{x} + kx = c\dot{y} + ky \tag{2.2}$$

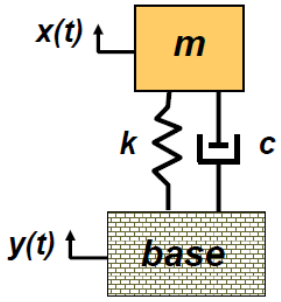

Figure 2-16: Equivalent mechanical system represented by a spring-mass damper system and a moving base [2]

In this form, equation 2.2 shows the dynamics of the system modeled in terms of stiffness, k, damping, c, and as well as base input displacement, y, and relative upper mass displacement, x. With a mount, both the spring and damper elements are combined into one package; however both are still quantified separately as they change somewhat independently of each other.

2.3.2 Quasi-Static Characterization

As was described in the objectives section of the first chapter, the main goal is to determine the mounts' abilities to suppress the magnitude of the output vibration at their respective resonance frequencies over a range of magnetic field magnitudes. As will also be seen in later chapters, the natural frequency calculation goes into data validation as well modeling.

In order to determine the natural frequency of any spring mass system, one must use the basic law

$$\omega_n = \sqrt{\frac{k}{m}} \tag{2.3}$$

where determining the natural frequency, ω_n , requires finding the stiffness of the spring involved and the amount of mass that the test setup has placed on it. Finding the spring constant, k, can be done multiple ways. The simplest is to use hook's law which states

$$F_k = k * x \quad \text{or} \quad k = \frac{F_k}{x} \tag{2.4}$$

Where F_k is the load force on the spring and x is its displacement [2]. This is most conveniently done by conducting a quasi-static test (QST). A typical force-displacement QST curve is shown below in figure 2-18 with the non-linear region ignored and spring rate determined using the fit line of the linear portion of the compression and extension plot. This linear relationship is applicable for a mount or spring that acts linearly. For MR mounts in squeeze mode, there exists aggregation of MR material chains and thus hysteretic content must be included [48].

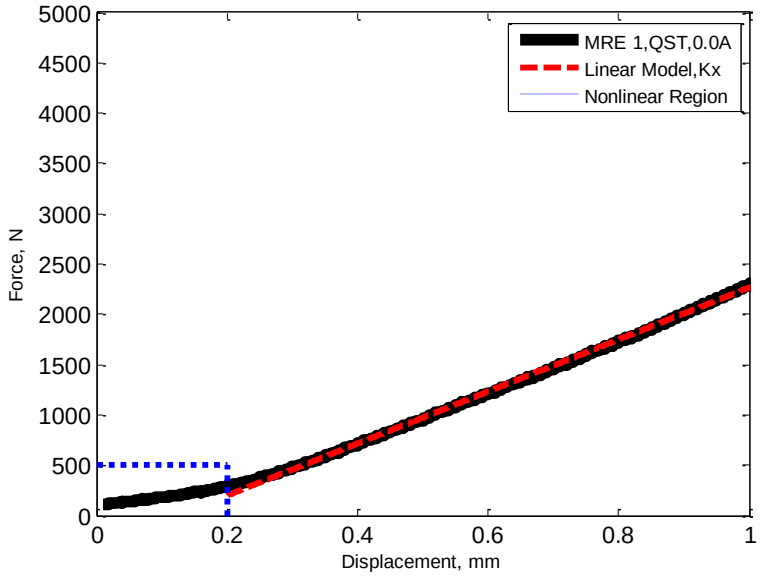

Figure 2-17: Force-displacement plotting method example on a MR fluid-elastic mount with MRF-145 fluid at 0 amp current, adapted from [11].

In order to determine the stiffness of a mount that experiences hysteresis the process is a bit more involved. Using the hysteretic force displacement curve along with line and area fitting techniques, the equivalent stiffness of the mounts can be determined [49].

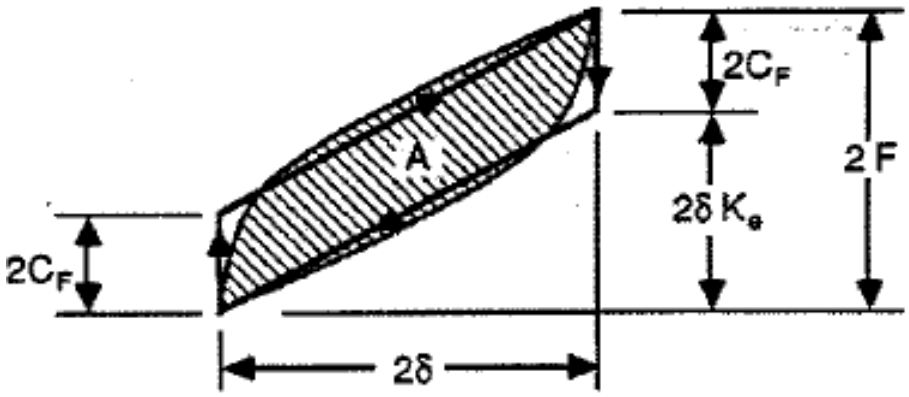

Figure 2-18: Example force-displacement curve showing method of calculation for materials with hysteretic content [49].

The second parameter that is determined from the QST is the equivalent damping of the system. Inman defines equivalent damping, C_{eq} and damping ratio as follows:

$$C_{eq} = \frac{\Delta E}{\pi \omega X^2} \qquad \zeta = \frac{C_{eq}}{2m\omega_n} \tag{2.5}$$

The damping is calculated using the energy dissipated, ΔE, as well as the QST displacement, X, test frequency, ω and the natural frequency, . The dissipated energy can either be found graphically by determining the area within the hysteretic loop [49] or analytically by multiplying π and the QST displacement by the hysteretic damping constant, β [2].

$$\Delta E = \pi \beta X^2 \tag{2.6}$$

This process was completed extensively and is detailed thoroughly in BM Southern's dissertation. However, since a significant amount of time had elapsed between the fabrication of the mounts and the testing date, the QST has to be conducted again for the mounts being used for the baseline test as well as any new mounts fabricated.

2.3.3 Dynamic Characterization

Lastly, in order to determine the effectiveness and usability of these mounts, one must employ the concept of base excitation and displacement transmissibility. The displacement transmissibility is defined as the ratio of the displacement of a mass resting on top of the spring/damper to the displacement input base, or in our case, the mount. In order to model the transmissibility of a base-excitation problem such as the one presented in this study, the following equation is used

$$\frac{X}{Y} = \sqrt{\frac{1 + (2 * \zeta * r)^2}{(1 - r^2)^2 + (2 * \zeta * r)^2}} \tag{2.7}$$

Where ζ is the damping ratio and r is the frequency ratio, $\frac{\omega}{\omega_n}$. Plotting this displacement ratio, $\frac{X}{Y}$ against the frequency ratio gives a characteristic transmissibility curve, assuming the input is sinusoidal. As is shown below in figure 2-20, a typical plot begins with a displacement transmissibility magnitude of 1 at $r = 0$, then the displacement transmissibility ratio increases until its peak at the resonant frequency, $\omega = \omega_n$ and then descends towards zero as r increases. The peak occurs at different magnitudes depending on the damping ratio of the system. [2]

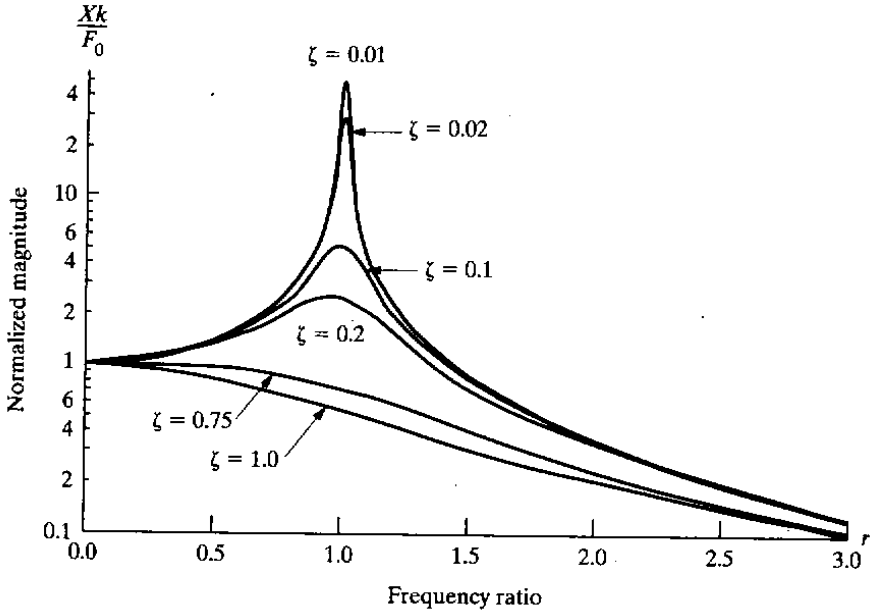

Figure 2-19: Typical transmissibility curves plotted against frequency ratio r with varying damping ratios, ζ, adapted from [2]

Chapter 3 |Testing Apparatus Design, Fabrication and Methodology

This chapter is devoted to the design of experiment for this study. This chapter begins by giving a brief over view of the magnetic principles to allow the reader ease of understanding of the relationship between MR fluid and electromagnetism. Next, it highlights the equipment already in hand prior to the initiation of the study, including the pre-fabricated mounts and the electromagnetic rheometer casing designed by BM Southern. It then delves into the many modifications made to the existing apparatuses to accommodate the testing for this study as well as the parts that were designed and custom fabricated for the experiment. It then summarizes the entire physical test set-up and provides a description of the data acquisition system used for the tests. The validation process of the setup is touched on and finally the chapter ends with an overview of the design of experiment.

3.1 |Magnetic Circuitry Principles and Existing equipment

3.1.1 Magnetic Circuitry Principles

As was discussed in earlier sections, MR devices are generally operated using a powered electromagnet, a permanent magnet or a combination of the two. But an elevated wire gauge or current past a certain threshold does not guarantee an adequate magnetic field as there are other factors that influence the magnitude of the magnetic field in a device. Magnetic permeability, μ, varies from material to material ranging from highly magnetically conductive materials such as steel and iron to substances such as aluminum and air which tend to degrade magnetic field intensity, *H*. As common sense would dictate, materials that readily pass magnetic flux should be used to increase the efficiency of the magnetic circuit whereas having air gaps should be avoided in the flux path of an MR fluid device. If air gaps are unavoidable, then a higher number of turns or a larger current should be used to achieve the desired field.

Utilizing Kirchhoff's law in magnetic circuit form

$$Ni = \sum H_n * L_n \tag{3.1}$$

we can view the relationship between magnetic field intensity, H_n , the Number of turns, N, the current, i , and the material length, L_n [23].

3.1.2 Existing Equipment: Electromagnetic Housings

Since this experiment was a second phase continuation of a project previously initiated by BM Southern, there were many artifacts left over from the initial static and quasi-static tests. Although some of the equipment was discarded, there were a few vital pieces that were used and adapted for the dynamic test. These items include the electromagnetic lower housing, the electromagnetic upper housing, spacer, wire wrapped coil-bobbin and two different mounts; the Rubber (RUB) and Steel (STE) core elastomeric mounts.

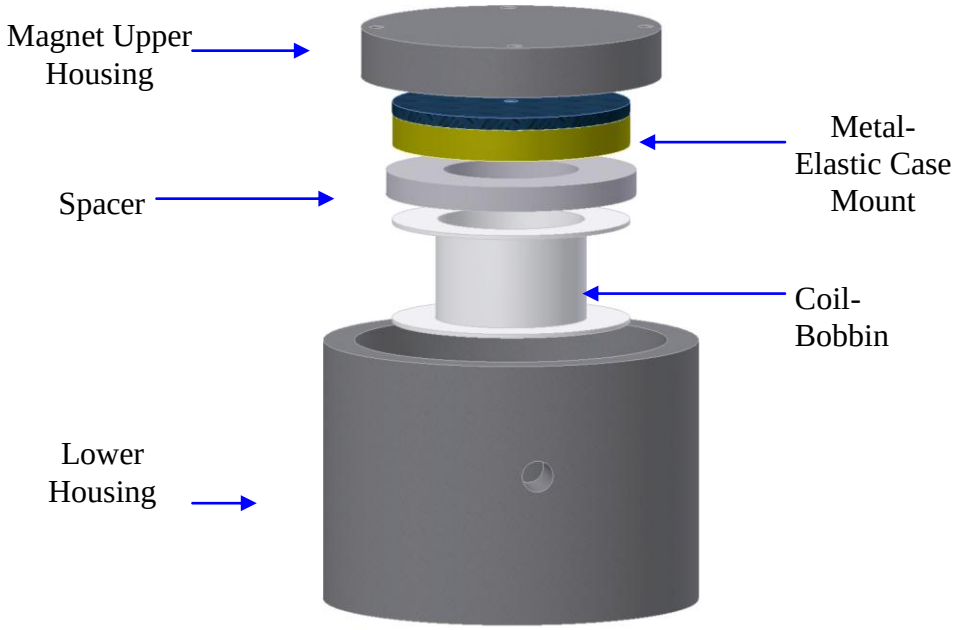

Figure 3-1: Isometric view of mount and magnetic system design, adapted from [11]

The lower housing is constructed of 1018 steel and houses a core that the wire wrapped coil-bobbin fits around. It also has side walls that allow the upper housing to fit into with an air gap of 1/16 in. between its outer diameter and the inner diameter of the lower housing. In the lower housing, a spacer made of 6061 Aluminum can be put in place to prevent shock or vibrations from jarring the coil-bobbin loose from the lower housing core. The spacer also provides a flush surface for the mount to rest on. The upper housing has a flat surface with a hole in the center to fit the mount's cap-screw on the upper pole plate of the mount while keeping it flush with the surface of the upper housing. Both the upper and lower housings have threaded holes for attachment to the testing rig. The specific dimensions of the upper and lower housings are listed in Table 3-1.

Table 3-1: Dimensions and material properties for the magnetic system components as well as packaging and testing dimensions, note the difference in coil turn number, adapted from [11].

Modeled Component	Outside Diameter in.	Inside Diameter in.	Component Height in.	Material Permeability *B-H*
Top-Assembly				
Upper Housing	3.000	*N/A*	0.250	1018 Steel
Upper-Pole Plate	2.375	*N/A*	0.125	1018 Steel
Elastomeric Casing	2.375	1.625	0.3125	Air
Magnetic-Pole Plate	1.625	*N/A*	0.125	1018 Steel
Fluid Cavity	1.625	*N/A*	0.1875	MRF-140CG
Spacer	2.500	1.350	0.250	6061 Alu
Bottom-Assembly				
Lower Housing Base	3.750	2.400	1.800	1018 Steel
Extruded Lower Housing	3.750	3.125	0.8125	1018 Steel
Magnetic Core	1.460	*N/A*	1.300	1018 Steel
800 Turn Electro Coil	2.375	1.460	1.048	24 AWG
Cosmos Coil-Bobbin 0680	2.375	1.460	1.048	N/A
Total-Assembly				
Package Dimensions	**3.75**	*N/A*	**2.613**	
Testing Setup	3.75	*N/A*	4.613	

For the lower housing, the coil-bobbin housing had to be designed specifically to fit a coil-bobbin that would be accommodating of the magnetic needs for the experiment. However, the choice of bobbin must not interfere with the design and operation of the housings and mounts. This design can be viewed in detail in figure 3-2 below. Finally, a coil with 24 AWG copper wire at 600 turns fit into the lower housing and to provide a large Ni value. This because with increase in current as well as time charged, electromagnets tend to drastically increase in temperature [23].This can cause the plastic housing to melt or the copper wiring in the coil to become damaged. In order to cage the temperature, one can use a coil with a smaller number of turns. In addition, it is necessary to limit the time charged and allow time between tests for the temperature to decrease before reapplying current to the coil.

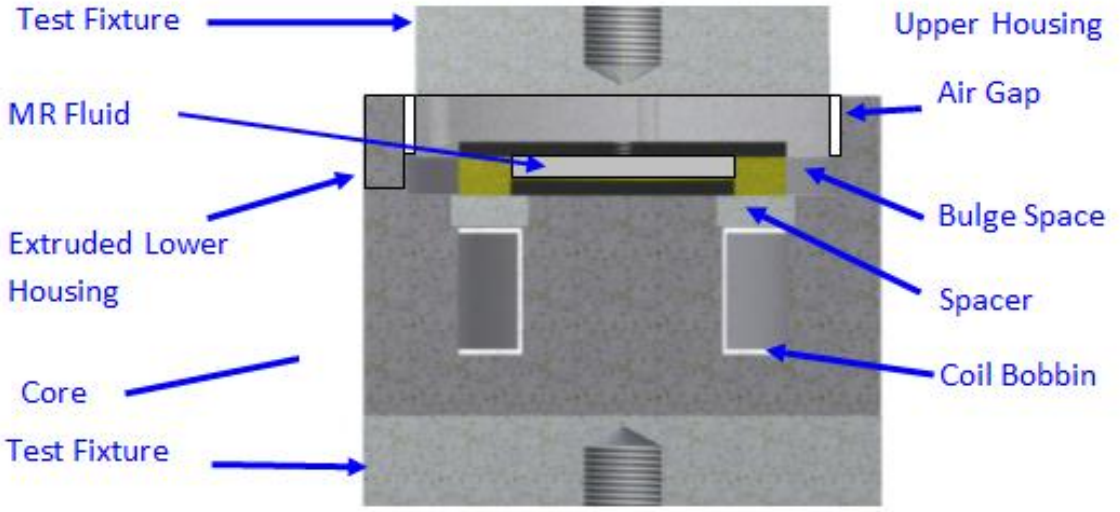

Figure 3-2: Cross-sectional view of empty metal-elastic casing and magnetic system with test fixtures, adapted from [11].

The electromagnet was powered by an Extech 80 watt switching mode DC power supply. This was chosen because of its compact size and because it allows the user to control either voltage or current. The power supply is able to produce 0.10-~40.00 V of voltage or 0.10-5.10A of current through positive and negative leads. The power supply also features a load limit in case the current applied to it is beyond its capacity, thus minimizing the possibility of shorting or blowing the circuit. This power supply, however, does not have a floating ground, which was not an issue within the scope of its use in this study [24].

3.1.3 Existing Equipment: Pre-Fabricated Mounts

Another set of artifacts that remained from the initial study were the active and passive mounts that BM Southern had fabricated. Although many were fabricated and tested, there were only two that were actually useful for this study. The mounts that were fabricated were the results of many iterations, including active mounts filled with MR fluid as well as passive mounts with different inserts. The ones that were usable were the final versions used for the establishment of baseline properties within that study. The STE and RUB mounts would serve the same purpose in this study as well.

Specifically, a mount made entirely of rubber (RUB) and a mount made with a rubber casing and a steel insert (STE) were used. The rubber casing for all of the active and semi-active mounts in this study were made from Poly-Tek 74-30 two part polyurethane RTV mold rubber. Using the 74-30 clear combination results in a clear/amber cured color and has a Shore-A hardness rating of 30 as well as a 2000 cP mixed viscosity. This specific blend was chosen for its ease of pouring, adequate shore hardness and its clear color which allows observation of the insert and fluid cavities of the mount [25]. The table below shows a comparison of familiar items and their hardness in comparison to the TVA design's elastomeric casing.

Table 3-2: Durometer rating comparison chart for conceptual understanding of the Shore-A hardness selected for the elastomeric casing material, adapted from [26].

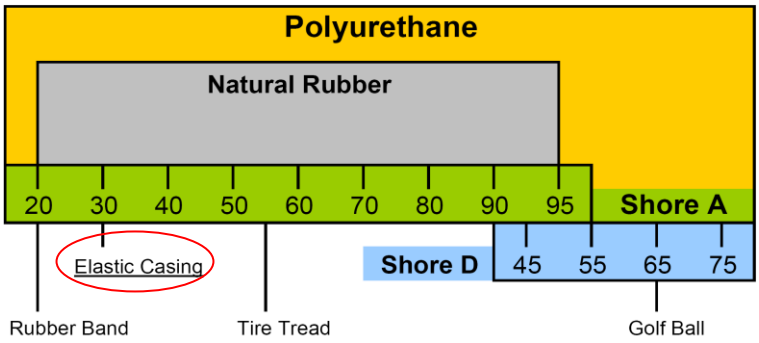

All of the mounts were fabricated with identical dimensions using a three part custom machined aluminum mold. This mold has the capability of making a solid elastomeric mount, an elastomeric mount with a cavity and a metal-elastic mount with a cavity.

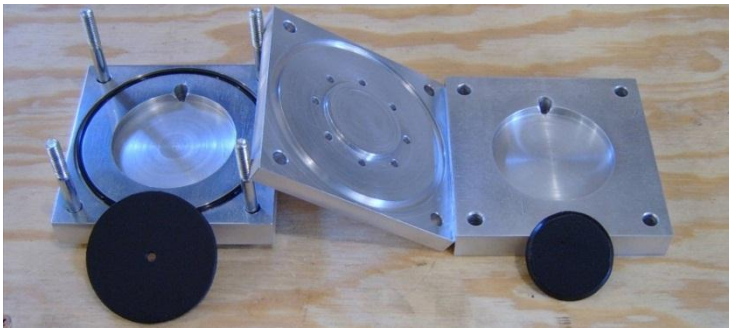

Figure 3-3: Three plate mold for manufacturing elastic mounts, adapted from [11].

For the RUB mount, the standard mount dimensions shown below were used and the mold was employed with its solid single piece capabilities using only the two outer parts of the mold. Therefore, the mount that was produced is a solid two-piece mount with no cavity, as the cavity was to contain an insert of the same material [11].

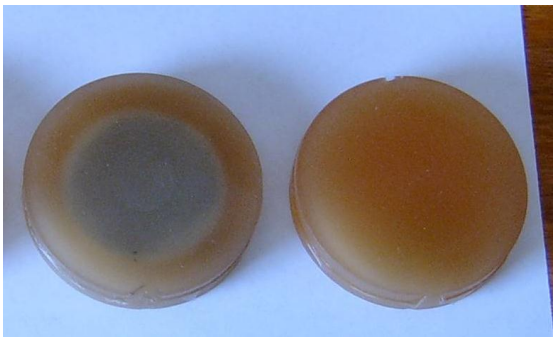

Figure 3-4: Elastic casing mounts 1018 steel (STE), and solid 30 D polyurethane (RUB), adapted from [11].

In order to produce the STE mount, the 3 part mold was employed in a two-step process. Firstly, after mixing the rubber, the mold with the middle cavity plate was filled with the polyurethane, then after partly curing, the mold was opened, separated and the 1018 Steel insert was placed inside of the cavity. Secondly, the mount was placed back in the mold with only the two outer plates and filled again with polyurethane and allowed to cure completely.

Table 3-3: Polyurethane metal-elastic and elastic casing dimensions with internal cavity dimensions for the specified insert, adapted from [11].

P.U. Casing with Type of Insert	**Mount *Height***	**Mount *Diameter***	**Insert *Height***	**Insert *Diameter***
	inch	inch	inch	inch
MRF	0.4375	2.375	0.1875	1.625
Air	0.4375	2.375	0.1875	1.625
30 D Polyurethane	0.4375	2.375	0.1875	1.625
1018 Steel	0.4375	2.375	0.1875	1.625

3.1.4 Existing Equipment: Roehrig Dynamic Characterization Test Rig

The equipment used for conducting the dynamic testing in this experiment was the Roehrig Electro Mechanical Actuator 2K-EMA testing rig, or EMA for short. The EMA that was used as a Dynamic Characterization Tester boasts a 0.010 to 7.000 inch stroke range, which is ideal for applications with very small displacements, such as the ones in this study. The maximum velocities are in excess of 10 feet per second and output frequencies range from 0hz to over 100hz. The EMA also features two polished chrome parallel uprights 1 ½ inch in diameter used for attaching a crossbar, temperature sensor and other tools and instruments. The aforementioned cross bar can be tightened to any height along the uprights. When conducting a static or quasi-static characterization test, a load cell attaches to this crossbar.

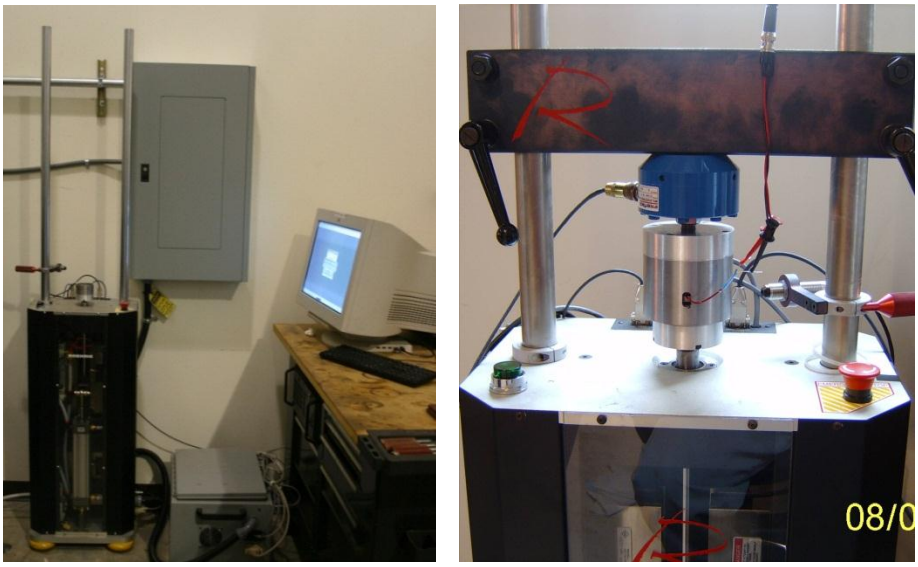

(a) (b)

Figure 3-5: Roehrig 2K-EMA Set-up with bare uprights, power-supply box, and PC (a), and uprights with cross bar and load cell assembly affixed (b), adapted from [11].

The load cell used can measure a maximum force of +/- 2000 lbs. (+/- 8.9kN). The EMA also has an input board with data ports inputting information from the load cell as well as an external infra-red (IR) temperature sensor. With knowledge of the pin-out configuration and modifications to the data-card, this input can be converted to take an external input from many other types of transducers, as is discussed later in this chapter.

The EMA has a 25 hp motor output and is controlled through a desktop PC using Roehrig's proprietary Shock Absorber Dynamometer Control and Analysis Software, Shock 6.3, released in 2009. Within this software, one can design and modify a number of custom wave-forms. The user also has the option to import inputs generated in other programs or collected data converted to the proper format, given that they are within the maximum stroke range and velocity limits. The EMA is controlled by a 16-bit motion control card and is powered through a 3-phase 220 volt power supply. These features make it the ideal tool for conducting our dynamic characterization test [27].

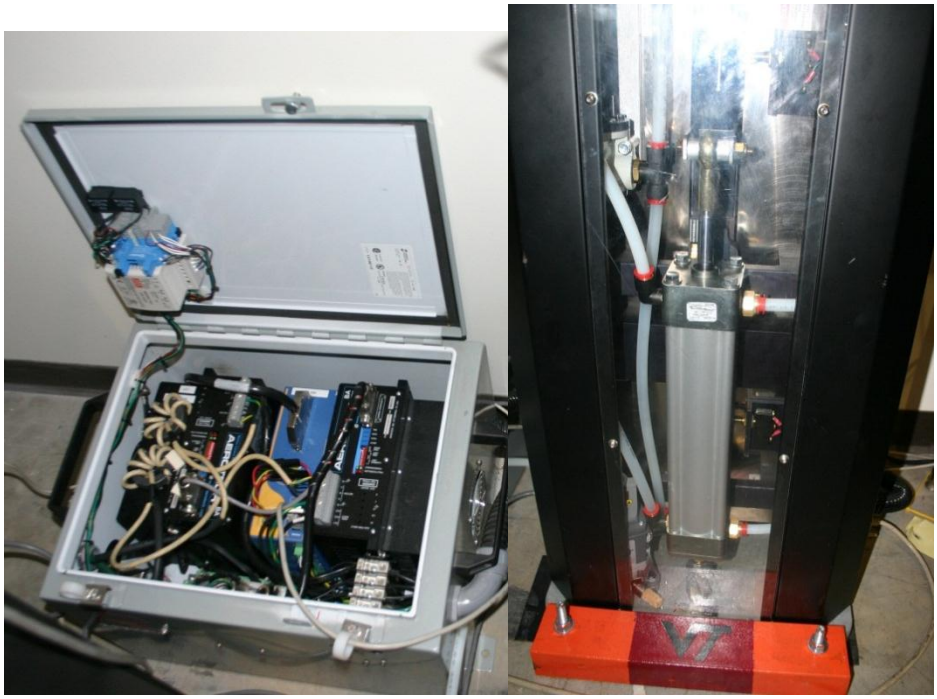

(a) (b)

Figure 3-6: Components of the Roehrig EMA (a) open power-supply box, and (b) front motor .

3.2 | Modification of Existing Parts, New Parts Fabrication, and Physical Dynamic Principles

3.2.1 Fabricated Parts: Floating mass brace assembly

The most important aspect of the dynamic characterization is being able to measure an output displacement to an input displacement. This poses a problem because, although setting an input is as easy as programming the EMA, having a floating mass that would be placed overtop the mount and allowing it to vibrate freely in the vertical direction was a much more difficult task. This required a slight modification of the standard Roehrig EMA set up.

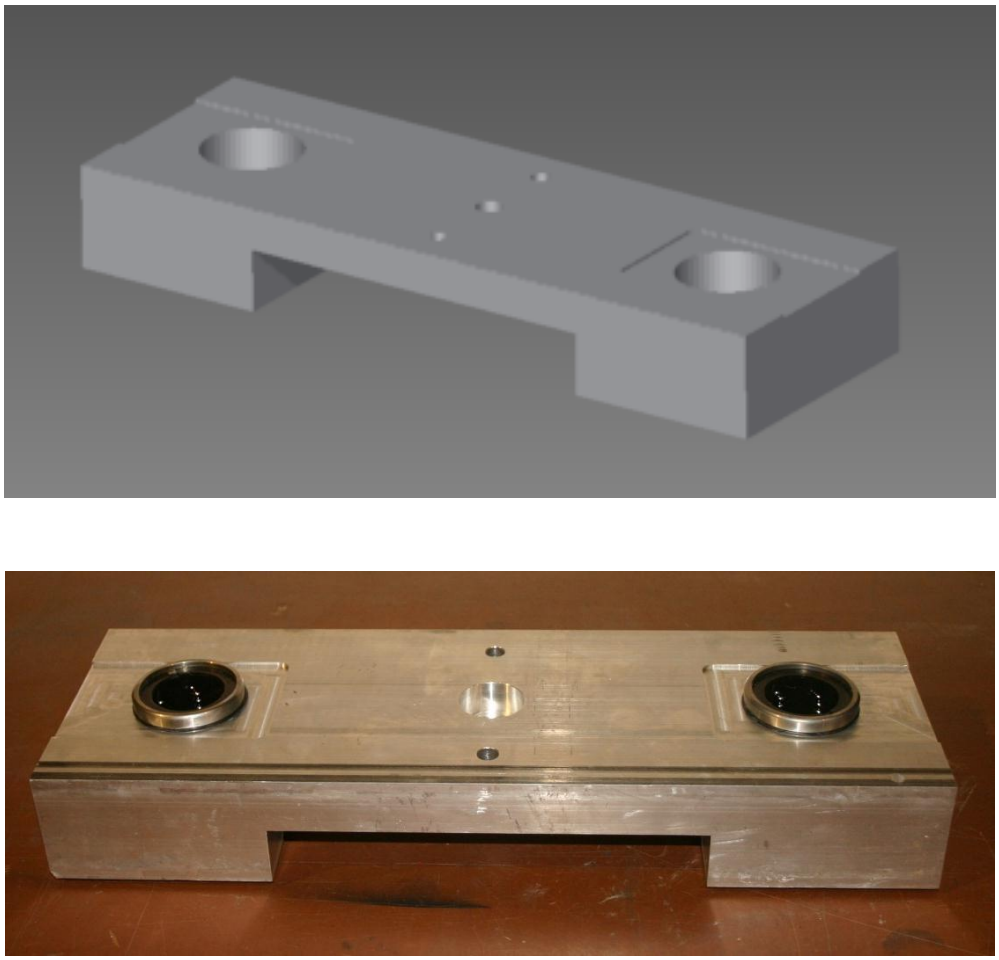

Figure 3-7: CAD Drawing of brace (top) and machined brace with bearings insert (bottom).

A brace assembly was designed to run along the existing 1 ½ inch diameter uprights of the EMA using INA KBZ24 self-lubricating sealed linear bearings [28]. These linear bearings fit into precisely machined holes on the braces. The upper housing of the electromagnet attaches to

the braces using the same size bolts that it would use to attach to the crossbar on the EMA. Having a second brace also allows the mass plates, each ~ 10lbs, to be tightened between the two. Two threaded upright rods were attached using bolts and washers and are then threaded through holes on either plate. The system would be experiencing input amplitudes of up to 0.5 inches peak to peak and frequencies of up to 60hz, so this was a necessary measure because it served the purpose of securing the required mass in place and keeping it from being thrown off during a test run. For experimental continuity, spacers were designed to fit in the space between the threaded upright rods and the holes in the mass plates. These spacers were machined to the exact diameters of the mass plates' holes thus maintaining their centered position throughout the entirety of the dynamic tests.

Each floating mass brace weighs approximately 19.5 lbs. and that weight, along with the mass of the upper magnetic housing and load cell, was then supplemented with the appropriate number of 10lb mass plates to meet the pre-load weight requirements for each experiment respectively.

Figure 3-8: Machined Aluminum spacers (left) mass plates with pre-existing holes (right) and spacers placed inside the weights (bottom).

3.2.2 Acquired Parts: External LVDT

As was mentioned in the dynamic principles section of chapter 2, in order to determine the transmissibility ratio for the mounts being tested in this study, one needs to be able to measure the input vibration and compare it to the output of the floating mass. Although the input vibration is automatically measured through the EMA's internal linear variable differential transducer (LVDT) , the vibration of the mass on the upper portion of the assembly is not. That is why an external LVDT was employed to fill that need. For this study, a Macros Sensors DC 750-2000 model LVDT was implemented. With its full scale output of 0 - ± 10V DC as well as a noise and ripple rating of < 10 mV rms , its resolution and signal to noise ratio was much more than was required as the minimum displacement required to be measured was ~0.01 inches peak-peak. This model has a has a usable range of ±2.00 inches (50 mm) which is adequate for measuring the output displacement of the upper plate [29].

Figure 3-9: LVDT Power supply (left) and multi-meter (right).

To be powered, the LVDT requires a ± 15V DC connection with a minimum of ± 25 mA current. The power supply used was a Power-One HAD 15-0.4-A. This power supply is able to produce the ±15 V DC and up to 400 mA current [30]. Lastly, to monitor the voltage output of the LVDT and to determine the zero point before each run, a simple multi-meter was employed and wired into the main circuit.

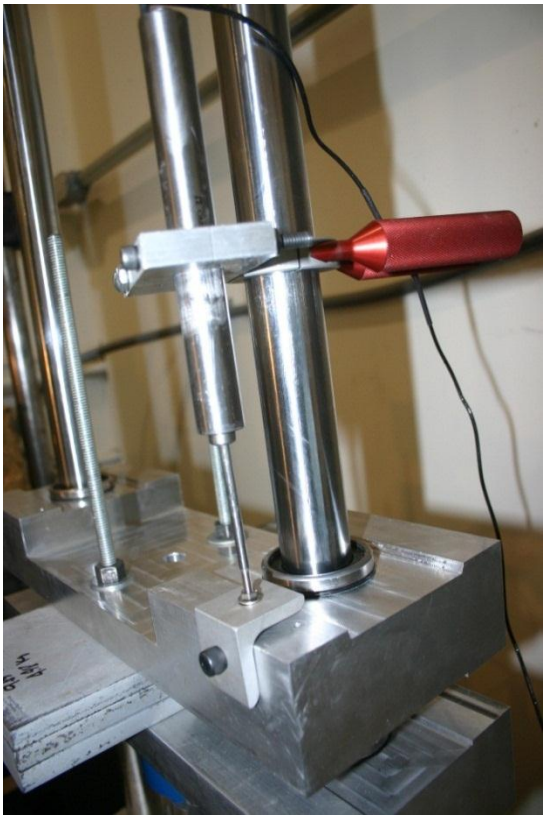

Figure 3-10: LVDT mounted to upper brace using custom machined bracket.

In order to properly measure the displacement of the upper floating mass, the LVDT's magnetic through-rod had to be attached directly to the mass itself. This was done by machining a bracket that was attached to the upper brace and to which the rod would attach to. The LVDT itself also had to be attached to a fixed surface in order to accurately measure the displacement at all instances. This was done by designing a bracket that would use the existing uprights on the EMA. Using the collars that were included with the EMA, the LVDT bracket is adjustable in height and can tighten around the LVDT using a clamping screw.

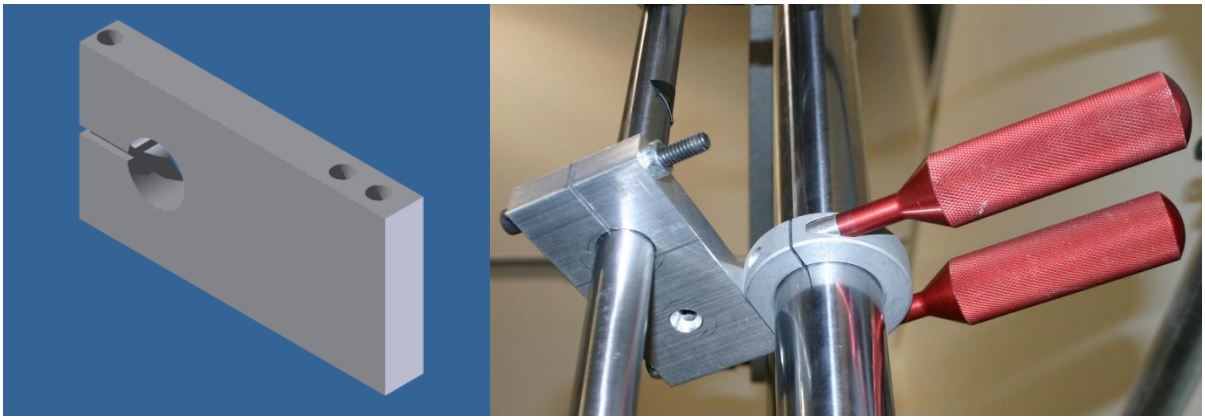

Figure 3-11: LVDT brace drawing (left) and mounted on uprights (right).

3.2.3 Modified Parts: MR Metal Elastic Mount

Lastly, due to the nature of the dynamic tests and the sometimes violent tendencies of any vibrational testing, the MR fluid mount had to be redesigned after initial failures of the design proposed by BM Southern.

Figure 3-12: Metal-elastic mount that failed under high amplitude testing.

As was shown in Table 3-4, the original MR-mount was designed to have a thickness of 0.4375 in. So, using a slightly modified version of the process BM Southern developed, a mount with a thickness increase of 25.7 % and diameter increase of 4.2 % was created. The mass of the mount also increased from 3.915 oz. to 4.85 oz. The insert cavity dimensions were not changed due to the fixed nature of the mold dimensions and so the amount of MR fluid still remained 0.95 oz.

Table 3-4: Original MRE dimensions and modified MRE dimensions

	MRE Original Dimensions	MRE Modified Dimensions
	Inch	Inch
Mount Height	0.4375	0.550
Mount Diameter	2.375	2.475
Insert Height	0.1875	0.1875
Insert Diameter	1.625	1.625

Figure 3-13: Original MRE mount (left)and modified MRE mount (right).

This design proved to be much more resilient and resistant to shock and vibration than the original designed which failed under the initial dynamic testing phase. The detailed instructions for fabrication of the mounts can be found in great detail in BM Southern's master's thesis [11]. The second major modification to the MR mounts that was made was the usage of a less dense MR fluid mixture. The original MRF mount was designed with MRF-145 mixture. Due to the lack of availability and discontinued manufacturing of that specific mixture, MRF-122 was used. The fluids react differently to magnetic field application due to the drastic difference in particle density. Mainly, clumping is less likely to occur in fluids with less percentage density when operated in squeeze mode [31]. The respective B-H curves are shown below. A comparison of Finite Element Magnetic Modeling models of flux density for the original design with MRF-145 and the redesigned MRF mount was then conducted.

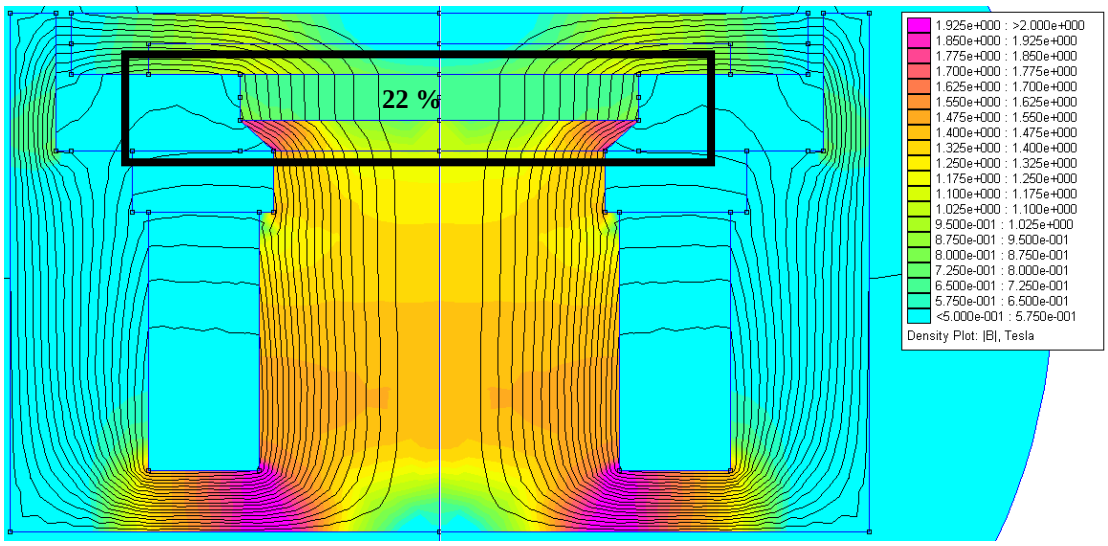

(a)

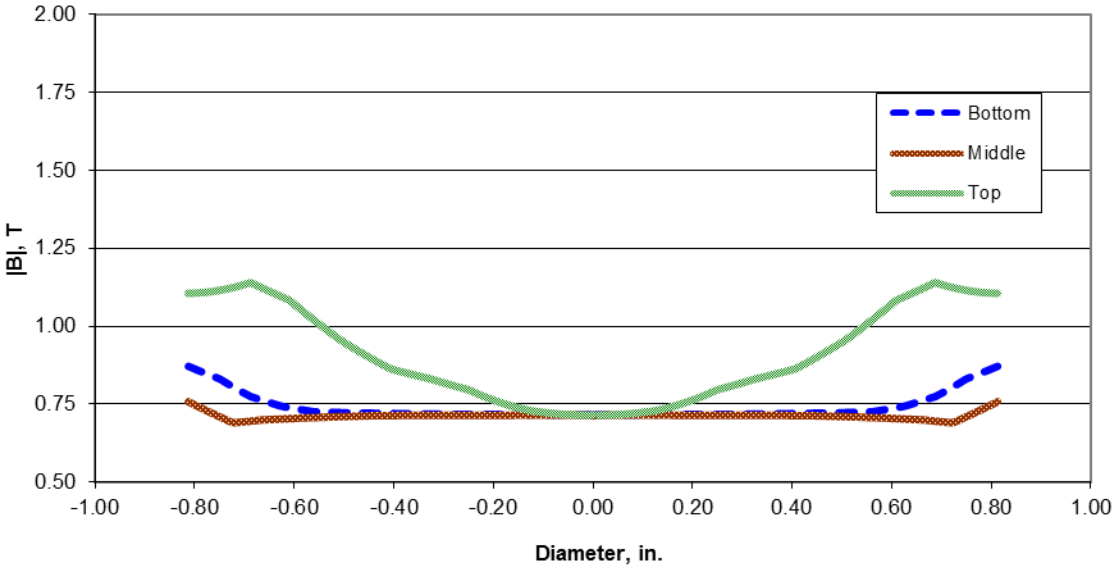

(b)

Figure 3-14: Simulated (a) Flux density for mount system and (b) magnetic flux magnitude for MRF-122 with 3 Amps of current supplied to the electro coil. adapted from [11].

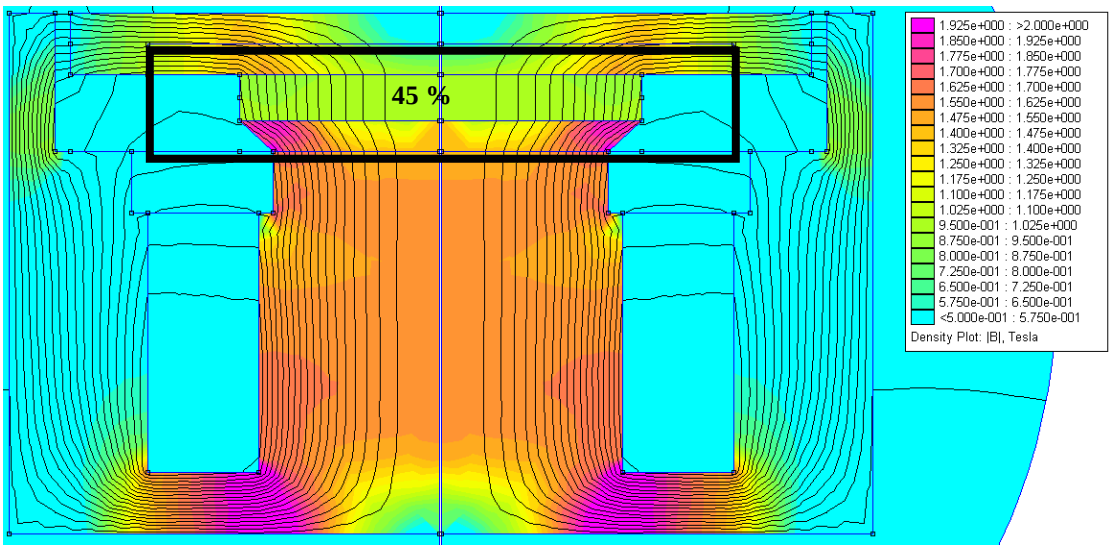

(a)

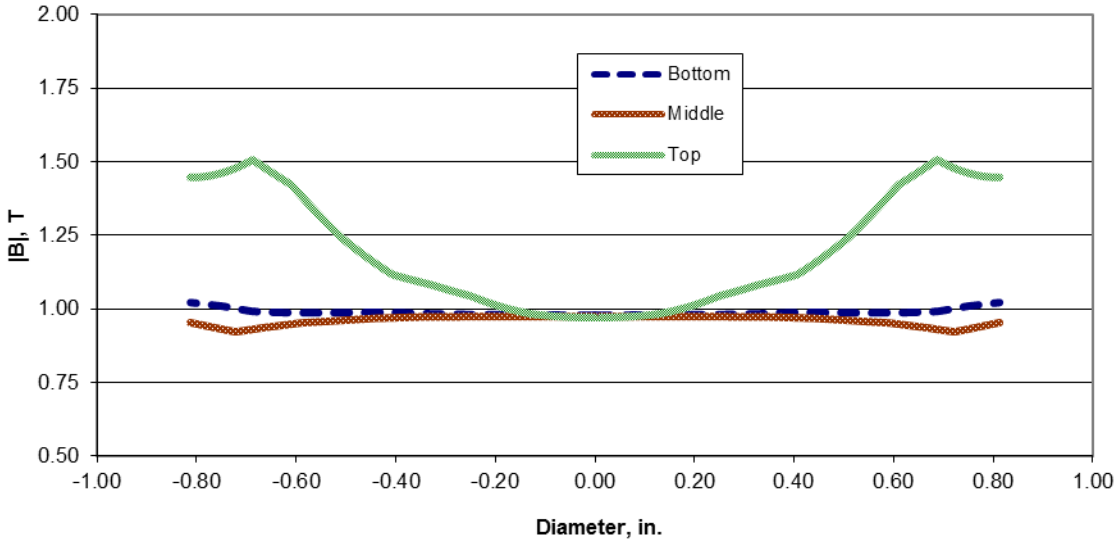

(b)

Figure 3-15: Simulated (a) Flux density for mount system and (b) magnetic flux magnitude for MRF-145 with 3 Amps of current supplied to the electro coil, adapted from [11].

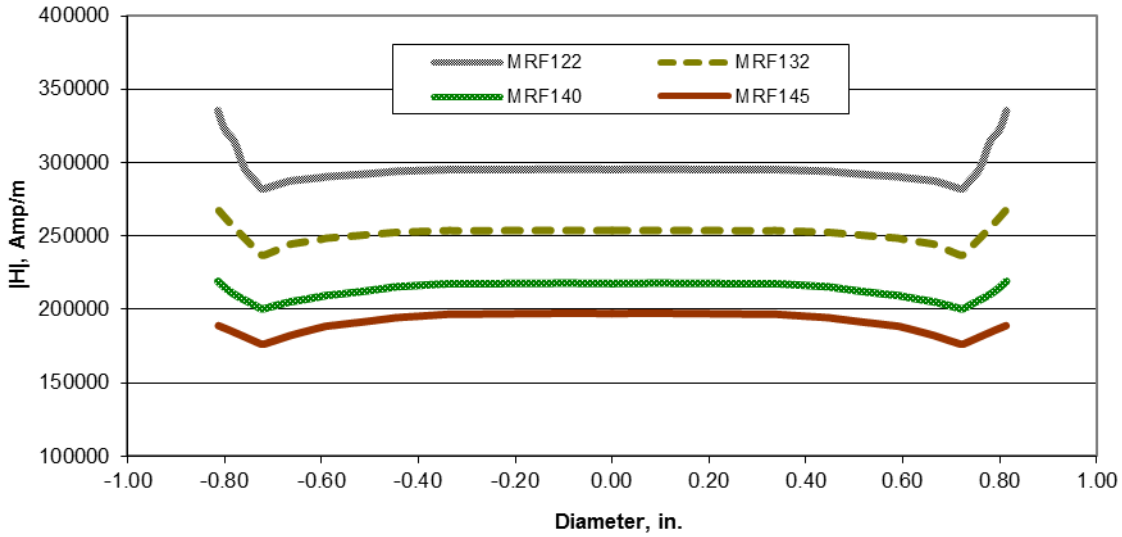

Figure 3-16: Magnitude of magnetic field intensity at the center of the fluid gap in the mount with various MR fluids including MRF-122 and MRF-145, adapted from [11].

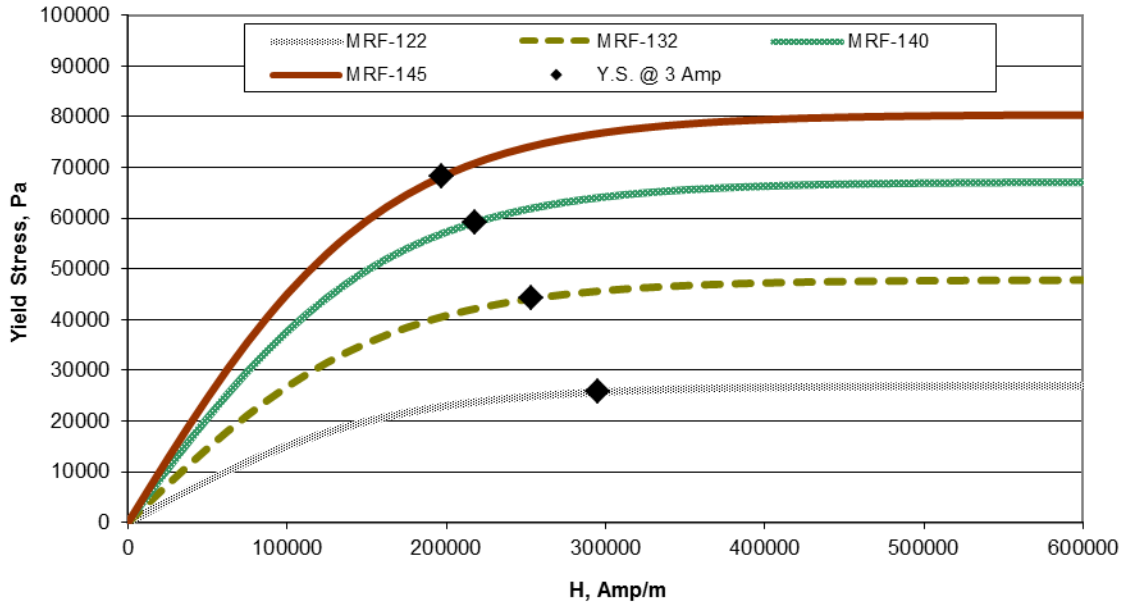

Figure 3-17: Yield stress in MR fluids marked with the maximum yield stress achieved in each fluid with various MR fluids including MRF-122 and MRF-145. adapted from [11]

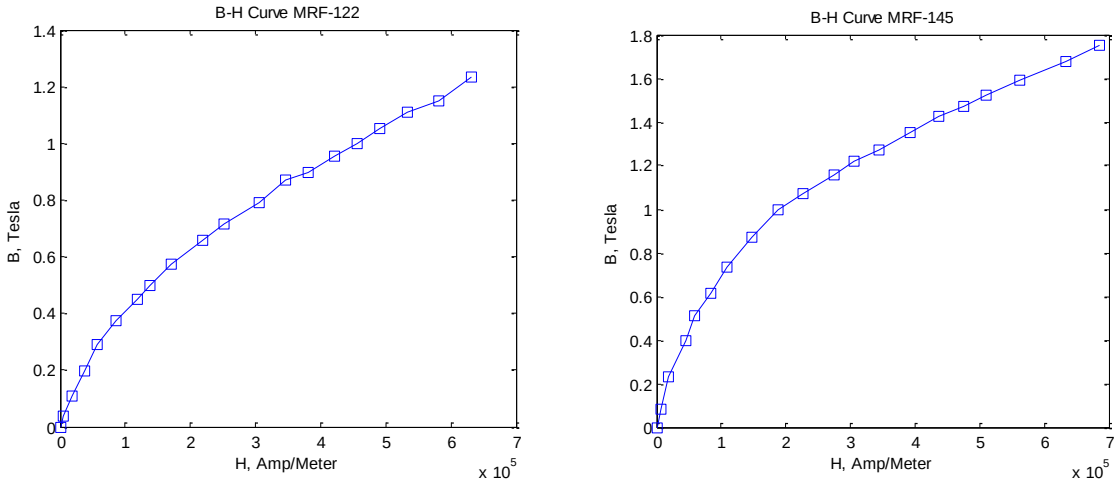

Figure 3-18: From the FEMM flux density models, we see there is a drop from 45% to 22% drop in flux density across the mount. This however is now the basis for the dynamic study.

3.3 |Final Experimental Set-up

3.3.1 Experimental Set-up

Using the materials and equipment discussed in the previous sections as well as the principles explained, the final experimental set-up was assembled. The assembly began with the Roehrig EMA as the base to which everything else would attach. The first step was attaching the lower electromagnet housing to the EMA's threaded actuator rod. The upper housing of the electromagnetic assembly as well as the load-cell were then attached to the lower floating mass brace using a 1 inch long threaded rod and nut. The lower brace, with the threaded rods fed through the bottom, was then placed on the uprights via its linear bearings. Using a small hand-crank hydraulic lift, the upper housing was loaded with the proper amount of mass for each for the respective experiment and mount while being elevated a few inches above the lower electromagnetic housing, allowing ample space for mount insertion.

Figure 3-19: Finalized completed assembly with rheometer, load cell and weights between the braces all mounted on the EMA.

After the weights were placed on the lower brace through the threaded uprights, the spacers were fed along the threaded uprights and through the existing holes in the masses thereby centering the masses. The upper floating mass brace was then fastened with bolts and washers to the bottom brace. Lastly the LVDT was fastened to the uprights using the collar and then its magnetic through-rod was attached to the upper assembly using the hole in the upper brace as

well as the custom machined bracket. In this situation, the input force was not being measured; rather, the load cell was being used as a convenient attachment piece between the lower brace and the upper magnetic housing.

3.3.2 Data Acquisition

Most of the data acquisition for this system was simplified due to the turn-key nature of the Roehrig EMA and software combination. The input displacement, input velocity, load-cell force reading, acceleration and test specimen temperature were all measured internally through equipment provided by and validated by Roehrig Inc. However, the major problem that was encountered was the data acquisition of the floating mass displacement.

This was resolved by using the EMA's data acquisition board and the existing connection for the IR Temperature Sensor. This was advantageous for multiple reasons. The first advantage was that the Roehrig EMA board features a sampling frequency of 4000 Hz and at a maximum input frequency of 60 Hz, this is far beyond the required sampling rate for this study. Secondly, having all of the data measurement coming from one board centralizes the information into one file, thus simplifying the collection of 100's of data files. Last, and most importantly, collecting data from multiple boards creates data sets that may be inconsistent and that are asynchronous. This would require a significant amount of processing to ensure synchronization prior to the analysis of the data itself. Additionally, the board filters out known system noise from all of the sensor data in a similar fashion thus adding to the continuity of all of the measured data.

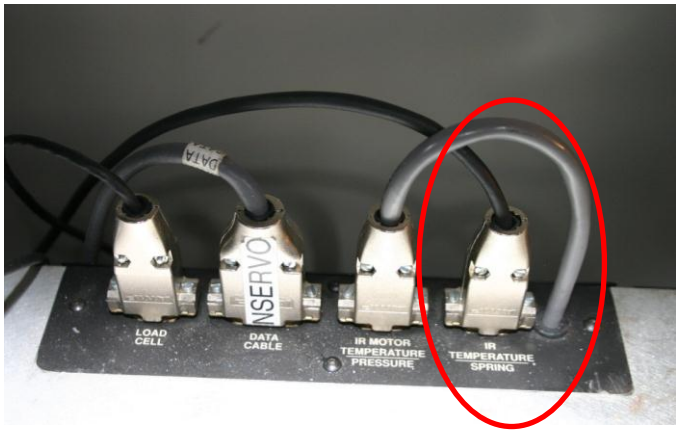

Figure 3-20: Data acquisition board with inputs for Load Cell, Data Cable (internal), Motor Pressure (internal) and IR sensor input converted for the LVDT input.

Using the EMA's board however, was not a simple plug and play task. The first step was to make a connector that would take the proper pin designations to the EMA from the LVDT. Next, after connecting and powering the LVDT, measurements for the maximum and minimum displacement capabilities were taken using the multimeter to monitor the output voltage. After having the max and min values, the mid-point was designated as a zero value. From that datum, output voltages were measured from precise incremental displacement changes and that information was entered into the data card.

3.3.3 Set-up Validation

In order to validate the set-up of the experiment, a set of validation tests were run to ensure that the calibration and outputs were still correct. In order to begin validation, an alternate set-up had to be used. As is depicted below in figure 3-22, the linear actuator of the EMA had to be directly linked to the external LVDT. This could only be done by attaching the floating braces directly to actuator on the EMA and having the LVDT attached to the upper brace in its normal fashion. Having this setup would ensure that the LVDT is reading exactly what is being output from the EMA actuator.

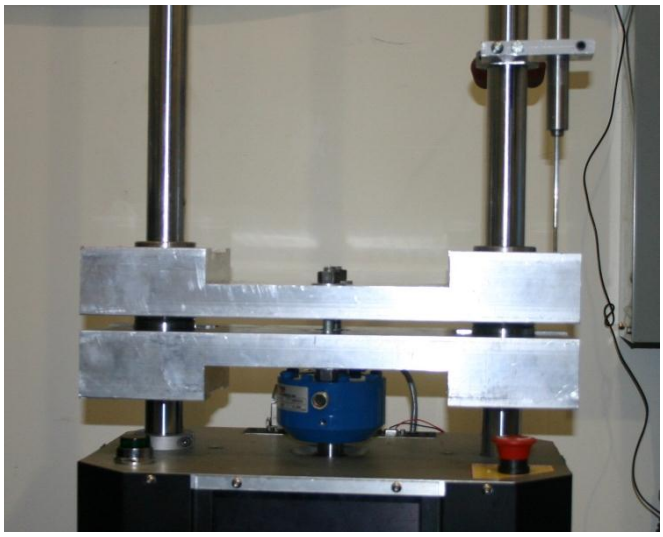

Figure 3-21: Validation set-up with direct attachment from LVDT to the actuator.

The first step of validation was to ensure that the LVDT was properly calibrated. Therefore, the calibration of the LVDT conducted in the previous section was done in multiple ways to ensure validity. Min and max, midpoint and incremental displacement voltage output measurements

were taken. The first method of incrementing the displacement was through the EMA's manual install feature, which allows the user to manually move the actuator to any desired point. Thus, having the LVDT at its determined zero point and moving the actuator in known positive and negative directions while noting the voltage outputs at each increment is an accurate way of calibration. Because the calibration and validity of the EMA's internal LVDT had to also be validated, the second form of calibration employed a similar process. However, instead of having the EMA actuator provide the displacement changes, a set of accurately machined parallel bars served the purpose of generating accurate displacements and equivalent voltage output values from the LVDT. Since the values were one and the same, they were entered into the EMA's data-card for usage as conversion factors.

Table 3-5: LVDT Displacement Values and Bit conversion values for entry into Data Card.

Displacement Inches	0.98	0.75	0.50	0.25	0.00	-0.25	-0.50	-0.75	-0.98
Card Value Bits	65534	58163	49811	41465	31138	24946	16588	8243	488

The next step was to validate the output of the EMA. Since the values of the LVDT's measurements were validated and confirmed, the next step was to ensure that a waveform produced by the EMA was indeed the waveform that was being imported through the software. Using the same experimental set-up as the LVDT calibration, a set of simple tests were conducted using sine and triangle waves of various amplitudes. The displacement readings from the LVDT were then compared to the input waveform and the validity was assessed.

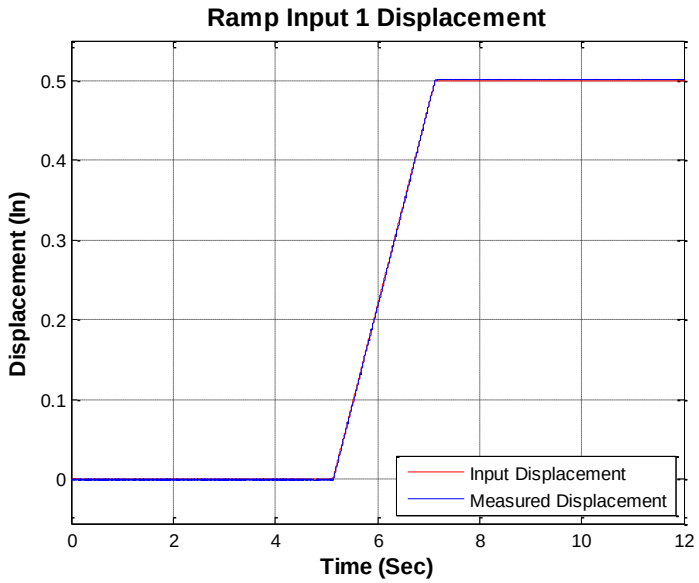

Figure 3-22: Comparison of 0.5 inch ramp input (Red) vs. waveform measured by LVDT (Blue).

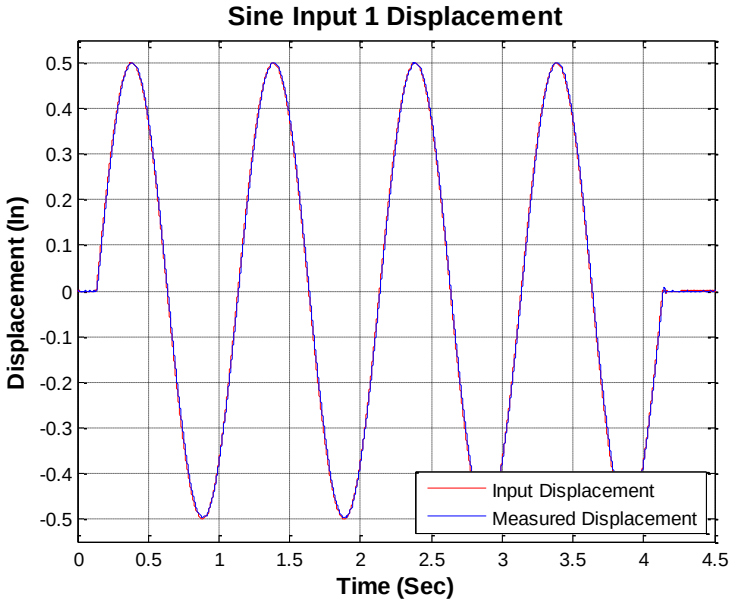

Figure 3-23: Comparison of 1 Hz 0.5 inch sine wave input(Red) vs. waveform measured by LVDT (Blue).

From the figures above, we see that both the static ramp and dynamic sine measurements were almost exactly tracking the input wave form thereby validating both the LVDT and the EMA test setup. Therefore, our equipment was fully validated and proven to provide accurate readings.

3.4 |Design of Experiment

3.4.1 Quasi-Static Test

For the first phase of characterization, a quasi-static test was run. In order to conduct the QST, a test set up similar to that of BM Southern's was employed. As is shown below, the upper and lower electromagnet housings were attached to the crossbar and the actuator respectively. The crossbar clamps were was then tightened and the tests were run.

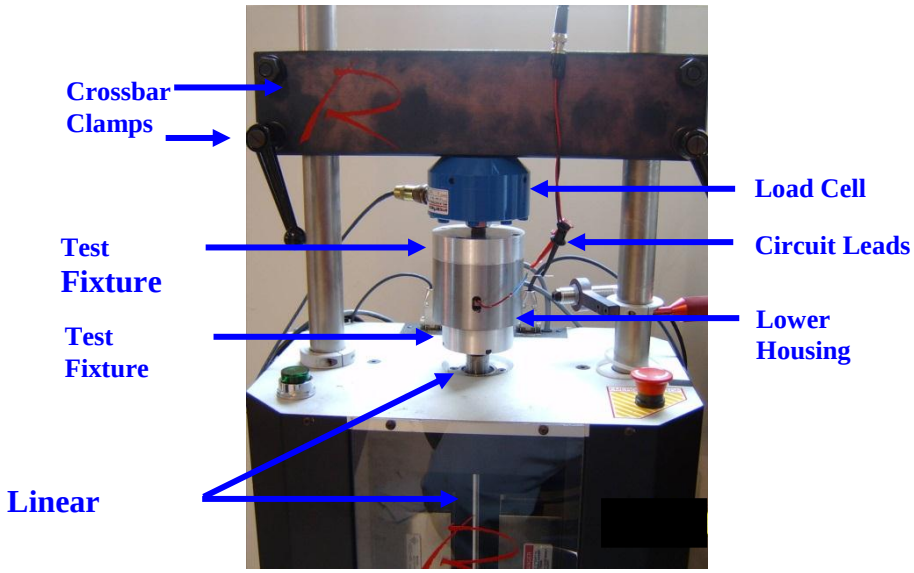

Figure 3-24: Test Setup of mount and magnetic system in the Roehrig EMA Dynamometer, adapted from [11].

In the quasi-static experimental testing, a ramp input from 0 to 0.0393inch (1 mm) over 3 sec. was used for the soft core mounts and a ramp input from 0 to 0.01968 inch (0.5 mm) over 3 sec. was used for the solid core mounts as illustrated in figure 3-25 . This was cycled through 5 times for each of the three test runs. The acquired force was measured against the compression and extension displacement [11].

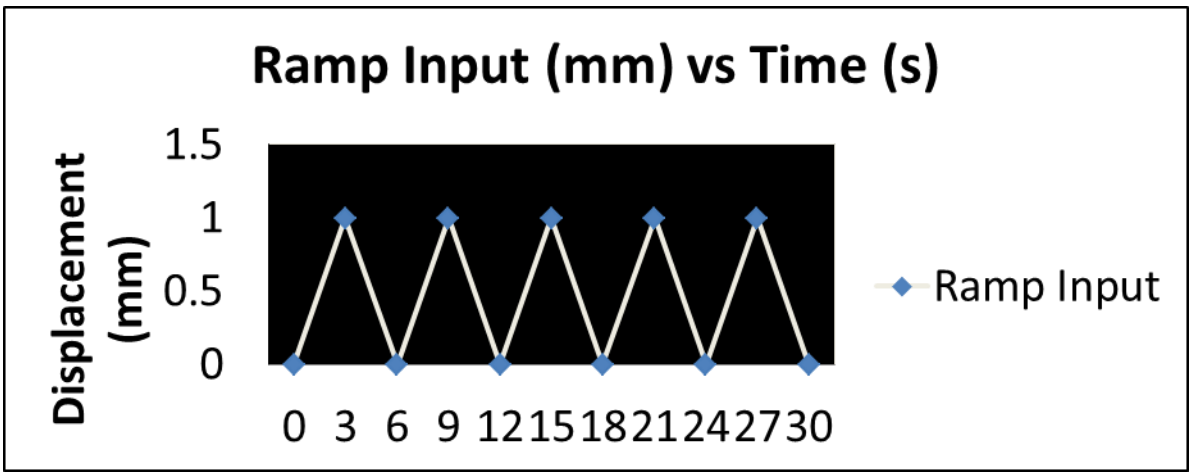

Figure 3-25: Ramp displacement input for quasi-static testing on the shock dyno.

The outputs of this test were plotted as force displacement curves and the method described in section 2.3.2 was employed to determine the stiffness and equivalent damping. The QST began by characterizing the STE and RUB mounts as a baseline for the MRF. This base would simulate stiffness and damping values that were less than that of a completely inactive MR mount as well as values that would be higher than that of a completely magnetized MR mount.

3.4.2 Dynamic Test

For the second phase of characterization a dynamic test was run. The custom test set up described in earlier sections was used for this stage. As is shown below, the upper and lower electromagnet housings were attached to the actuator and lower mounting brace respectively.

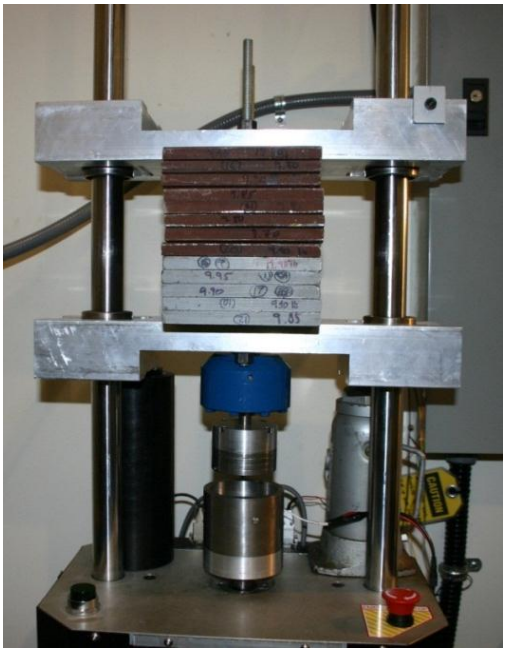

Figure 3-26: The Completed dynamic test assembly with pre-load.

The upper housing was attached to the brace via the load cell. Then a stack of the appropriate amount of weights was secured between the two braces and the LVDT was attached to the upper plate via the custom attachment bracket. In order to implement a preload and circumvent an initial non-linearity in the mounts, an initial deflection of 0.006 inches (0.15 mm) was chosen and subsequently, a pre-load weight for each mount was determined and placed onto the mass braces. Table 3-6 below shows the values for each mount.

Table 3-6: Preload weights and Percent of deflection with pre-load weight attached.

	Pre-load Weight (lbs.)	% Deflection
RUB	75	~1.5
STE	~170	~1.5
MRF	~170	~1.1

With the floating mass determined, an appropriate input had to be chosen for adequate dynamic test results. The method of simulating various frequencies chosen was a chirp signal. A chirp signal is one that sweeps from a given initial frequency to an indicated maximum frequency. The rate of increase is also user defined. For our specific test, a chirp signal that sweeps from 0hz to 60hz was chosen. This was because the highest natural frequency calculated using equation 2.3 was found to be around 20 Hz, and to accurately display the dynamics of the system, a maximum value of 3 times that was chosen. The rate of increase was 1hz per second, giving adequate time for the system to react through each frequency as well as being able to recognize the frequency response accurately from a time-displacement plot.

Table 3-7: Numerical Parameters Used in Simulink Chirp Generator

Simulation Input	Initial Frequency	Target Frequency	Simulation Time	Fixed-step Size
Chirp	0 Hz	60 Hz	60 sec	1/100

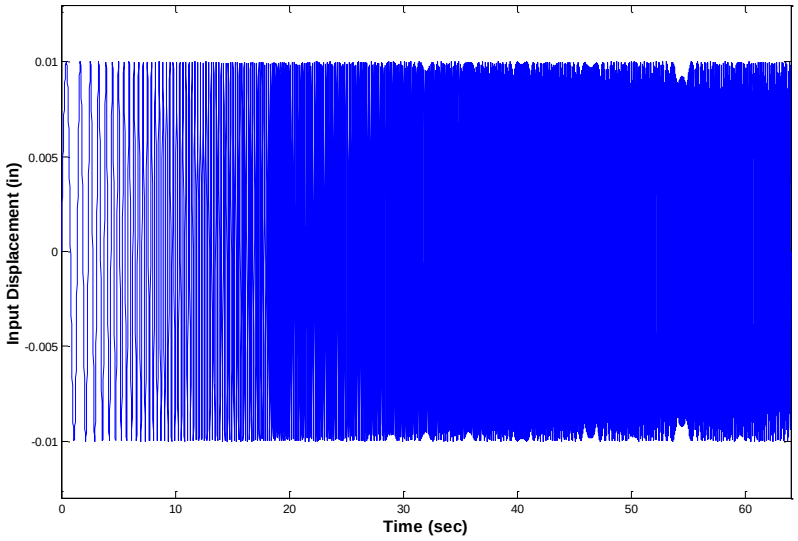

Figure 3-27: Original chirp input waveform from 0-60 Hz

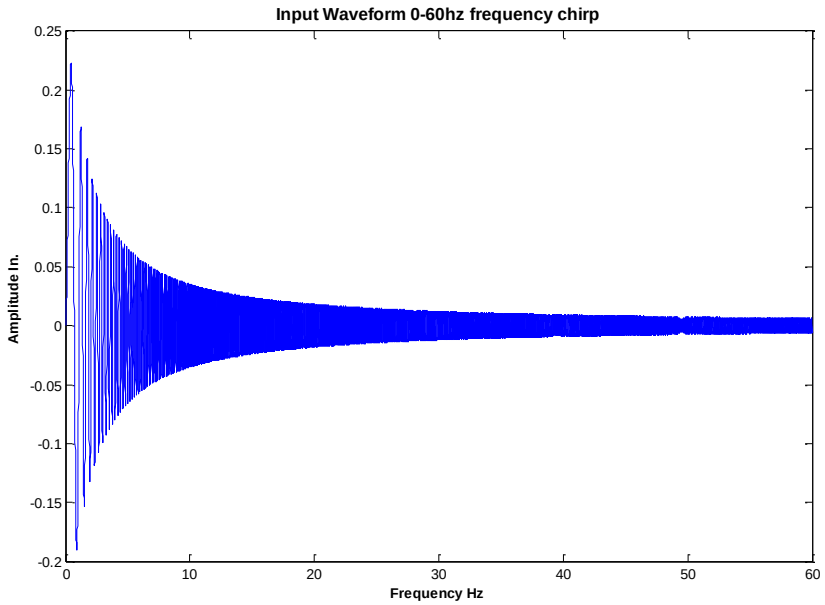

Figure 3-28: Customized decreasing amplitude chirp waveform used in this study.

Also, due to the nature of the higher frequency nature of the dynamic tests and an initial amplitude of 0.25 inches, a modified chirp signal was employed. By filtering the signal through the transfer function below, the chirp signal's amplitude was gradually reduced, thus drastically reducing the violent nature of the input and response at the higher frequencies while still maintaining the frequency content throughout the test. This is not the most accurate way to achieve this, however, this proved to be a simple and adequate method for this study.

$$TF = \frac{1}{\frac{1}{2\pi * 1.5} + 1} \tag{3.1}$$

The data acquisition software and DAQ board has the ability to record many system measurements. The ones that that were of value for this study were input displacement, velocity, force, and the output displacement (measured with external LVDT).

The time-displacement curves were plotted, however they were not directly used to analyze the dynamic characteristics of the mount. An example of the time traces are included in figure 3-39.

The proper method of displaying and analyzing the dynamic test data is by generating a transmissibility plot. To generate transmissibility plot there are two methods, the force - displacement and the displacement-displacement methods. In this experiment, the latter was used because of the measurement capabilities of the sensors used. The equation generates a plot using a ratio of the output displacement to the input displacement. However, since transmissibility is plotted against the frequencies, the input and output plots had to be converted into the frequency domain.

$$H(\omega) = \frac{G_{XX}}{G_{XY}} = \frac{X^*(\omega) \cdot X(\omega)}{X^*(\omega) \cdot Y(\omega)} \tag{3.2}$$

Equation 3.2 above shows the equation for the FRF transmissibility estimator, $H(\omega)$ being defined as a ratio of the cross spectrum, $G_{xy}(\omega)$ to the auto spectrum, $G_{xx}(\omega)$. The auto spectrum can be defined as the frequency content of the input, $X(\omega)$, multiplied by its complex conjugate, $X(\omega)^*$. Additionally, the cross spectrum is defined as the frequency content of the output, $Y(\omega)$, multiplied by the complex conjugate of the input, $X(\omega)^*$. This ratio was then plotted against either the input frequency range or against the normalized frequency ratio, r.

In order to remove unwanted content from the frequency domain of the displacement data, it was averaged over 15 overlapping blocks. This averaging removes noise and the possibility of outliers skewing the data and creating peaks that did not exist. Secondly, Matlab's built in smoothing filter was applied to the resulting transmissibility calculation to produce a smooth and characteristic transmissibility curve. The smoothing filter in matlab acts by using a moving smoothing filter and a summing span specified by the user or a default of 5 spans.

Much like the QST, this portion of the test also began by characterizing the STE and RUB mounts as a baseline for the MRF. This base served to simulate transmissibility plots that represent the upper and lower limits in terms of vibration transmissibility. We then ran the dynamic tests on the MRF mount, beginning with no magnetic field applied and increasing the current by 0.2 amp until the 2.0 amp maximum.

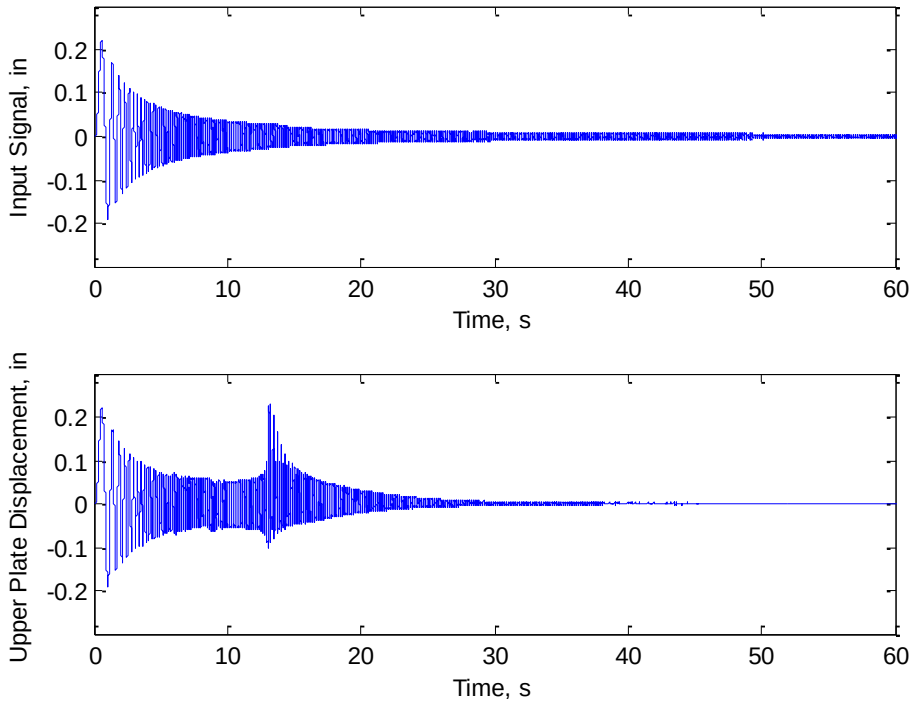

Figure 3-29: Example of time traces for MRF at 0.0 amps of current of measured input (top) and output displacement (bottom) by internal and external LVDT's respectively.

Chapter 4 | Results and Discussion

This section shows the results of the experiment conducted in this study and presents a discussion and explanation of the results. Specifically, this chapter begins with a presentation of the results of the Quasi-Static Test and compares it with the results of similar tests conducted in prior studies. Secondly, the chapter turns to the results of the dynamic testing. First it presents the validation results, followed by the results of the dynamic testing of the passive and MR mounts. Finally, a discussion of the results and conclusions is presented.

4.1 |Quasi-Static Test results

4.1.1 Necessity of QST

Approximately four years had elapsed since the RUB and STE mounts were first fabricated. Some of the properties had changed due to extended storage and even due to the testing they endured. Also, due to the failure under dynamic testing of the MR mount design presented by BM Southern, a new MR mount was designed that was more resilient to the impacts and higher input frequencies from the actuator. Therefore, the mounts' characteristics had to be re-confirmed using a similar process outlined by BM Southern discussed in detail in section 2.3.2 of this study. This would provide us with evidence that the mounts were still usable and would also provide us with values to use for the validation process of the dynamic test data analysis.

4.1.2 Acquired Data

The mounts tested were the RUB, STE and MRF. To ensure quality and consistency of the results, each mount endured a set of three tests. For each test, the actuator went through 5 cycles of compression and extension. Then the average values of force vs. displacement for the 5 cycles were plotted and the stiffness and damping values of each of the mounts were extracted from those plots by methods described in earlier sections.

First, the RUB mount was tested, representing values well below lower limit of damping and stiffness for the MR mounts.

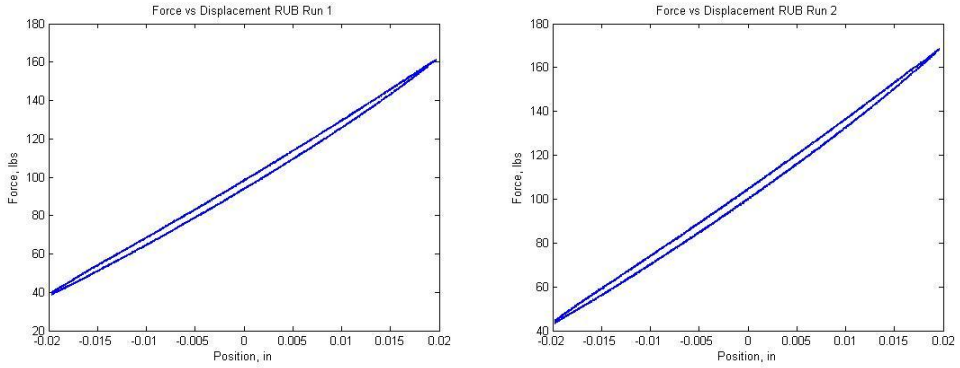

(a) (b)

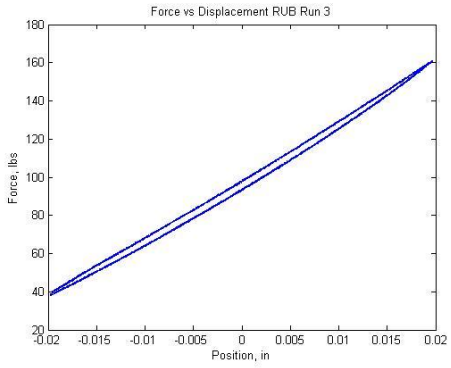

(c)

Figure 4-1: Plots for (a) 1st test, (b) 2nd test and (c) 3rd test of the 5-cycle averaged QST for the RUB mount at 0.0 amps current.

Secondly the STE mount was tested, representing values well above the upper limit for the mounts.

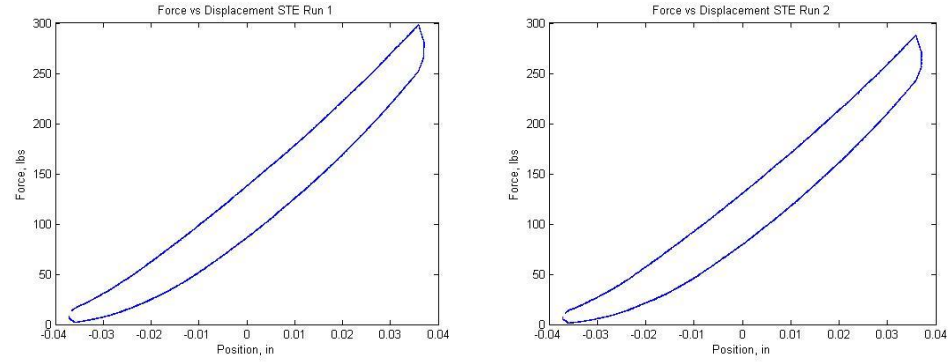

(a) (b)

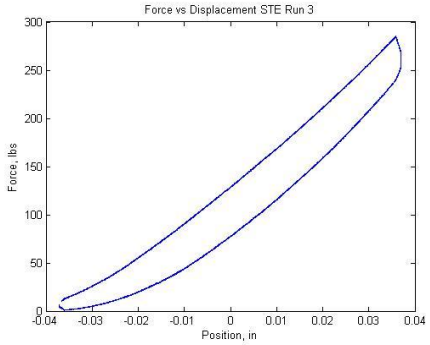

(c)

Figure 4-2: Plots for (a) 1st test, (b) 2nd test and (c) 3rd test of the 5-cycle averaged QST for the STE mount at 0.0 amps current.

Lastly, for use in the validation process of the dynamic test data in the next section, the MRF mount was tested at 0.0 amps current.

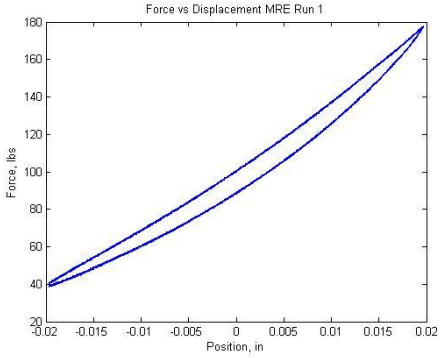

(a)

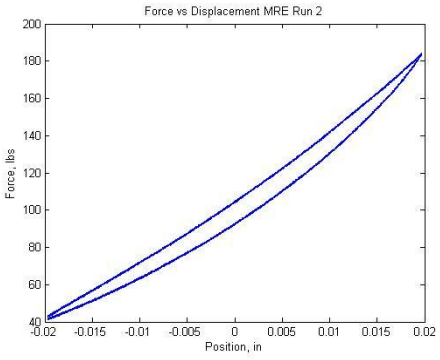

(b)

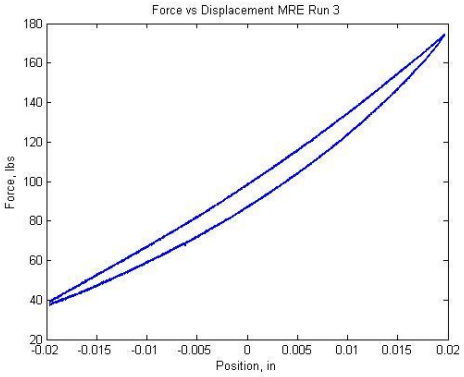

(c)

Figure 4-3: Plots for (a) 1st test, (b) 2nd test and (c) 3rd test of the 5-cycle averaged QST for the MRF mount at 0.0 amps current.

4.1.3 Summary of Results and Comparison to Earlier Studies

The results above showed a few trends. First, as was expected, the RUB mount provided the least amount of stiffness and lowest damping ratio, with an average stiffness value of 2913 lb/in and an average damping ratio of 0.0204. Also as expected, the RUB mount exhibited the least hysteretic content and acted almost completely linearly. Thus the stiffness calculation method for mounts exhibiting hysteretic behavior and the one for linear springs gave way to similar values.

Secondly, the STE mount, again as expected, exhibited stiffness values that were much higher than that of the RUB mount with an average stiffness value of 4450.5 lb/in and average damping ratio value 0.1088. The hysteretic content in the steel was much more evident and prominent as the stiffness and damping from the mount was limited to the smaller portion of the elastomer around the steel insert since the steel is a non-compressible material.

Lastly, the MRF mount showed reasonable median values. With an average stiffness value of 3681.2 and an average damping ratio value of 0.0663, these were well within the upper and lower limits established by the baseline testing. The amount of hysteretic content was also more than that of the RUB mount but significantly less than that of the STE mount, as was expected.

Table 4-1: Table of Stiffness, K and Damping Ratio, ζ values and averages for each mount per run.

	Stiffness Value, K $(\frac{lb}{in})$	Ave. Stiffness Value, K, $(\frac{lb}{in})$	Damping Ratio, ζ	Ave. Damping Ratio, ζ
RUB Run #1	2950.1	2981.3	0.0202	0.0204
RUB Run #2	3077.9		0.0203	
RUB Run #3	2915.9		0.0208	
STE Run #1	4142.6	4450.5	0.1081	0.1088
STE Run #2	4500.5		0.1105	
STE Run #3	4708.5		0.1077	
MRF Run #1	3968.5	3681.2	0.0678	0.0663
MRF Run #2	3276.3		0.0652	
MRF Run #3	3798.9		0.0659	

Table 4-2: Original stiffness Values from BM Southern's study compared with newly acquired values from this study.

	New Stiffness, K $(\frac{lb}{in})$	Original Stiffness, K [11] $(\frac{lb}{in})$	% difference
RUB	2981.3	2265	31.6
STE	4450.5	4855	8.69
MRF	3681.2	2806	31.2

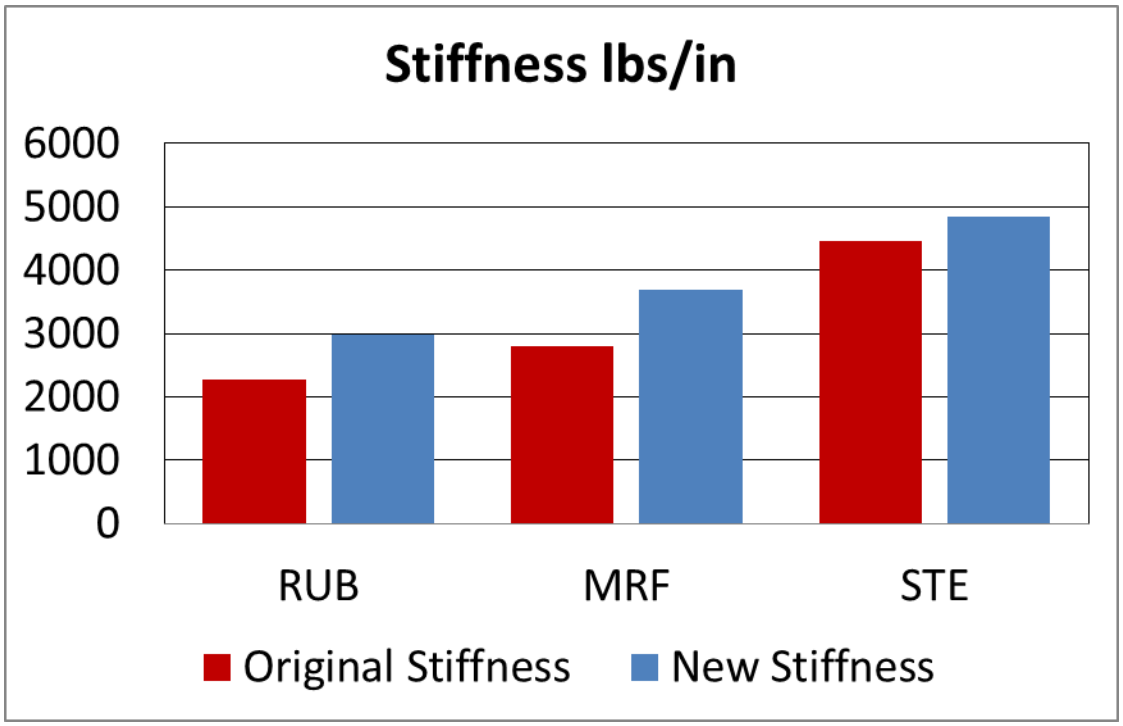

Figure 4-4: Stiffness value, k, comparisons from BM Southern's study (red) and the values found in this study (blue) for each mount tested in this study

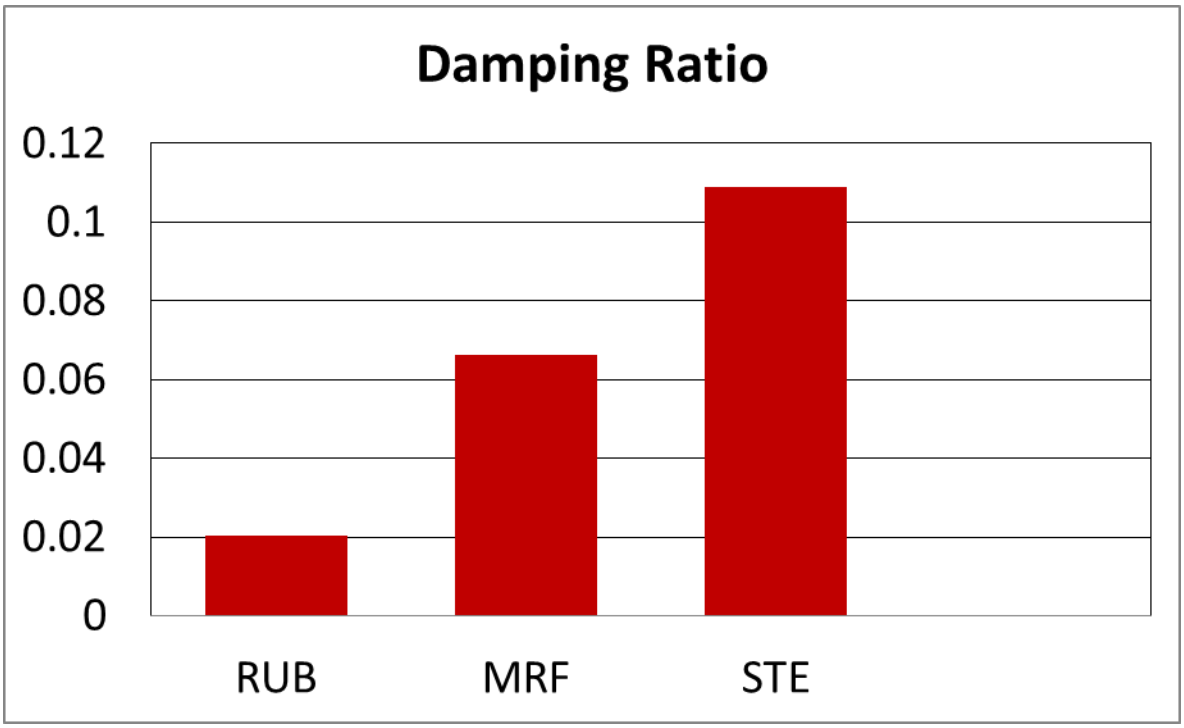

Figure 4-5: Damping ratio values, ζ, shown for each mount tested in this study

4.2 |Dynamic Test Results

4.2.1 Validation Results

In order to confirm the transmissibility and frequency domain analysis techniques, the natural frequency and damping ratio values were plugged into equation 2.7 from the previous chapter to model results from both the baseline testers as well as the MR mount. When compared to the actual plots for transmissibility, the natural frequency and damping values were confirmed. Having done this for multiple plots and for multiple mounts indicates that the plots confirm the legitimacy of the frequency domain analysis technique with which the data for this test was analyzed. Shown below are the confirmation plots.

To ensure continuity and repeatability of test results, each dynamic test was run a total of 5 times. In order to eliminate the effects of external factors and of extended periods of testing, the tests were run with similar environmental conditions and the test runs were spaced out.

As is observed from all three sets of results below, the tests confirm that the system parameters determined from the QST, when plugged into the model, substantiate the values that were received independently from the dynamic tests for multiple independent testing subjects. Although all three plots match the model for their mount fairly well, the MRF and STE show better tracking of the theoretical model waveform than the RUB mount.

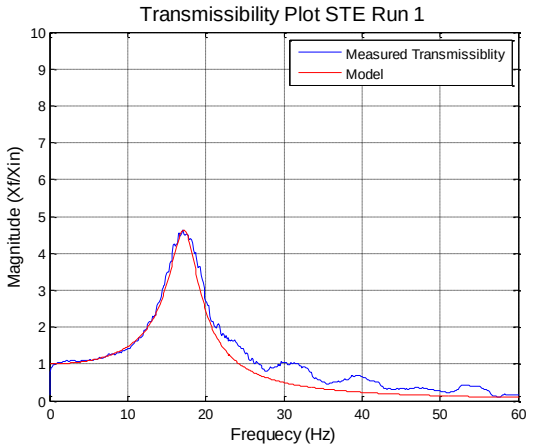

(a)

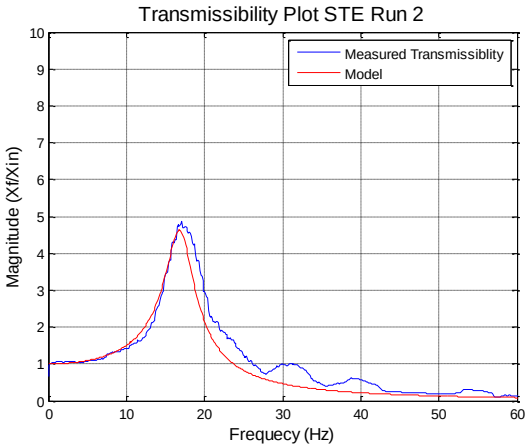

(b)

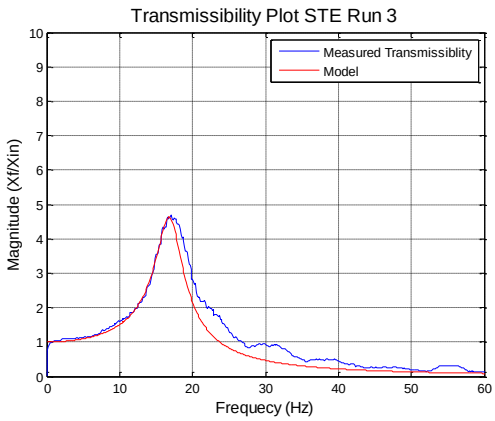

(c)

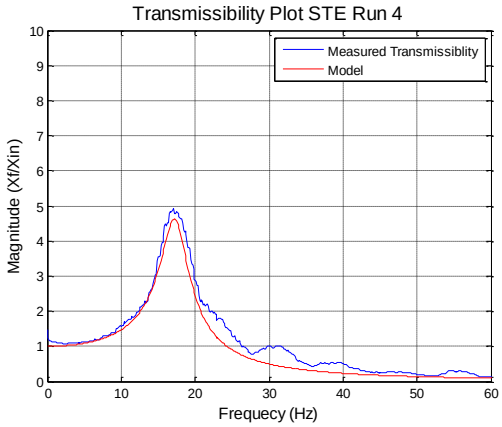

(d)

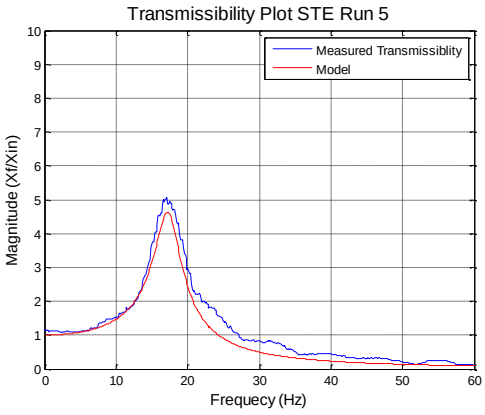

(e)

Figure 4-6: Transmissibility plots of STE (blue) plotted with Model for STE overlaid (red).

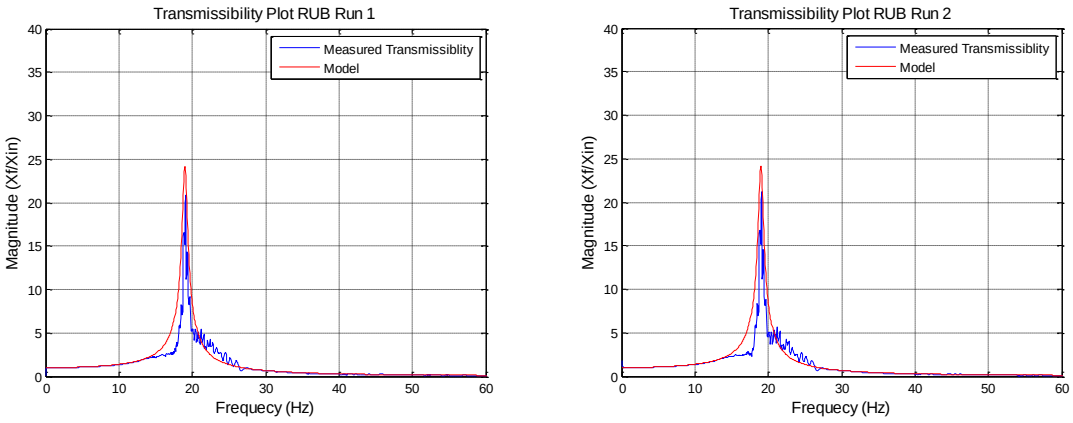

(a)

(b)

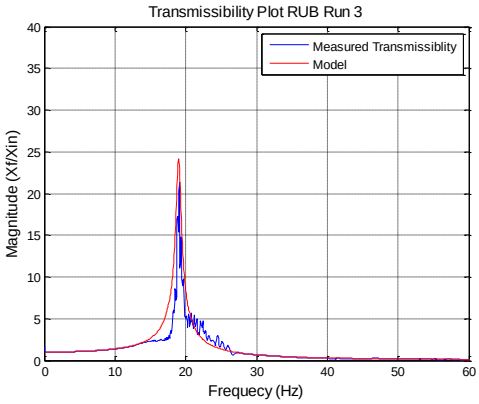

(c)

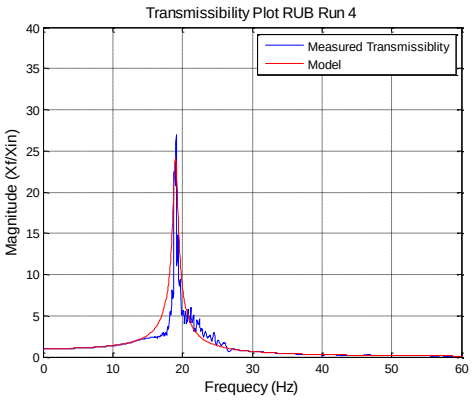

(d)

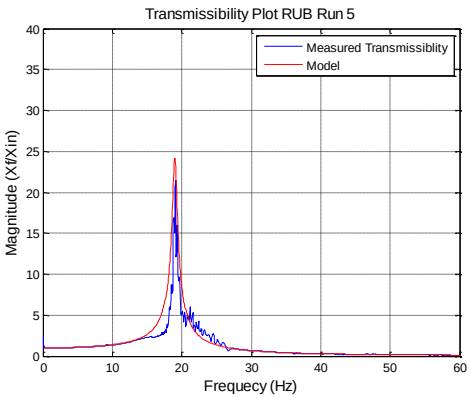

(e)

Figure 4-7: Transmissibility plots of RUB (blue) plotted with Model for RUB overlaid (red).

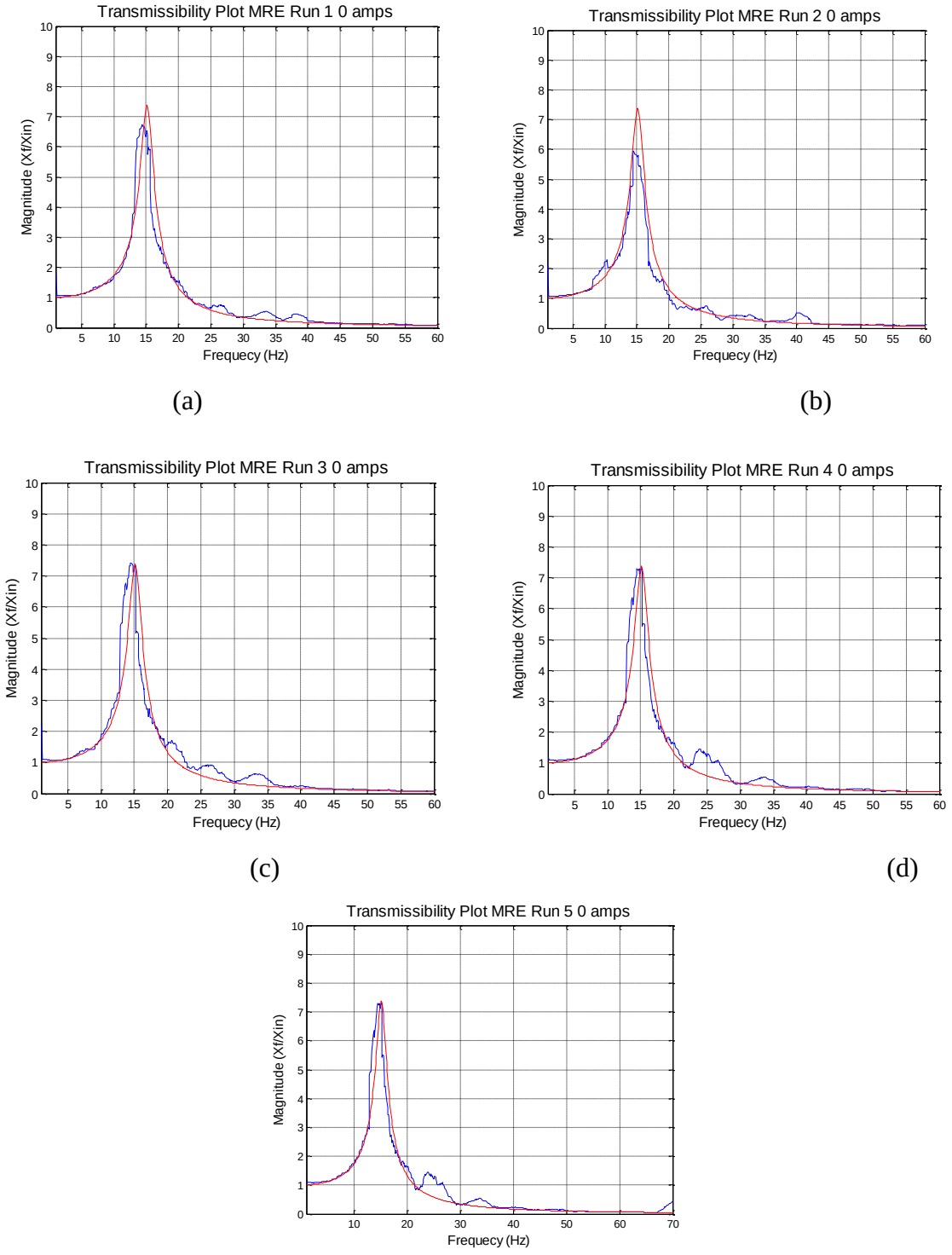

Figure 4-8: Transmissibility plots of MRF (blue) plotted with Model for MRF overlaid (red).

4.2.2 Presentation of Results: MRF mount dynamic tests

With all of the validation conducted and the frequency domain methods confirmed, this section presents the results of the dynamic testing conducted in this study. This section presents the results grouped by how the data was taken in order to be able to identify trends that may have shown up. The testing was bunched into 2 groups. The first 2 sets of tests ran the mount all the way through the entire current range sequentially from 0 amps to 2 amps using 0.2 amp increments. The last 3 sets were organized by input current to the electromagnet, holding the current constant and running the mount through the test 3 times in a row before incrementally increasing the current by 0.2 amps from 0 amps to 2 amps. A detailed justification for this is found below.

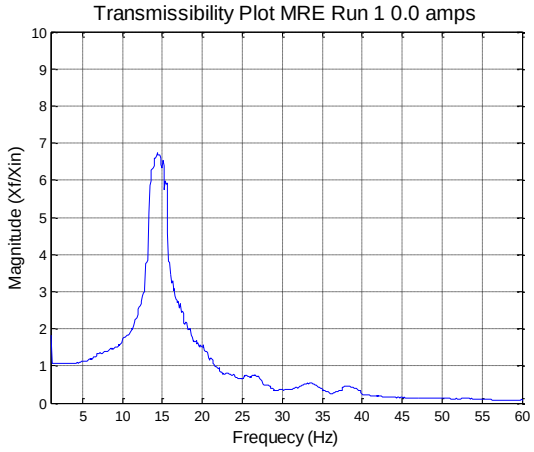

(a)

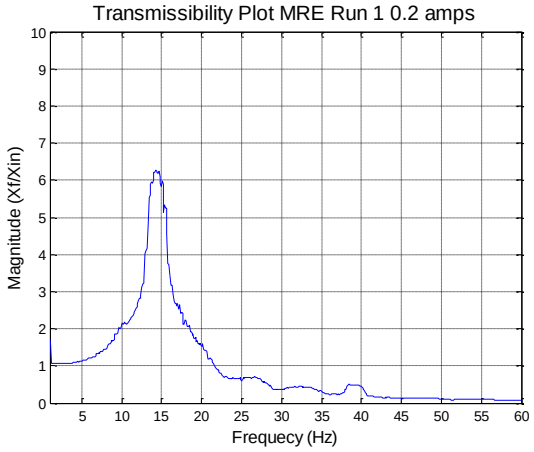

(b)

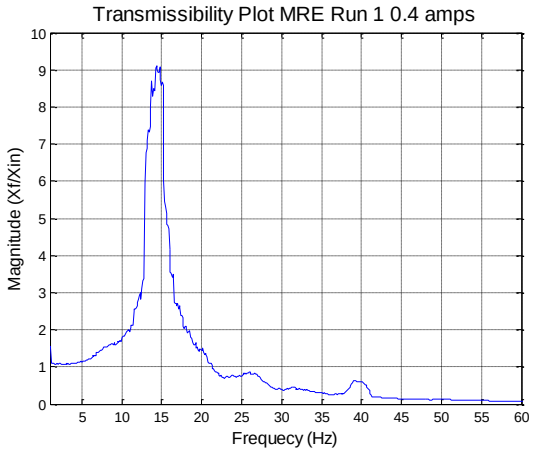

(c)

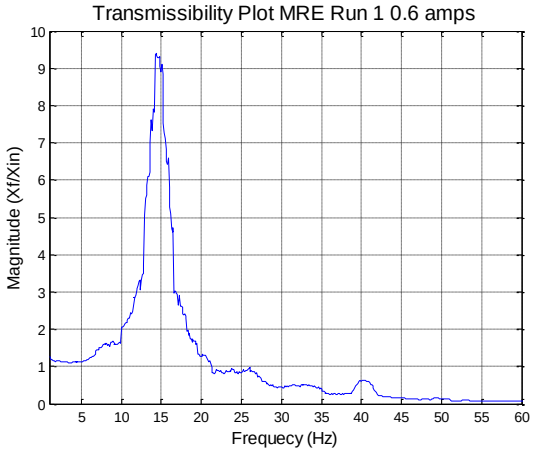

(d)

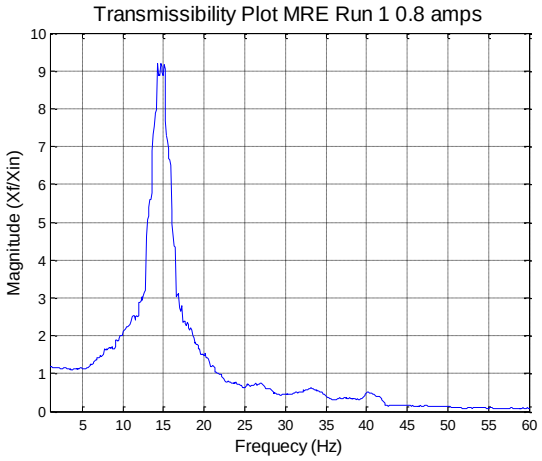
Transmissibility Plot MRE Run 1 0.8 amps
Magnitude (Xf/Xin)
Frequecy (Hz)

(e)

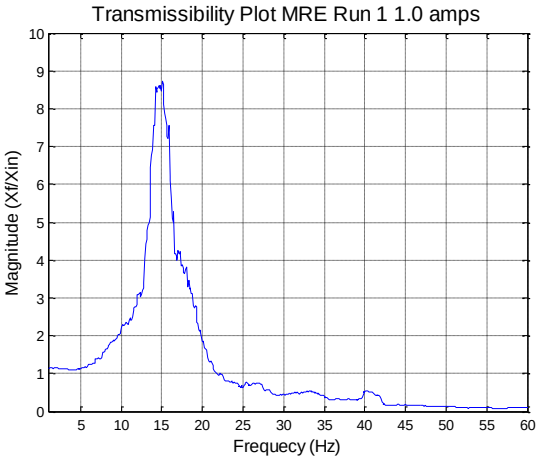
Transmissibility Plot MRE Run 1 1.0 amps
Magnitude (Xf/Xin)
Frequecy (Hz)

(f)

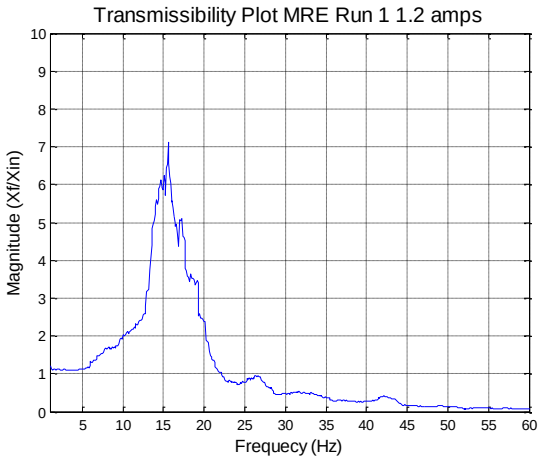
Transmissibility Plot MRE Run 1 1.2 amps
Magnitude (Xf/Xin)
Frequecy (Hz)

(g)

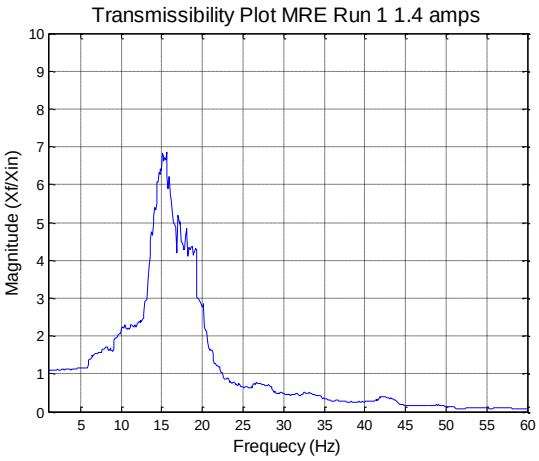
Transmissibility Plot MRE Run 1 1.4 amps
Magnitude (Xf/Xin)
Frequecy (Hz)

(h)

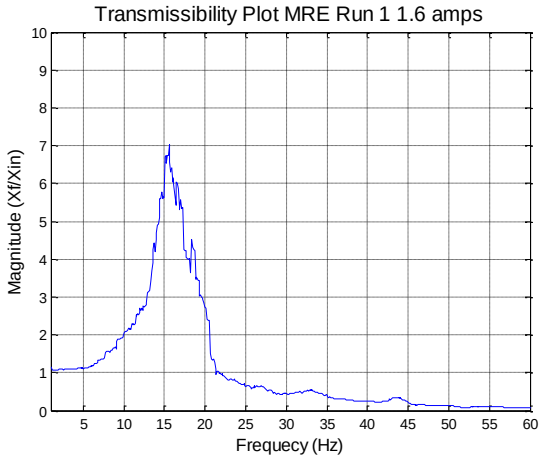
Transmissibility Plot MRE Run 1 1.6 amps
Magnitude (Xf/Xin)
Frequecy (Hz)

(i)

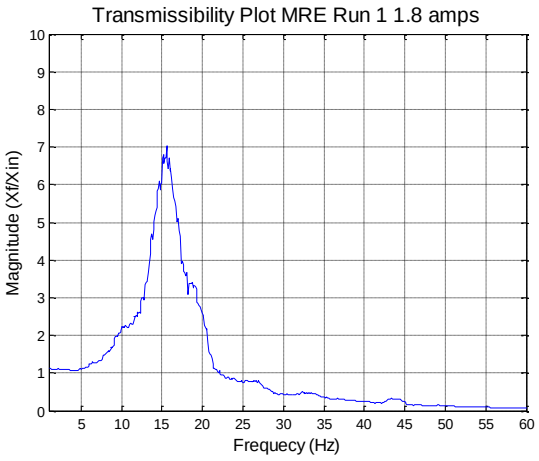
Transmissibility Plot MRE Run 1 1.8 amps
Magnitude (Xf/Xin)
Frequecy (Hz)

(j)

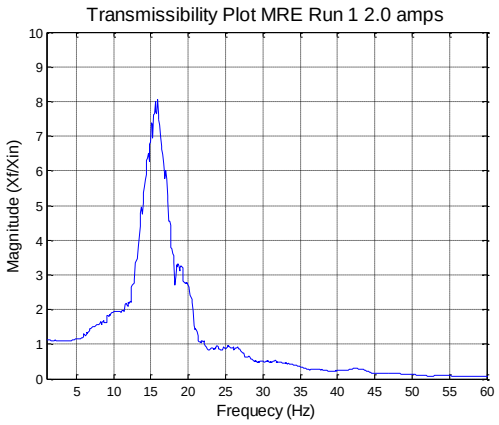

(k)

Figure 4-9: Transmissibility Plots for MRF mount for 1st test run shown from 0.0 amps to 2.0 amps

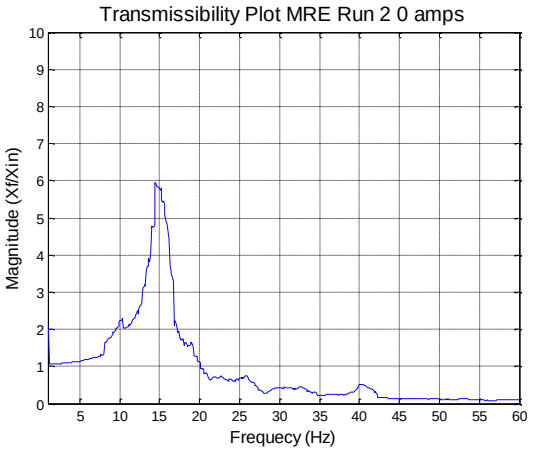

(a)

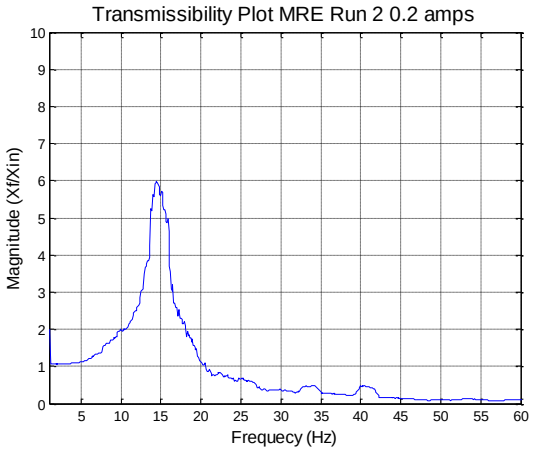

(b)

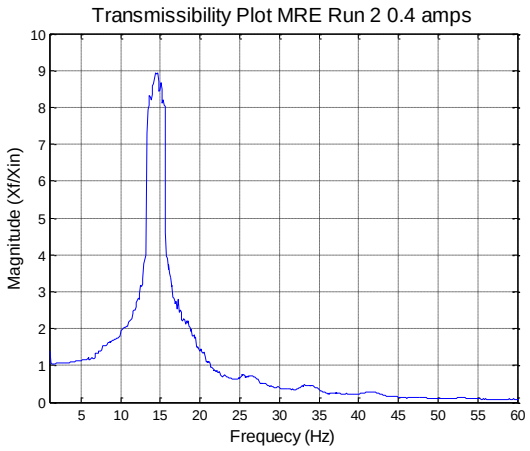

(c)

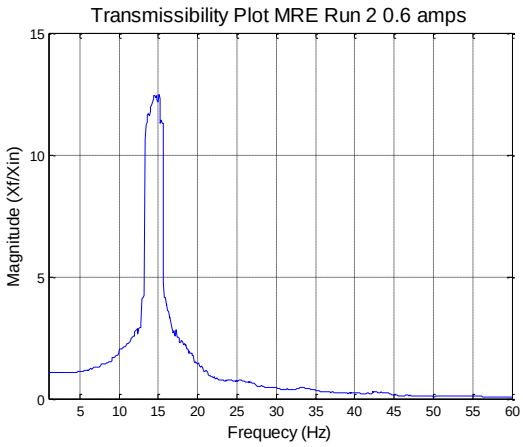

(d)

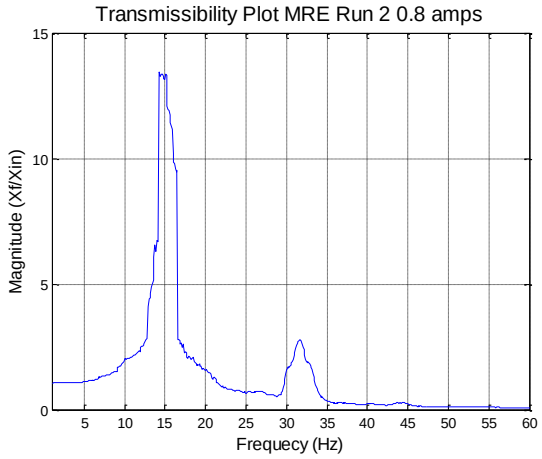
Transmissibility Plot MRE Run 2 0.8 amps
Magnitude (Xf/Xin)
Frequecy (Hz)

(e)

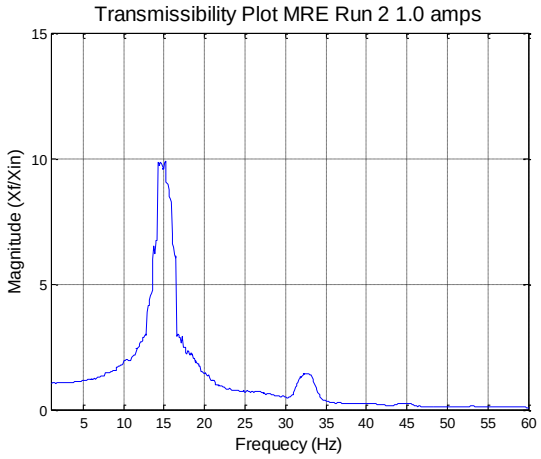
Transmissibility Plot MRE Run 2 1.0 amps
Magnitude (Xf/Xin)
Frequecy (Hz)

(f)

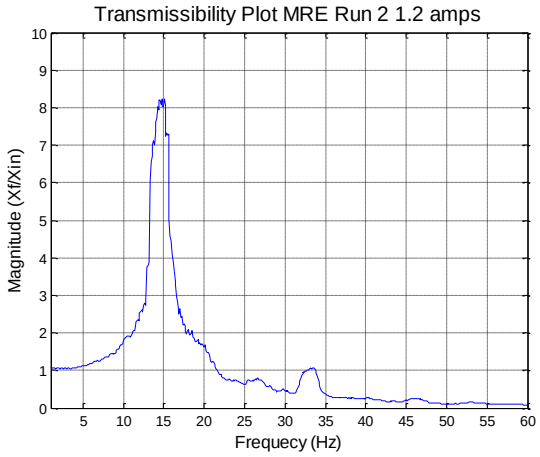
Transmissibility Plot MRE Run 2 1.2 amps
Magnitude (Xf/Xin)
Frequecy (Hz)

(g)

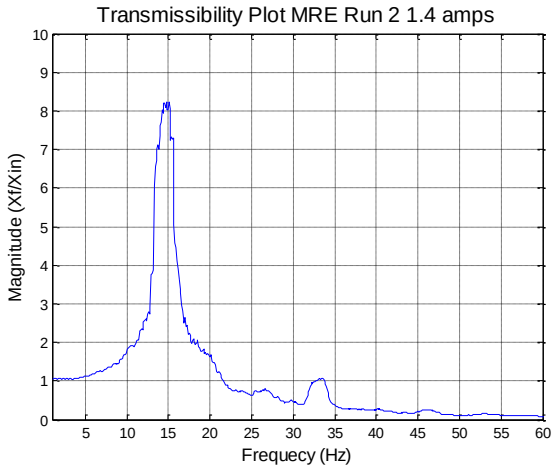
Transmissibility Plot MRE Run 2 1.4 amps
Magnitude (Xf/Xin)
Frequecy (Hz)

(h)

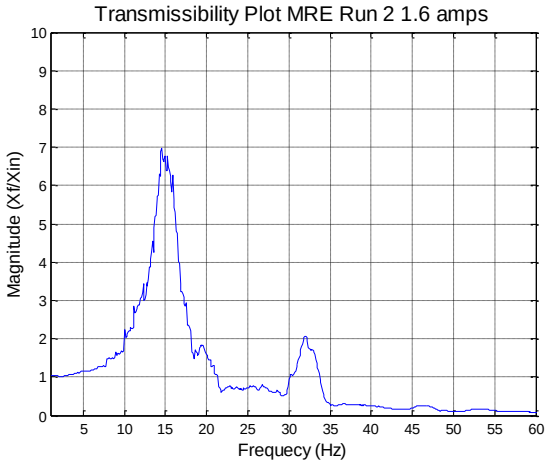
Transmissibility Plot MRE Run 2 1.6 amps
Magnitude (Xf/Xin)
Frequecy (Hz)

(i)

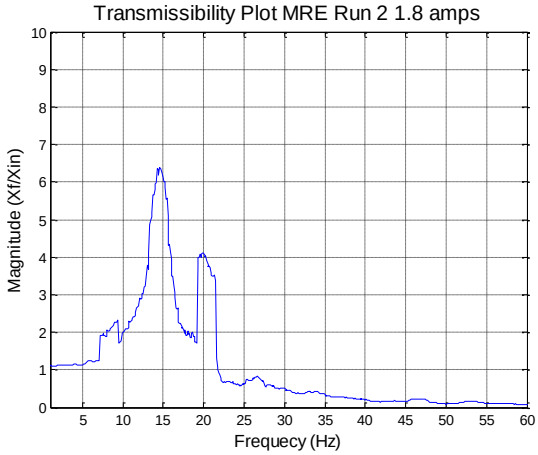
Transmissibility Plot MRE Run 2 1.8 amps
Magnitude (Xf/Xin)
Frequecy (Hz)

(j)

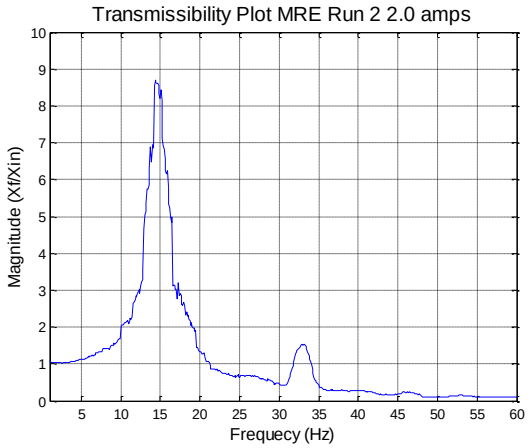

(k)

Figure 4-10: Transmissibility Plots for MRF mount for 2nd test run shown from 0.0 amps to 2.0 amps

The first two sets of test results showed a few obvious trends. For the first test run, when the mount was completely inactivated, the peak transmissibility ratio amplitude was ~ 6 and as the current was increased, the transmissibility increased as well, until between 0.8-1.0 amps where the maximum amplitude occurs. After which the amplitude dipped between 1.0 and1.4 amps before it began to increase again.

These tests were conducted consecutively with minimal zero time. One can see that the first test runs' resulting waveforms appear to be relatively smooth. However, after completing the 2nd set of dynamic tests directly following the first, some odd behavior was noticed. Firstly, the waveform was not nearly as smooth as the first test run. Next, a somewhat similar trend to the first tests was noticed except at a much more exaggerated level in terms of amplitude. Lastly, a second peak appeared at ~33 Hz consistent with the dynamics of a two-degree of freedom system. Despite filtering and smoothing, this 2nd peak was persistent in all but one of the plots, at 1.8 amps, indicating that it was not an outlier but that the mount was behaving this way. This can be seen in figure 4-7.

Having seen this behavior, it was decided to vary the last three data testing procedures in order to observe if leaving a significant amount of time between each magnetization and subsequent dynamic test would still yield the same unexpected behavior or if it would eliminate it. The results of the remaining three test runs are presented below in figures 4-9, 4-10 and 4-11.

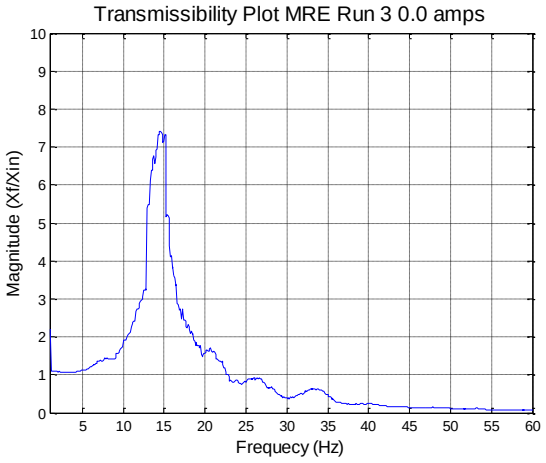
Transmissibility Plot MRE Run 3 0.0 amps
Magnitude (Xf/Xin)
Frequecy (Hz)

(a)

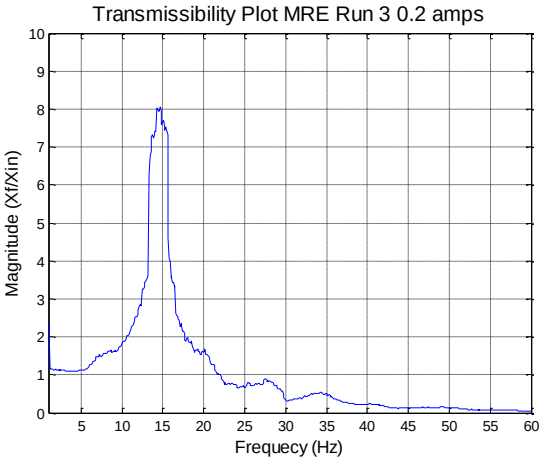
Transmissibility Plot MRE Run 3 0.2 amps
Magnitude (Xf/Xin)
Frequecy (Hz)

(b)

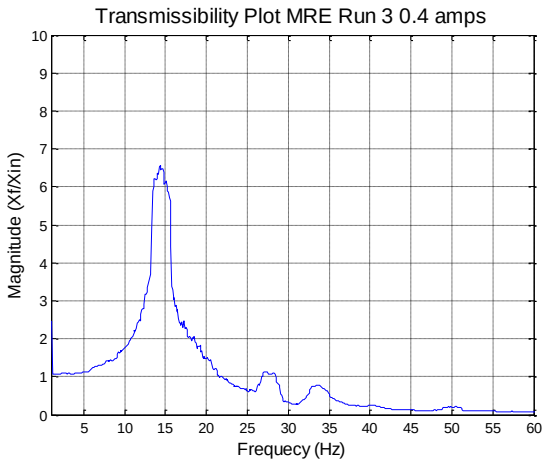
Transmissibility Plot MRE Run 3 0.4 amps
Magnitude (Xf/Xin)
Frequecy (Hz)

(c)

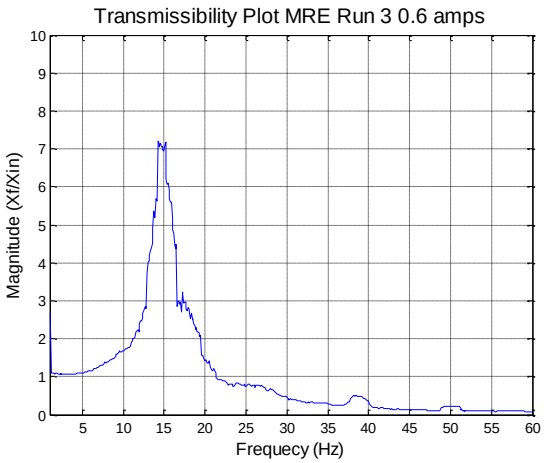
Transmissibility Plot MRE Run 3 0.6 amps
Magnitude (Xf/Xin)
Frequecy (Hz)

(d)

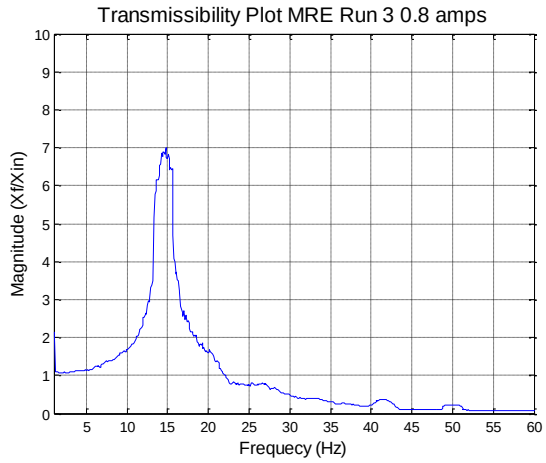
Transmissibility Plot MRE Run 3 0.8 amps
Magnitude (Xf/Xin)
Frequecy (Hz)

(e)

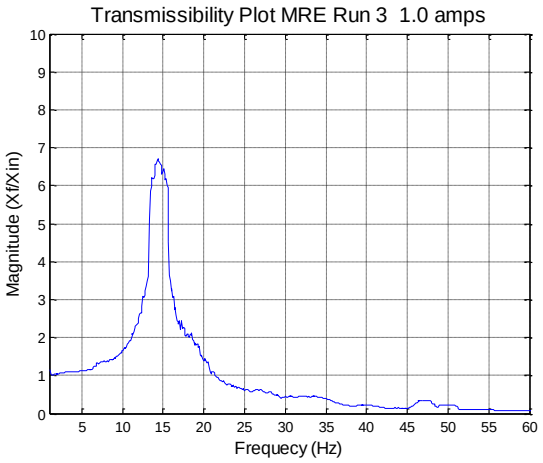
Transmissibility Plot MRE Run 3 1.0 amps
Magnitude (Xf/Xin)
Frequecy (Hz)

(f)

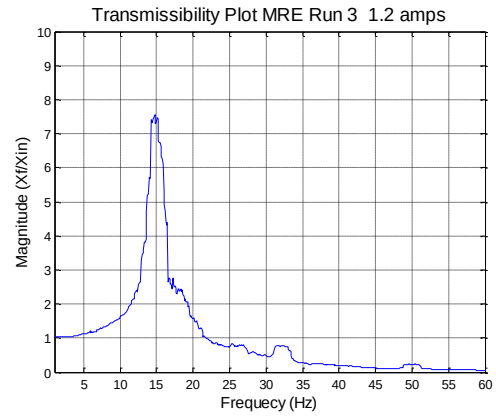

(g)

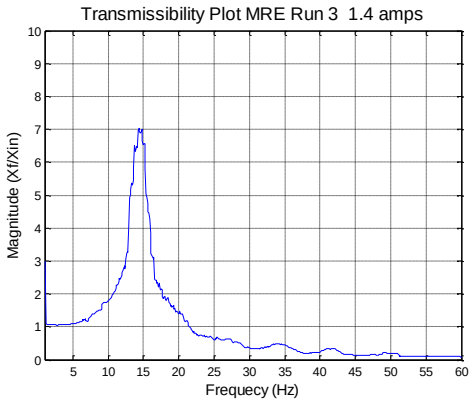

(h)

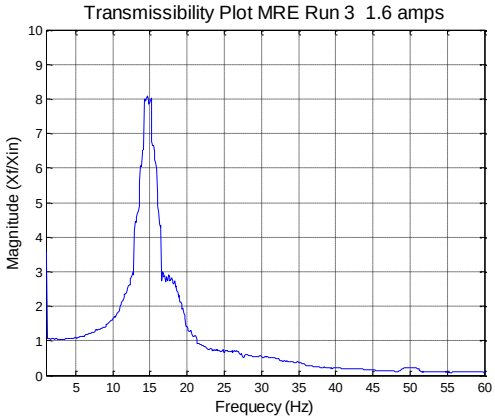

(i)

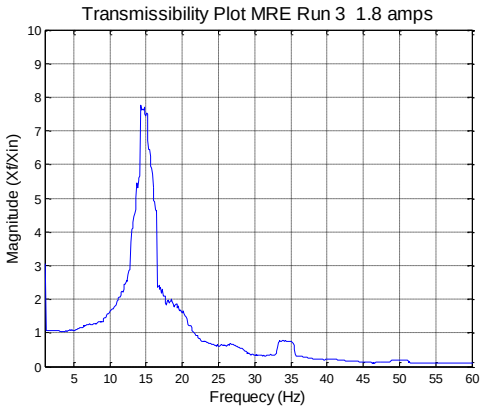

(j)

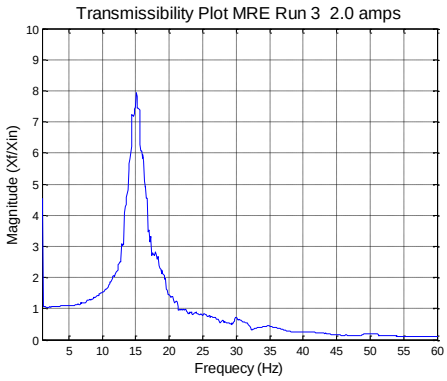

(k)

Figure 4-11: Transmissibility Plots for MRF mount for 3rd test run shown from 0.0 amps to 2.0 amps

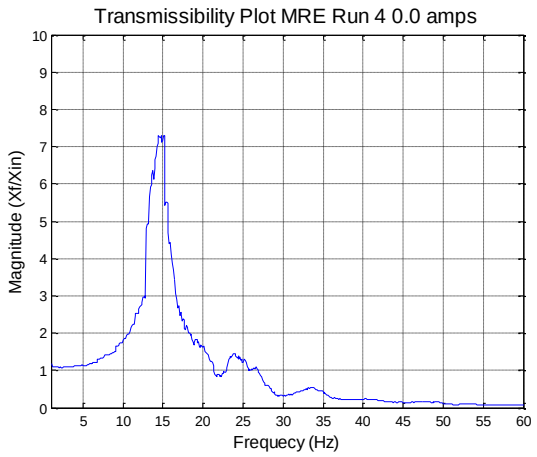
Transmissibility Plot MRE Run 4 0.0 amps
Magnitude (Xf/Xin)
Frequecy (Hz)

(a)

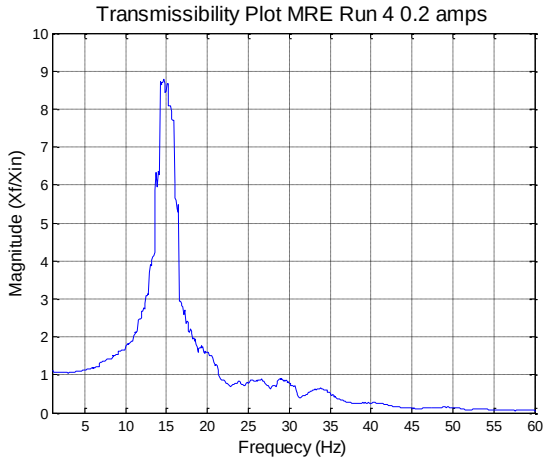
Transmissibility Plot MRE Run 4 0.2 amps
Magnitude (Xf/Xin)
Frequecy (Hz)

(b)

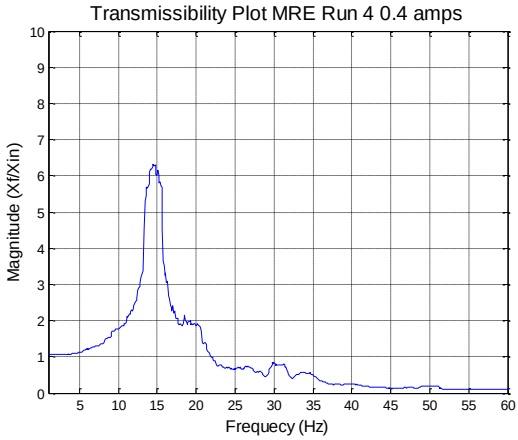
Transmissibility Plot MRE Run 4 0.4 amps
Magnitude (Xf/Xin)
Frequecy (Hz)

(c)

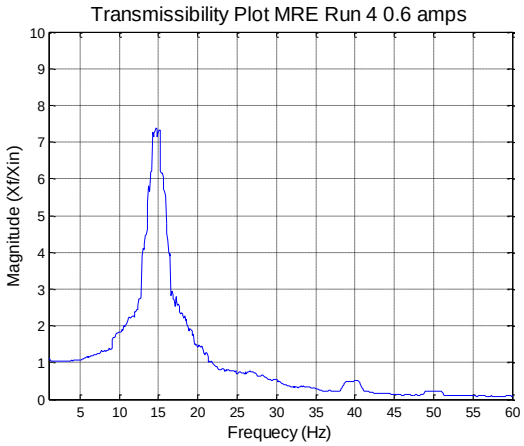
Transmissibility Plot MRE Run 4 0.6 amps
Magnitude (Xf/Xin)
Frequecy (Hz)

(d)

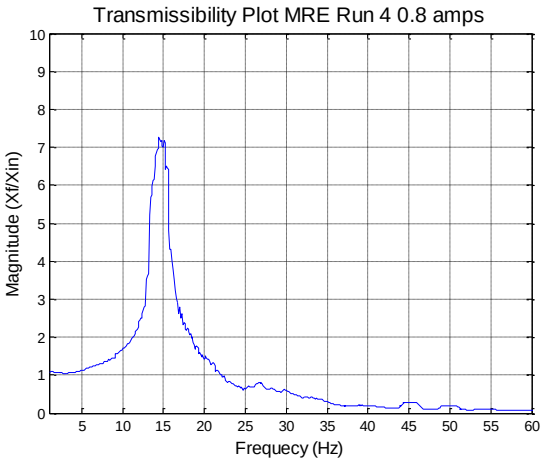
Transmissibility Plot MRE Run 4 0.8 amps
Magnitude (Xf/Xin)
Frequecy (Hz)

(e)

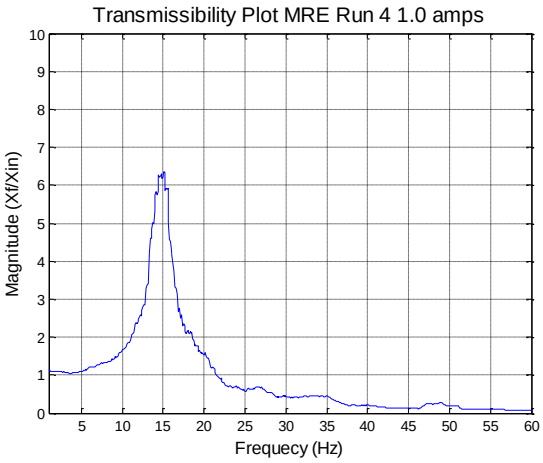
Transmissibility Plot MRE Run 4 1.0 amps
Magnitude (Xf/Xin)
Frequecy (Hz)

(f)

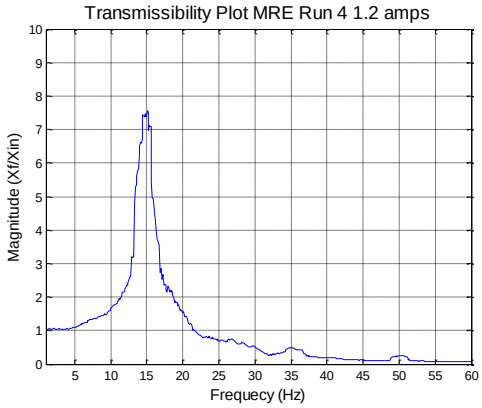

(g)

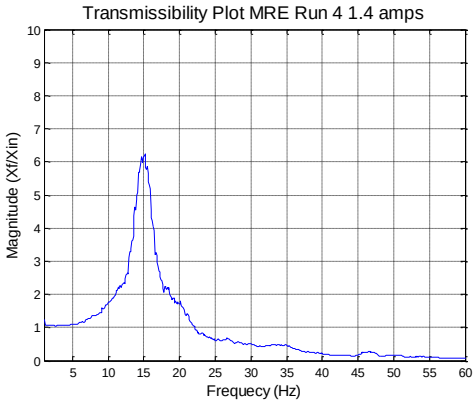

(h)

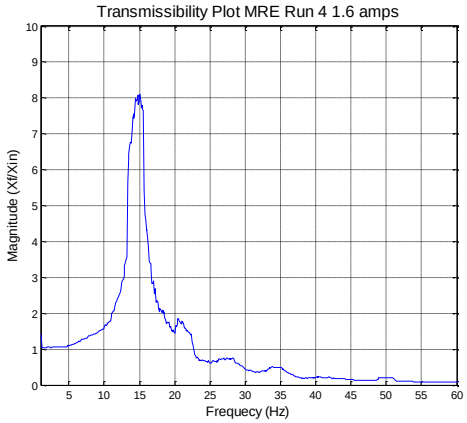

(i)

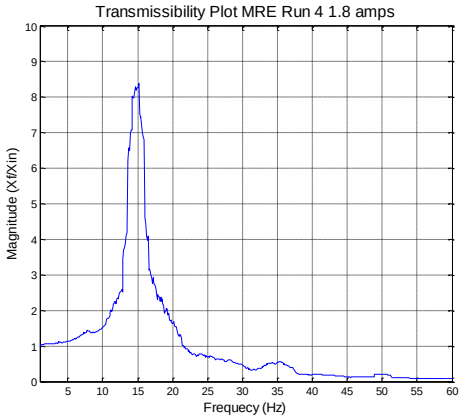

(j)

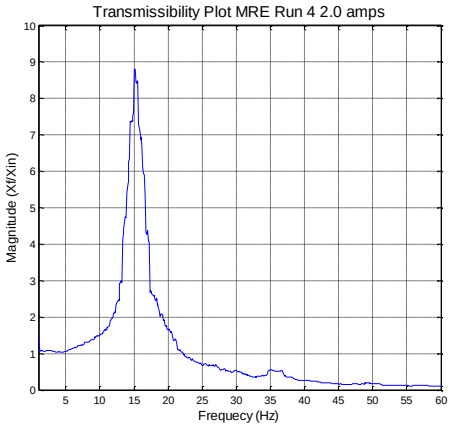

(k)

Figure 4-12: Transmissibility Plots for MRF mount for 4th test run shown from 0.0 amps to 2.0 amps

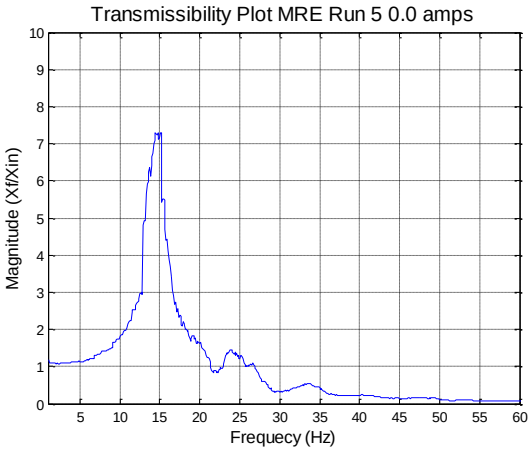
Transmissibility Plot MRE Run 5 0.0 amps
Magnitude (Xf/Xin)
Frequecy (Hz)

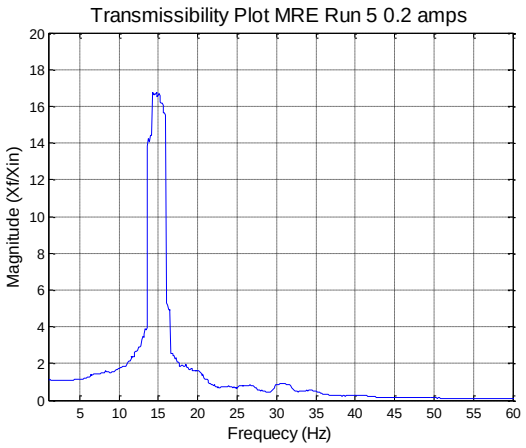
Transmissibility Plot MRE Run 5 0.2 amps
Magnitude (Xf/Xin)
Frequecy (Hz)

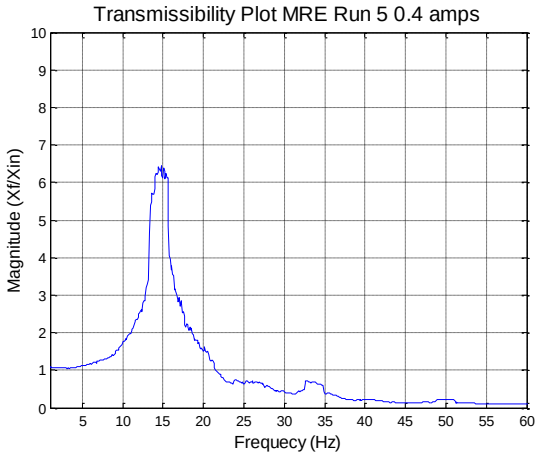
Transmissibility Plot MRE Run 5 0.4 amps
Magnitude (Xf/Xin)
Frequecy (Hz)

(c)

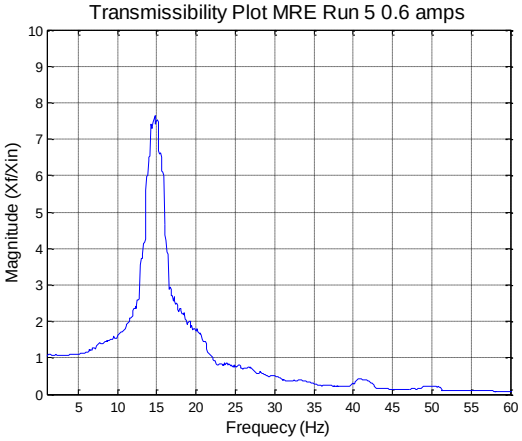
Transmissibility Plot MRE Run 5 0.6 amps
Magnitude (Xf/Xin)
Frequecy (Hz)

(d)

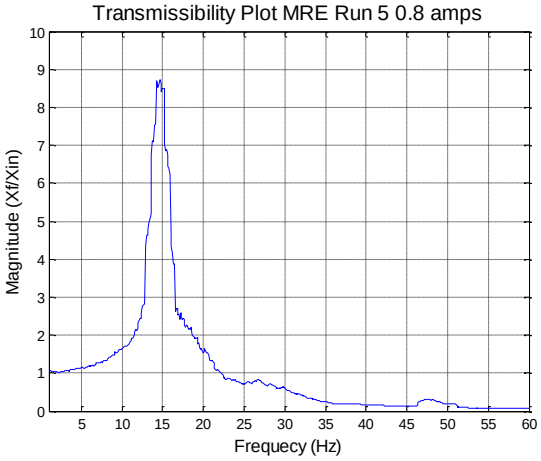
Transmissibility Plot MRE Run 5 0.8 amps
Magnitude (Xf/Xin)
Frequecy (Hz)

(e)

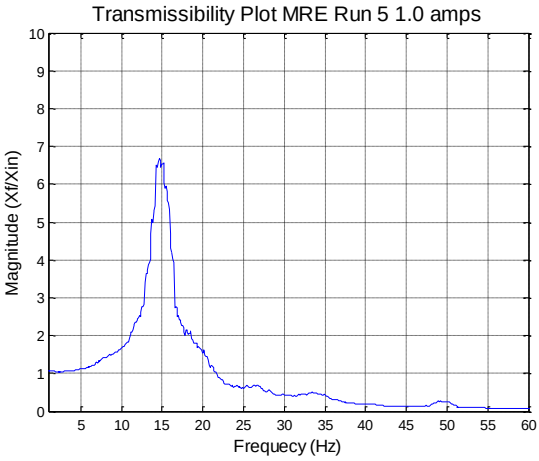
Transmissibility Plot MRE Run 5 1.0 amps
Magnitude (Xf/Xin)
Frequecy (Hz)

(f)

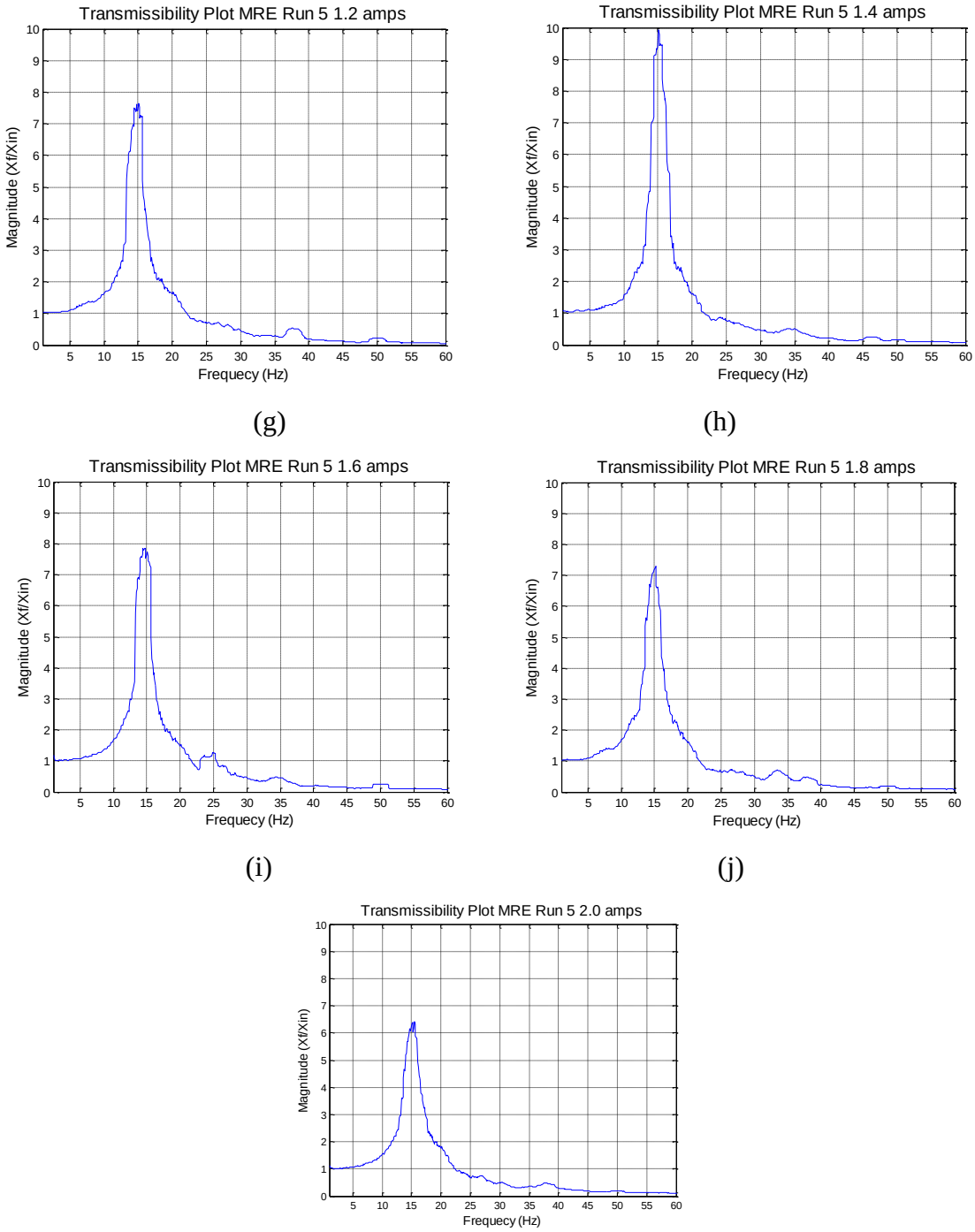

Figure 4-13: Transmissibility Plots for MRF mount for 5th test run shown from 0.0 amps to 2.0 amps

From observing the results of the 3rd, 4th and 5th set of tests, we see that the similar trend of an initial increase followed by a decrease and an eventual increasing trend towards the maximum current value. The 2nd resonance peak that appeared in the data set from the 2nd test run was eliminated and the values subsequent results were consistent and reproducible. A more in depth analysis and comparison is presented in the later sections.

After viewing the results above, it was determined that the 2nd testing Run posed a vast majority of the outliers within this study in comparison with the other 4 test runs. The average standard deviation for the averaged values of the MRF test runs drop from 1.562 to 1.276, an 18.3 % drop, when omitting the 2nd test run data. Thus for the sake of accuracy of the data, the entire data set from the 2nd test run was removed from analysis. This was not found to be problematic as 4 sets of data remained and were adequate for analysis. Having done this will provide a much more accurate and reliable set of final values for making final conclusions within this study.

4.2.3 Presentation of Results: Passive mounts test

The results of the passive mount tests are presented in this section beginning with the RUB mount. The RUB mount exhibited very consistent results throughout the 5 dynamic test runs. There was no significant migration of resonance frequency with an average value of 19.11 Hz and a standard deviation of 0.04. The average value for transmissibility was found to be 22.3 with a standard deviation of 0.259. The largest peak transmissibility value was observed in the 4th test run with a magnitude of 26.93.

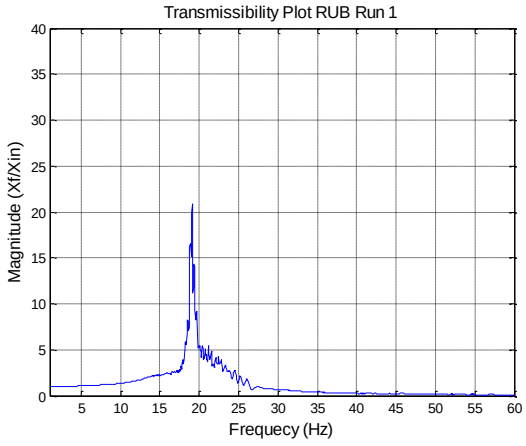

(a)

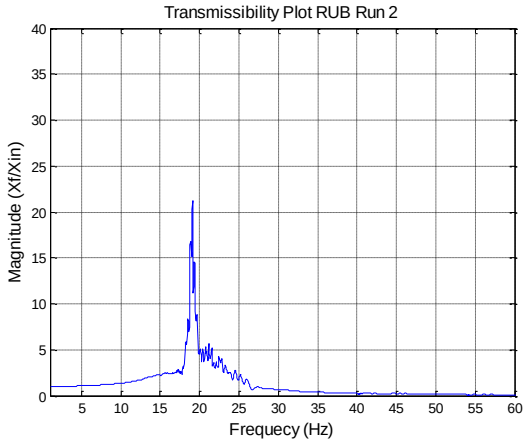

(b)

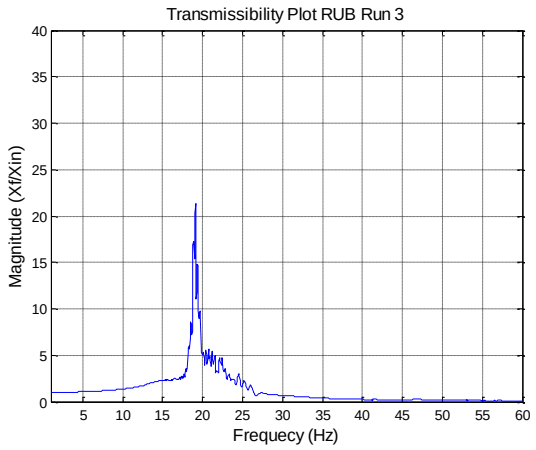

(c)

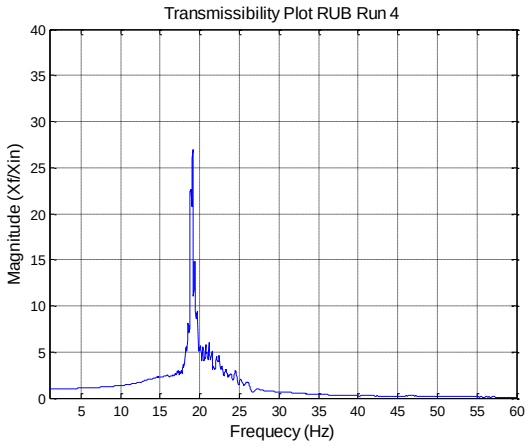

(d)

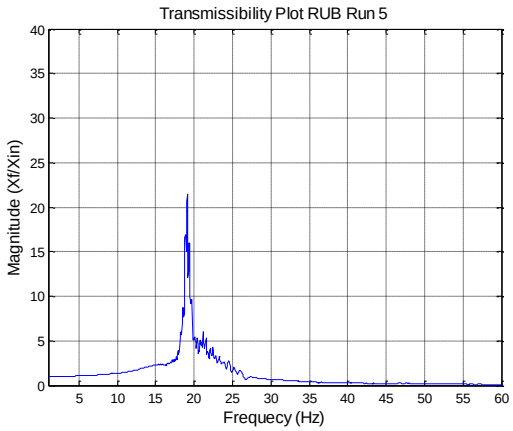

(e)

Figure 4-14: Transmissibility plots for RUB passive mount

For the STE mounts, the results were very similar in nature to the RUB mounts in that they also exhibited very consistent results throughout the 5 dynamic test runs. There was also no significant migration of resonance frequency with an average value of 17.215 and a standard deviation of 0.24. The average transmissibility value was 4.875 with a standard deviation of 0.18. The peak transmissibility was observed in the 5th test run with a magnitude of about 5.073. A complete table of these values is provided in Appendix C.

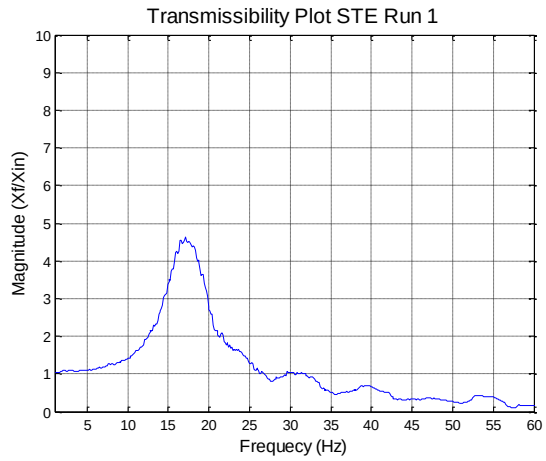

(a)

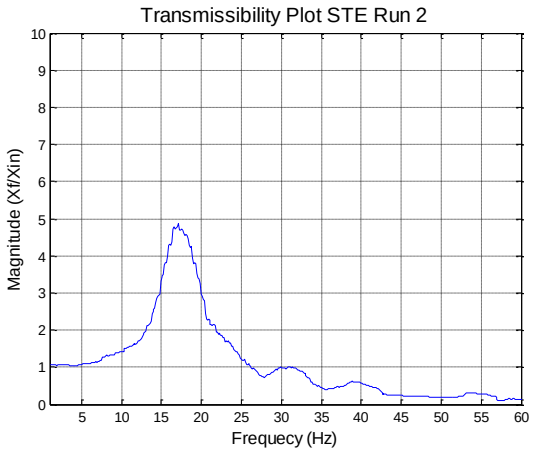

(b)

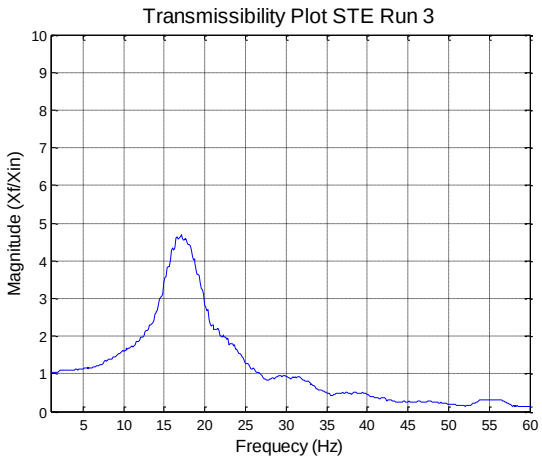

(c)

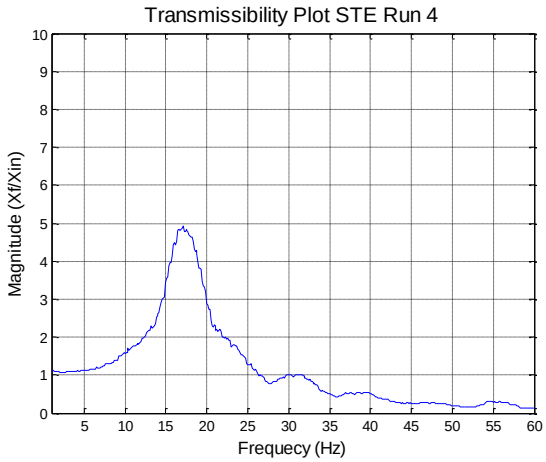

(d)

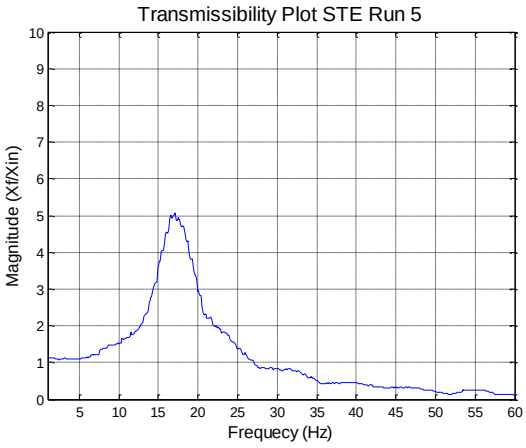

(e)

Figure 4-15: Transmissibility plots for STE passive mount

4.2.4 Summary of Results

These results, as mentioned in the previous section and will be explained in the coming section, do not include data collected from the 2nd test run. The first parameter to observe from a transmissibility plot is the migration of the resonance frequency, ω_n. As expected, all of the resonance frequency values were observed as increasing with increase of supply current and subsequently, the stiffness of the mount. An average increase of 11.04% was observed with a 1.55 Hz frequency differential. The Largest increase in resonance frequency was observed from Run 1 with a 13% increase showing a move of 1.83 Hz. Conversely, the smallest observed frequency percentage and differential was from Run 4 with 9.2 % and 1.33 Hz respectively. The adequacy of these results is based on application, however we see a great deal of promise from this result.

Table 4-3: Average resonance frequency values from 0 amps to 2.0 amps

Supply Current (Amps)	Average ω_n values Excluding Run #2 (Hz)
0	14.08
0.2	14.21
0.4	14.37
0.6	14.60
0.8	14.75
1	14.83
1.2	15.11
1.4	15.26
1.6	15.31
1.8	15.46
2	15.64

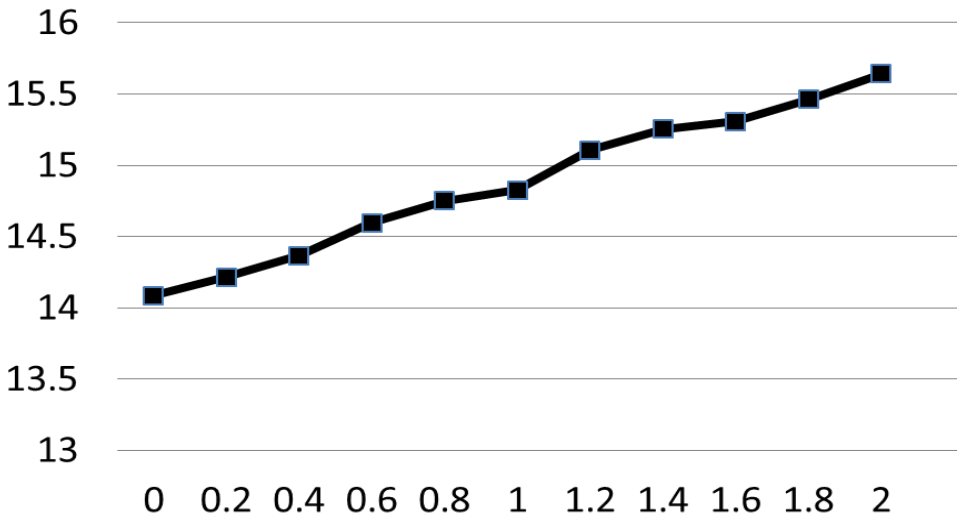

Figure 4-16: Average values of peak resonance values for MRF mount over 5 test sets plotted against current level of electromagnet

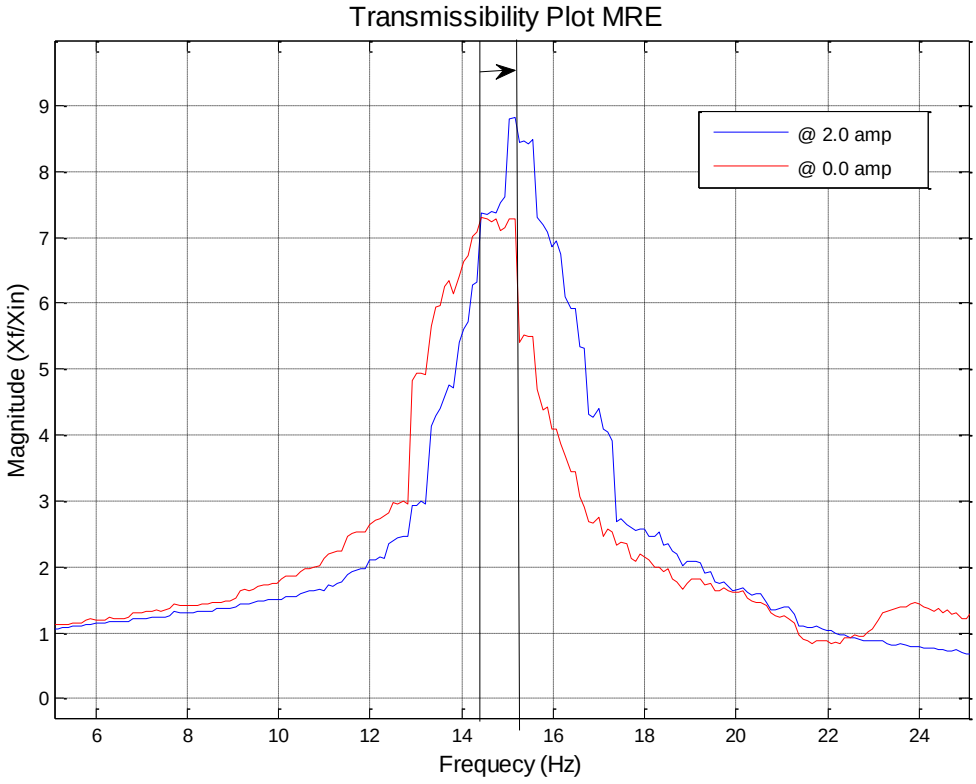

Figure 4-17: Lowest observed resonance peak at 0.0 amp (red) compared with highest observed resonance peak @ 2.0 amp (blue)

The second and arguably more important parameter to observe from a transmissibility plot is the change in the magnitude of transmissibility. A similar trend was observed from each of the test run data sets. As is apparent from figure 4-14 below, this trend showed an increase in peak transmitted displacement initially as the electro-magnet was activated, however a significant dip in peak transmitted displacement occurs at ~1 amp current before returning to an average peak transmissibility ratio of about 7.75.

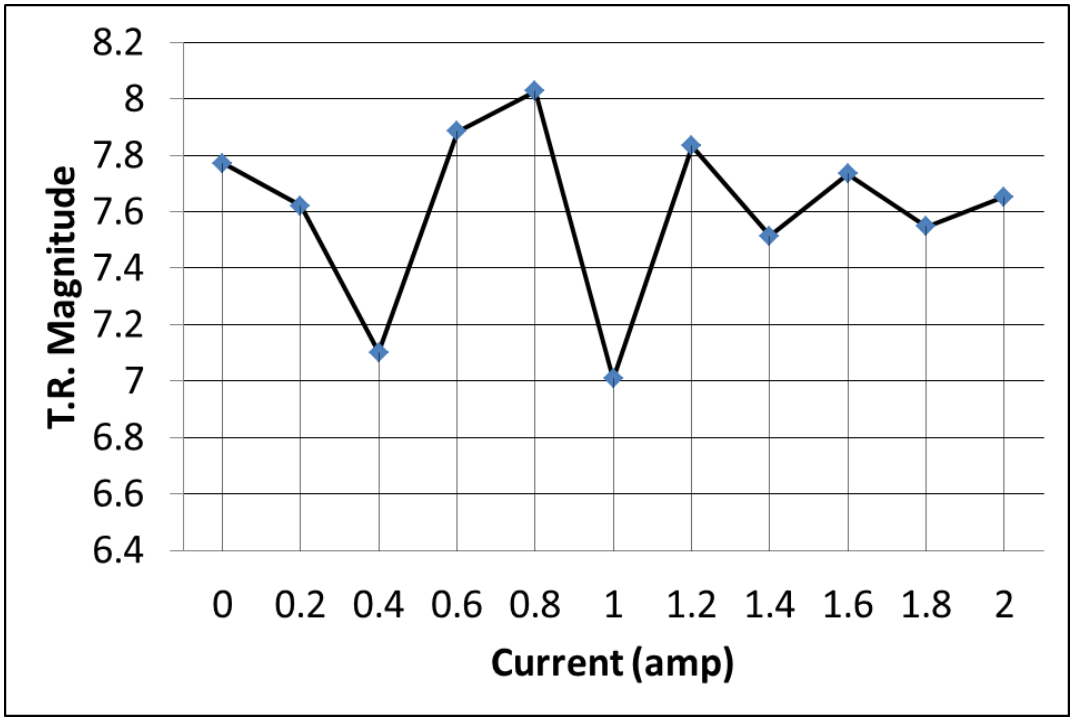

Figure 4-18: Average values of Transmissibility of MRF mount over 5 test sets plotted against current level of electromagnet

The largest average magnitude transmitted was at 0.8 amps, with 8.03 and the peak transmissibility magnitude was observed at 1.4 amps of current on Run 5 with a magnitude ratio of 9.92. The lowest average value of 7.01 was found at 1.0 amp. One thing to note is that although it appears to go against logic, there are points where the transmissibility drops despite increase in current. This phenomenon is due to the fact that the ratio is actually a ratio of stiffness to natural frequency, and thus the stiffness. Although both values may increase, the rate of increase may differ and as such, the ratio my spike or dip depending on what the values are at which point in the test.

Table 4-4: Average values for peak magnitude between 0 amps and 2.0 amps

Supply Current (Amps)	Average Peak Magnitude Values Excluding Run #2
0	7.77
0.2	7.62
0.4	7.10
0.6	7.88
0.8	8.03
1	7.01
1.2	7.83
1.4	7.51
1.6	7.74
1.8	7.55
2	7.65

The second part of the evaluation is a comparison between the passive mounts in this study and the active mounts that were designed. The RUB mount was supposed to simulate a lower limitation below an active metal elastic mount.

The STE mount was intended to serve a similar purpose but with values that were not attainable in the upper limit due to the fluid's inability to act as a true solid. In addition, due to the lack of solid core mounting platforms in application, the performance of the MRF mount was not compared to the STE mount.

The MRF mount's performance was only compared to the RUB mount's performance as it also represents a passive elastomeric mount of similar dimensions and for use in similar applications. As was indicated above, the MRF mount's average peak transmissibility never exceeded a magnitude of 8.03 (@ 0.8 amps) while the average magnitude value for the RUB mount was more than double that, at 22.3. Thus, the active MRF mount, at its worst, a 59.24% decrease in transmissibility over the passive RUB mount. At its best, the MRF mount saw a 68.58% decrease in transmissibility over the RUB mount. However, due to the much lower stiffness

levels of the RUB mount as well as the lower preload, the resonance frequency was much higher than its MRF counterpart.

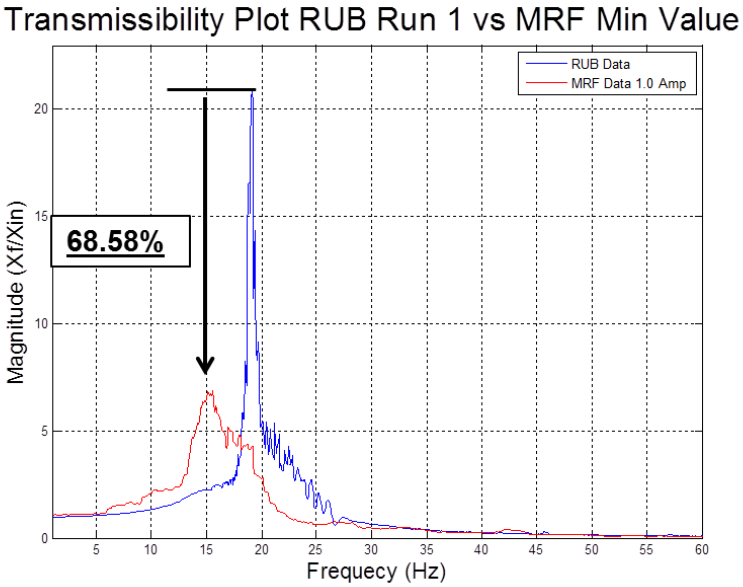

(a)

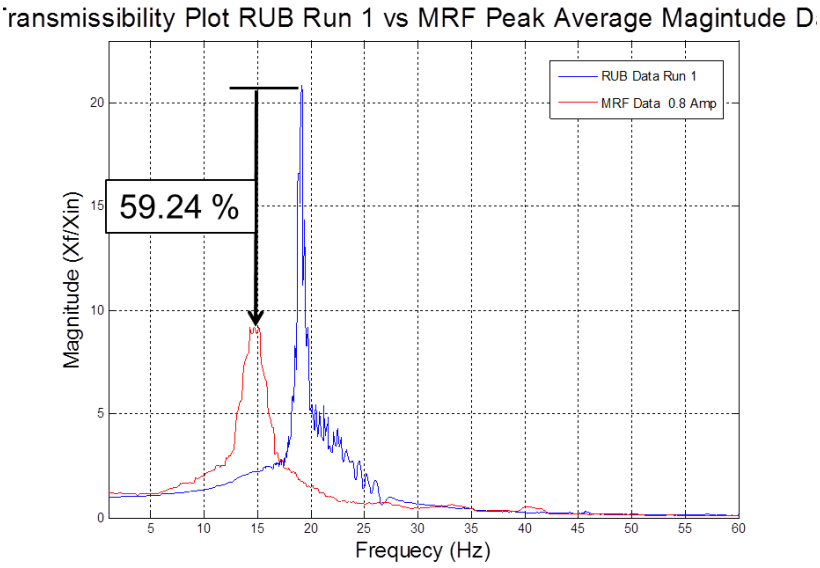

(b)

Figure 4-19: Comparison transmissibility plots (a) of RUB run 1 vs. lowest observed transmissibility ratio of MRF at 1.0 amp. and (b) highest observed transmissibility ratio of MRF at 0.0 amp

A more complete set of tables with all of the values can be found in Appendix C.

4.3 |Conclusions and discussion

4.3.1 Quasi-Static Test (QST)

Two conclusions can be drawn from the QST results. The first conclusion is that over 4 years' time, the RUB and STE mounts' properties changed significantly. One cause of this may have been the prolonged storage and inactivity of the mount. Another possible cause of this may have been the testing that the mounts were subject to. The mounts were tested thoroughly by BM Southern and they were also tested fairly strenuously for this study. Another possible cause of this change in properties is the RTV polyurethane rubber itself. 4 years of storage in an uncontrolled environment where heat, cold, and humidity conditions were neither monitored nor controlled may have had an effect after prolonged exposure. These and other factors contributed to a 31% and 9% increase in stiffness for the RUB and STE mounts respectively.

The second conclusion that can be drawn from the QST was the fact that the newly designed mount proved to be much more resilient than the previous mounts. Even under QST and low frequency sinusoidal dynamic testing during BM Southern's study, one of the initial MRF design mounts failed. However, there was a drastic change in the stiffness and damping properties with a dramatic increase in stiffness of about 30% and almost 1000 lb/in, as was shown in earlier sections. However, even with this change in design, the mount still required minor repair after the final dynamic tests because of initial signs of failure.

(a) (b)

Figure 4-20: Failed Mount from BM Southern's Quasi-Static Test [11](a) and failed mount from the dynamic test in this study (b)

Although the designs and materials first used by Wang et al., and improved upon by York et al. and BM Southern, appeared to be ideal for static applications. However, when put through dynamic testing, they were not adequately designed and require further development.

4.3.2 Dynamic Tests

The results of the dynamic tests point to a few different conclusions. The first and most important of which is that the MRF active mounts are effective at mitigating vibrations from a base excitation input. When compared to a rubber mount of similar dimensions and for use in similar applications, the MRF mount out- performed drastically. Even when employed passively and without magnetic field present, it still performed much better than the RUB due to its higher inactive stiffness and damping values. This shows that a passive Metal-Elastic mount of the same dimensions but filled with a fluid of the same viscosity as inactive MRF-122 would provide much better damping than a simple rubber mount. Such a mount would be a potential next in line subject for establishing baseline properties and future comparison

When activated, the mount's properties changed with the electromagnet's increasing influence. It was found that peak attenuation of input vibrations was seen most prominently when there was 1 amp of current input to the electromagnet. When employed semi-actively, this would prove an ideal operating point for the mount if similar mass and input vibration conditions were present. With ~60% decrease average transmissibility and ~70% observed at 1.0 amp, this proves a very promising advance in mounting technologies.

The fact that the resonance peak decreases despite the increase of stiffness due to the magnetic field appears to be against logic. This occurs, however, because the increase in stiffness and subsequently, the natural frequency, is not proportional to the increase in damping, and thus, from one current level to the next, the damping ratio may increase or decrease depending on the ratio of the increase in stiffness to that of the equivalent damping.

Also promising is the amount of resonance frequency migration that was observed. With an average of 1.33 Hz, or ~11% migration, we see the possibility of developing a control system that could potentially allow the mount to subdue the peak transmissibility completely. By quickly changing the properties of the mount at the proper times, the resonance points could be drastically reduced if not avoided completely. This change of magnetic field over time could prove to be another interesting point to investigate.

As was noted earlier, the data from the second test run of the MRF dynamic transmissibility tests was omitted from analysis due to a prominent existence of outliers. In fact, it caused the standard deviation of the 5 test runs to almost double for about half of the current level tests and it caused the overall standard deviation to grow by nearly 22 percent. The causes of this are not certain but the results point to a phenomenon being characterized by a few researchers in the field called clumping. Basically, this "clumping effect" occurs when MR fluid is exposed to higher current levels for an extended period of time. When clumping becomes evident, the iron particles in the fluid become trapped in the chains that were formed under magnetic field.

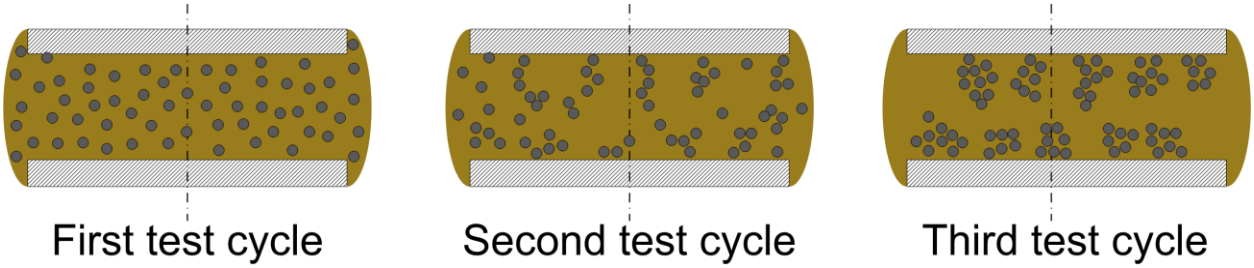

Figure 4-21: After multiple cycles, clumping can become evident in some cases, adapted from [56]

Therefore when the magnetic field is taken away, the carrier fluid is able to move freely but some of the chains of particles cannot. This effect was studied heavily by A. Farjoud et al. The main tell of the clumping effect is a drastic increase of both force and displacement transmission through the fluid and thus produce unexpected stiffness and damping values [56] much like the ones observed in the results of this study. For this reason, the 2nd run of the dynamic testing was omitted and the testing process was changed so that the likelihood of this happening wouldn't be as large.

To summarize the results, we found a ~60% decrease in transmissibility observed peak resonance and a 70% observed at 1.0 amp. We also found an average of 1.33 Hz, or ~11% positive migration of resonance frequency over the range of input current to the electromagnet. In conclusion, these results are indicative of the potential that these MRF mounts have to become prominent in active and semi-active vibration suppression technology. Their ability to attenuate input vibration and migrate resonance frequency show that these mounts, although still yet to be fully developed and understood, perform very well and show much promise.

Chapter 5 |Summary and Recommendations

This chapter is the culminating chapter of the research study. The first section begins by briefly summarizing every step taken in this study and a brief presentation of the results and conclusions. The second and final section begins by mentioning some recommendations that the author has for making the study more complete as well as suggesting ideas for future work involving the development and characterization of the MR mounts examined in this study.

5.1 |Summary and Conclusions

This section broadly summarizes the many steps taken in this study beginning with the major objectives, the objectives delivered upon and the conclusions for the research. After an extensive literature review, the objectives were then completed.

The first chapter served as a brief overview and guide to the remainder of the thesis. It began by providing a background section featuring the history of vibration isolation and absorbers and their uses in current applications. It then turned the discussion to magneto-rheological fluid and their potential uses in tunable vibration absorbers. Next, a section was presented that lists the deliverable objectives of this research study and the driving factors that inspired the pursuit of these goals. The approach section discussed the method by which the objectives are achieved. An outline section laid out the organization of the chapters in this document. And finally, a contributions section highlighted what contributions this work will be making to the field of development of tuned vibration absorbers.

The first chapter acted as the introduction to the entire work. First a brief introduction outlined that the main purpose behind conducting this research study was to design and improve upon designs for mounting devices that attenuate input vibrations in vehicles and heavy machinery. It then listed the objectives for this study as follows. They were to better understand the dynamic characteristics of a special class of hydraulic mounts that use MR fluid, determine the factors that influence dynamic isolation properties of the MR mounts, Conduct experiments that allow us to quantify the dynamic isolation improvements of the MR mounts, and provide recommendations for future studies that that can help with the practice implementation of the MR mounts. It then outlined the process by which these objectives were sought and gave way to the remainder of the study.

After an extensive literature search and review of previous work by Wang et al. , York et al. and finally BM Southern, the study was initiated. The first steps included determining which tests would be required for dynamic characterization and what sort of test assembly would be necessary to accomplish this task. From the literature search as well as basic understanding of base-excitation problems, a test rig was designed using both existing equipment left behind from BM Southern's initial static testing as well as newly acquired and fabricated parts. A dynamic test rig was set up to simulate a base excitation problem with a floating mass, a spring/damper, an electromagnet for magnetic flux, and an actuator for input vibrations. This accomplished the second objective listed.

There were three mounts that were tested in this study as the spring/damper, the first was a mount 0.4375 height and 2.375 in diameter made completely of PolyTek 74-30 RTV polyurethane (RUB) . The second was a mount similar in dimensions and of the same material. However, this second mount featured a cavity with an insert in the center 0.1875 inches high and 1.625 in diameter made of steel (STE). The last was a metal-elastic mount with a steel upper pole plate and a smaller lower pole plate encased entirely in the same rubber material and with the same dimensions (MRF). This mount however failed under initial dynamic tests and a new mount was designed. This new mount was 25.7% thicker, thus adding in resiliency to dynamic shock. Also, the MR fluid type in the new mount was changed to MRF-122 due to lack of availability and discontinued manufacturing of the MRF-145 used in the previous study.

For linear actuation and vibration input, a Roehrig EMA dynamometer was used. The EMA boasts a displacement range of 0.010 to 7.000 inches and can produce input vibration frequencies from 0Hz to over 100Hz. It also had a pair of polished parallel uprights that were ideal for mounting auxiliary equipment to. Additionally, a set of internal measurement capabilities including a +/- 2000lb load cell, and internal displacement transducer and temperature gauge were also found featured on the EMA. Finally, it had a data acquisition board that, with some modification, was capable of taking an external input. Mounted on this linear actuator is the electromagnetic house featuring an electromagnet with a 600 turn 24 AWG copper wire coil. The upper electromagnetic house was attached to the load cell which was fastened to a custom machined and fabricated weight assembly. This weight assembly consisted of an upper and lower brace between which the stacks of weights were fastened securely. This entire assembly featured

ball bearings that ran along the polished uprights of the EMA allowing friction-free motion in the vertical direction.

Also attached to the uprights using a custom machined bracket, was a linear variable differential transducer (LVDT) for measuring the output displacement of the floating mass assembly as the EMA could not measure that. This data was collected through the Roehrig's external input on its data acquisition card. This allowed all of the data that was being collected including the force, base displacement, velocity, and temperature as well as output displacement to be packaged into one file per test run. This also synchronized the data acquisition so that when the data was being analyzed, there would be no need to adjust the data sets so that they all began with the same time interval, thus eliminating another source of experimental uncertainty and error.

After designing this experimental set-up, validation had to be conducted for all of the external input. This was done by fixing the upper assembly directly to the actuator thus creating a direct linkage between the LVDT's measurement and the input. The inputs chosen were a ramp input and a 1Hz sine wave. The measured output displacements matched the profile of the inputs perfectly, thereby verifying the LVDT's measurements.

The next step was to establish the stiffness and damping characteristics of the three mounts for 2 reasons. The first was to identify if any changes had occurred in the pre-fabricated mounts in the 4 year span that they had been stored. Also, it was necessary to determine the characteristics of the new mount design. Secondly, it was necessary to attain these characteristics in order to model the expected outputs of the dynamic tests. After conducting a quasi-static test (QST) in the same fashion that BM Southern had previously, average stiffness and damping ratio values were computed. These were to be used for later validation of the frequency domain analysis of the dynamic test results.

The next step was to conduct the dynamic tests themselves. The method for this was to have the EMA set-up as described earlier and to excite the base with a custom frequency chirp. This input signal swept from a lower frequency to a higher frequency. The wave amplitude was diminishing in nature so that as the higher frequencies were approached, the amplitude would be decreasing according to a specific transfer function. This was in order to input higher frequencies while minimizing violent shaking and possible damage to the testing apparatus and injury to the user. Each passive mount (RUB & STE) was loaded with a pre-determined pre-load to initiate ~1.5% deflection of the mount. Then they were run through 5 test runs each with zero current applied to

the electro magnet. Next the MRF mount was run through the same cycle of 5 test runs with no current applied.

With the input and output displacement data in hand, frequency domain methods were employed to first determine the frequency content. The displacement transmissibility ratio equation was used to convert those values into dimensionless magnitude values plotted against input frequency. However, with real-world systems there exist external factors that make this slightly more difficult to do. With input noise coming from the sensors, cables, the EMA and other sources both inside and outside the data acquisition board, averaging and filtering techniques had to be applied in order for the waveforms to be characteristic of the dynamics of the system. Next the results from these passive mount tests were then used to verify the frequency analysis methods employed earlier. Validation of three different mounts evaluated with the same averaging and filtering techniques would be sufficient to verify the accuracy of the remainder of the plots. Upon completion, the plots matched closely to the models that were generated previously using the characteristics of the mounts thus validating the data processing techniques. Finally, the remaining dynamic tests were conducted by applying the proper pre-load to the MRF mount and running the dynamic test while increasing input current. The input increase was set to be from a passive 0.0 amps to a completely charged 2.0 amps. This increment resolution was able to show trends as the current increased and the mount was run. The MRF mount was run through two groups of dynamic tests. The first group consisted of 2 test runs that ran the mount from 0.0-2.0 amps consecutively without any stoppage time between increments. However after recognizing evidence of the MR phenomenon called clumping in the results from the second test run, the scheduling was adjusted. Therefore, the second group consisted of the last 3 test sets run in order of input current. The current was held constant for 3 identical test runs, then the mount was allowed ample time to return to its original uncharged state before recommencing the testing for the next incremental increase in current.

The results from the test were then analyzed. Firstly, the quasi-static results showed that the mounts that were stored did indeed experience a change in stiffness and damping due to the extended period storage and uncontrolled temperature and humidity conditions in which they were stored. It is also possible that the many tests that were run on the mounts could have affected their characteristics; however that was thought to be less likely. Secondly, the new mount that was fabricated was found to have a significantly higher stiffness and damping ratio

than previous mounts and proved to be much more resilient than the previous mount designs, one of which failed under static and quasi-static testing conducted by BM Southern. This completed the 3rd of the objectives listed for this study.

From the dynamic test results there were also some very important conclusions drawn. Firstly, when compared with its passive rubber counterpart, the MRF mount performed drastically better. At its worst, the MRF mount managed to reduce the transmissibility ratio ~60 % over the rubber mount and at its best was found reduce it about ~70% (at 1.0 amp of current). Even when acting passively, the MRF mount proved to perform much better. Also, the resonance was seen to have migrated on average, about 11% from its original passive state. This also showed promise for the mount to be employed semi- and fully actively in mechanical systems. These results were indicative of the potential that these MRF mounts have to become prominent in active and semi-active vibration technology. Finally a list of recommendations was given for future research with these mounts. This completes the 4th objective of this study.

In conclusion, a dynamic testing rig was designed, assembled and validated using the available tools. A new MRF mount was then designed to withstand the more violent inputs that were anticipated. Then a quasi-static test (QST) was run to determine the stiffness and damping characteristics of the new active mount as well as to confirm the characteristics of the passive mounts involved in the study. Next an initial validation of the frequency domain analysis techniques was conducted and finally the dynamic test was run a total of 5 times. From this data, a conclusion was met that the MRF mount design was able to mitigate a satisfactory amount of input vibration and possess an acceptable amount of resonance migratory ability. Thus, have the potential to become working solutions for the vibration suppression industry. This successfully completes the first and overall objective of this research study.

5.2 |Recommendations and Future Work

Although this study shows two completed experimental studies and the subsequent results were found to be favorable, there always exists room for further investigation of the behavior of the MR mounts. This section therefore presents recommendations from the author for revisions to the design of experiment as well as the experimental set-up, including mount and electro-magnet design. Also listed are some potential future work ideas that could follow from this research study's results.

5.2.1 Recommendations

Although the results from this study were satisfactory, there are still some modifications that would have been desirable and will act as recommendations for future researchers desiring to continue this research. The first set of recommendations involves the mount design and the experimental set-up. As is obvious, because the mount was not designed to be applied for a specific application or machine, the changes that could be made would revolve around specifications from sponsors and interested parties. However, the most important change that the author suggests is to explore different materials of elastomer for the casing of the mounts. As was seen by both BM Southern as well as the author of this study, the polyurethane casing was not as strong as desired. It was also prone to cracking, separating, and under some circumstances, complete mount failure. When put through heavier testing and under significant load of prolonged periods of time, the mounts do not show the resiliency and durability required for application. Therefore, it is recommended that new materials with higher shore durometer ratings that can withstand extended periods of higher amplitude and frequency inputs are explored. Also recommended, is to observe the effects of time and environmental conditions on the durability and characteristics of the mounts. Under prolonged storage, ideal storage conditions should be observed as suggested by the manufacturer. Lastly, the mounts may also benefit from being periodically cycled through the input signal to maintain their elasticity characteristics.
Although the testing apparatus was adequate and simplified a great deal of the testing process, the range limitation of 100 Hz could prove problematic as tougher, more durable mounts are produced in the future and testing at higher frequencies could become relevant. Also finding an actuator with a higher resolution for input and data measurement could be used to look more closely at smaller input and output trends.

Another recommendation is with the electromagnet itself. A major hindrance in the conducting of any of the tests, be they QST or dynamic, was the limitations of the electromagnet itself. Because of its properties, the electromagnet would become very hot to the touch and require a halting of testing in order to allow it time to cool off. Running it while hot could damage both the magnet and the mounts that are being tested. Therefore an electromagnetic assembly that would be better at channeling the heat away from the electromagnet and test subject or a permanent magnet would prove to be a much more convenient option for both testing and application
Also, in order to better market the mounts, a much more compact electromagnetic assembly would prove to be much more attractive to potential investors and clients of this technology. Therefore the author's final recommendation would be designing a single-piece electromagnet housing which could prove to be a better overall design for a permanent mount solution.

5.2.2 Future Work

There are many possible routes stemming from this research that could be explored in the future. A list of possible ideas is presented below. However, the list is not all encompassing or limited to the ideas posed here

Mount Fabrication and Design:

- As was expressed earlier, exploring the effects of different materials can be advantageous to the development of this research area. One could test the different materials for durability, longevity, cost and other parameters.
- This study was limited to the MRF-122 mixture, however there exist many different compositions of MR fluids as well as different ferromagnetic materials. An idea for a future study could include a study on the effects of the different MR fluids on stiffness, damping and transmissibility.
- Fabricating passive metal elastic mounts, with the same design and dimensions as the ones tested in this study could prove to be an interesting idea for a comparative study.
- Developing a new MRF mount design by performing a design parameter optimization to minimize the need for physical testing for MR effect

Mount Evaluation and Testing

- Conducting a parametric study on the mounts varying factors such as pre-load, input frequency range, input type (sin, step, ramp etc.) and amplitude and including factors not considered in the preceding studies like a controlled temperature and zero time between test runs.
- Exploring the effects of a varying magnetic field input-type such as sinusoidal inputs and chirp signals as opposed to the step inputs given in the preceding studies.
- A further exploration into the clumping phenomenon encountered in Run 2 of the MRF dynamic test, replicating the conditions and evaluating the likelihood of its occurrence and observing the trends of its effect
- Conducting durability testing of all of the mount designs could show weaknesses in design of the mounts
- Developing a control policy for use with MR mount in specified system, possibly based on JW Koo et al.

References

1. Yu, Y., Peelamedu, S. M., Naganathan, N. G. and Dukkipati, R. V. Automotive Vehicle Engine Mounting Systems: A Survey. *Trans. ASME, J. Dynamic Systems, Measurement, and Control*, 2001, 123, 186-194.

2. Inman, D.J., Engineering Vibration, *Third Edition*, Pearson Education, Inc., Upper Saddle River, New Jersey, 2008.

3. Hong, S. R., Choi, S. B. and Han, M. S. Vibration Control of a Frame Structure Using Electro-Rheological Fluid Mounts. *International J. Mechanical Sciences*, 2002, 44(10), 2027-2045.

4. Rabinow, J., "The magnetic fluid clutch." AIEE Trans. 67, p. 1308, 1948.

5. Weiss, K. D., Duclos, T. G., Carlson, J. D., Chrzan, M. J. and Margida, A. J. High Strength Magneto- and Electro-Rheological Fluids. *Society of Automotive Engineers, SAE Technical Paper* , 1993, No. 932451

6. Zhang, Xin-Jie, Mehdi Ahmadian, Michael Craft, and Kong-Hui Guo. "Dynamic Testing and Modeling of an MR Squeeze Mount." (2011).

7. Farjoud, Alireza. "Mathematical Modeling of Magnetorheological (MR) Rotary Brakes." Thesis. Nanyang Technological University, 2007. Print.

8. Li, W and Du, H. 2003. "Design and experimental evaluation of a magnetorheological brake," The International Journal of Advanced Manufacturing Technology, 21:508-515.

9. Cho, S.W., Jung, H.J. and Lee, I.W. 2005."Smart passive system based on magnetorheological damper," Smart Materials and Structures, 14(4):707-714.

10. Chen J.Z. and Liao W.H. 2010. "Design, testing and control of a magnetorheological actuator for assistive knee braces," Smart Materials and Structures, 19(3):035029.

11. Southern, Brian M. "Design and Characterization of Tunable Magneto-Rheological Fluid-Elastic Mounts." Thesis. Virginia Polytechnic Institute and State University, 2008. Print.

12. Rabinow, J., *Magnetic Fluid Torque and Force Transmitting Device*. 1952: United States (US), 2575360.

13. Ginder, J. M., L. C. Davis, and L. D. Elie. *Rheology of Magnetorheological Fluids: Models and Measurements*. in *Proceedings of the 5th International Conference on Electro-Rheological Fluids, Magneto-Rheological Suspensions and Associated Technology, 10-14 July 1995*. 1996. Sheffield, UK: World Scientific.

14. Ashour, O., C. A. Rogers, and W. Kordonsky, *Magnetorheological Fluids: Materials, Characterization, and Devices.* Journal of Intelligent Material Systems and Structures, 1996. 7(2): p. 123-130.

15. Rosensweig, R. E. *Directions in Ferrohydrodynamics*. in *Proceedings of the Thirtieth Annual Conference on Magnetism and Magnetic Materials, 27-30 Nov. 1984, Journal of Applied Physics*. 1985. San Diego, CA, USA.

16. Carlson, J.D., Weiss, K.D., "A growing attraction to magnetic fluids," *Machine Design*, Vol. 66, No. 15, p. 61-64, 1994.

17. Weiss, K.D., Duclos, T.G., Carlson, J.D., Chrzan, M.J., and Margida, A.J., "High strength magneto - and electro - rheological fluids," *Society of Automotive Engineers*, Vol. 932451, 1993.

18. Carlson, J. D. and K. D. Weiss, *Magnetorheological Materials Based on Alloy Particles*. 1995: U.S.

19. Berkovsky, B. M., V. F. Medvedev, and M. S. Krakov, *Magnetic Fluids: Engineering Applications*. 1993, New York: Oxford University Press.

20. Raj, K. and R. Moskowitz. *Commercial Applications of Ferrofluids*. in *5th International Conference on Magnetic Fluids, 18-22 Sept. 1989, Journal of Magnetism and Magnetic Materials*. 1990. Riga, USSR.

21. Lemaire, E. and G. Bossis, *Yield Stress and Wall Effects in Magnetic Colloidal Suspensions.* Journal of Physics D: Applied Physics, 1991. 24(8): p. 1473.

22. Genc, S., *Synthesis and Properties of Magnetorheological Fluids,* in *School of Engineering*. 2002, University of Pittsburgh. Goncalves, F.D., "Characterizing the Behavior of Magnetorheological Fluids at High Velocities and High Shear Rates," Ph.D. Dissertation, Virginia Polytechnic Institute and State University: Blacksburg, VA, 2005.24.

23. Goncalves, F.D., "Characterizing the Behavior of Magnetorheological Fluids at High Velocities and High Shear Rates," Ph.D. Dissertation, Virginia Polytechnic Institute and State University: Blacksburg, VA, 2005. Ahn, Y.K., Yang, B., Ahmadian, M., Morishita, S., "A Small-sized Variable-damping Mount Using Magnetorheological Fluid," *International Journal of Vehicle System Dynamics*, Vol. 16, p. 127-133, 2005.

24. *LORD Corporation - Magneto-Rheological (MR)*. Web. 10 Mar. 2011. <http://www.mrfluid.com

25. Lord Materials Division, "Designing with MR Fluids," *Engineering Note*, p. 1-5, 199927.

26. Carlson, J.D., Jolly, M.R., "MR fluid, foam and elastomer devices," *Mechatronics*, Vol. 10, p. 555-569, 2000.

27. Mazlan, S.A., Ekreem, N.B., Olabi, A.G., "The performance of magnetorheological fluid in squeeze mode," *Smart Materials and Structures*, Vol. 16, p. 1678-1682, 2007.

28. Goncalves, F.D., Koo, J.H., Ahmadian, M., "A Review of the State of the Art in Magnetorheological Fluid Technologies – Part 1: MR fluid and MR fluid models.," *The Shock and Vibration Digest*, Vol. 38, 2006.30.

29. York, D., Wang, X., Gordaninejad, F., "A New MRF-E Vibration Isolator," *Journal of Intelligent Material Systems and Structures,* Vol. 18, p. 1221-1225, 2007.

30. Winslow, W. M., *Method and Means for Translating Electrical Impulses into Mechanical Force*. 1947: U.S.

31. Winslow, W. M., *Fluid Controlled Hydraulic Device*. 1953: U.S.

32. General Motors LLC. *Corvette 2011*. Detroit: General Motors LLC, 2010. *Corvette 2011*. General Motors LLC, July 2010. Web. 6 May 2011. <http://www.chevrolet.com/assets/pdf/en/overview/11_corvette_catalog.pdf>.

33. Carlson, J. D. and B. F. Spencer, Jr. *Magnetorheological Fluid Dampers: Scalability and Design Issue for Application to Dynamic Hazard Mitigation*. in *workshop on structural control*. 1996. Hong Kong, China. AFP 53.

34. Carlson, J. D., M. J. Chrzan, and M. O. James, *Magnetorheological Fluid Dampers*. 1994: U.S.

35. Bansbach, E. A., *Torque Transfer Apparatus Using Magnetorheological Fluids*. 1998: U.S.

36. Carlson, J. D., *Low-Cost Mr Fluid Sponge Devices.* Journal of Intelligent Material Systems and Structures, 1999. 10(8): p. 589-94.

37. Kordonski, W. I. and S. D. Jacobs, *Model of Magnetorheological Finishing.* Journal of Intelligent Material Systems and Structures, 1996. 7: p. 131-137.

38. *Principal Diagram Anti-Earthquake*. Rimpex Rubber. Web. 6 May 2011.

39. Adiguna, H., Tiwari, M., Singh, R., Tseng, H.E., Hrovat, D., "Transient response of a hydraulic engine mount," *Journal of Sound and Vibration*, Vol. 268, p. 217-248, 2003.

40. Christopherson, J., Jazar, G.N., "Dynamic behavior comparison of passive hydraulic engine mounts. Part 1: Mathematical analysis," *Journal of Sound and Vibration*, Vol. 290, p. 1040-1070, 2005.

41. Vahdati, N., Ahmadian, M., "Variable Volumetric Stiffness Fluid Mount Design," *Shock and Vibration*, Vol. 11, p.21-32, 2004.

42. Wang, X., Gordaninejad, F., Hitchcock, G., "A magneto-rheological fluid elastomer vibration isolator," *Smart Structures and Materials*, Proc. of SPIE Vol. 5760, p. 217-225, 2005.

43. Choi, S.B., Hong, S., Choi, Y., Wereley, N., "Vibration control of flexible structures using MR and piezoceramic mounts," *Smart Structures and Materials*, Proc. of SPIE Vol. 5390, p. 127-134, 2004.

44. Vahdati, N., Ahmadian, M., "Single Pumper Semi-active Fluid Mount," *Proc. of ASME 2003 IMECE* 2003, International Mechanical Engineers Conference, Washington, D.C, 2003.

45. Nguyen, T., Schroeder, C., Ciocanel, C., and Elahinia, M., "On the Design and Control of a Squeeze-Flow Mode Magnetorheological Fluid Mount," *Proc. of the ASME 2007 IDETC/CIE,* Las Vegas, Nevada, 2007.

46. Koo, J.H., Ahmadian, M., Setareh, M., Murray, T.M., "In Search of Suitable Control Methods for Semi-Active Tuned Vibration Absorbers," *Journal of Vibration and Control,* Vol. 10, p. 163-174, 2004.

47. University of Michigan Transportation Reasearch Center, *Mechanics of Heavy Trucks and Truck Combinations,* 1993.

48. Hayt Jr., William H., and John A. Buck. *Engineering Electromagnetics*. 7th ed. New York: McGraw Hill, 2006. Print.

49. Extech Intsruments, "80W Switching Mode DC Power Supply," User Manual, 2007.

50. Polytek Development Corp. , "Mold Making and Casting," *Manual and Catalogue,* 2007.

51. Redwood Plastics Corp., "Hardness Comparison Chart," Redco Polyurethane Brochure, 2008.

52. Roehrig Engineering Inc. Advertisement. *2K-EMA*. Web. 5 May 2011. <2K-EMA:>.

53. INA Bearing Corp., "Linear ball beraings KBZ24-OP-OP," Datasheet.

54. "Macro Sensors DC 750 and SE 750 Series General Purpose AC-Operated LVDT Position Sensors." *LVDT Position Sensors*. Macro Sensors, 2009. Web. 05 May 2011. <http://www.macrosensors.com/DC_SE_750.html>.

55. Power-One, "HA Power Supply Series-Dual Output Linears," Installation Instructions.

56. Farjoud, Alireza. "Physics-based Modeling Techniques for Analysis and Design of Advanced Suspension Systems and Experimental Validation." Diss. Virginia Polytechnic Institute and State University, 2011. Print.

57. Lange, U., Richter, L., Zipser, L., "Flow of Magnetorheological Fluids," *Journal of Intelligent Material Systems and Structures*, Vol. 12, p. 161-164, 2001.

Appendix A: Custom Fabrication Design Schematics

This section includes technical drawings for the custom fabricated pieces used in this study. These are available to allow future researches to produce identical dynamic testers and for use as a basis for designing testers to be used with other mount and suspension devices.

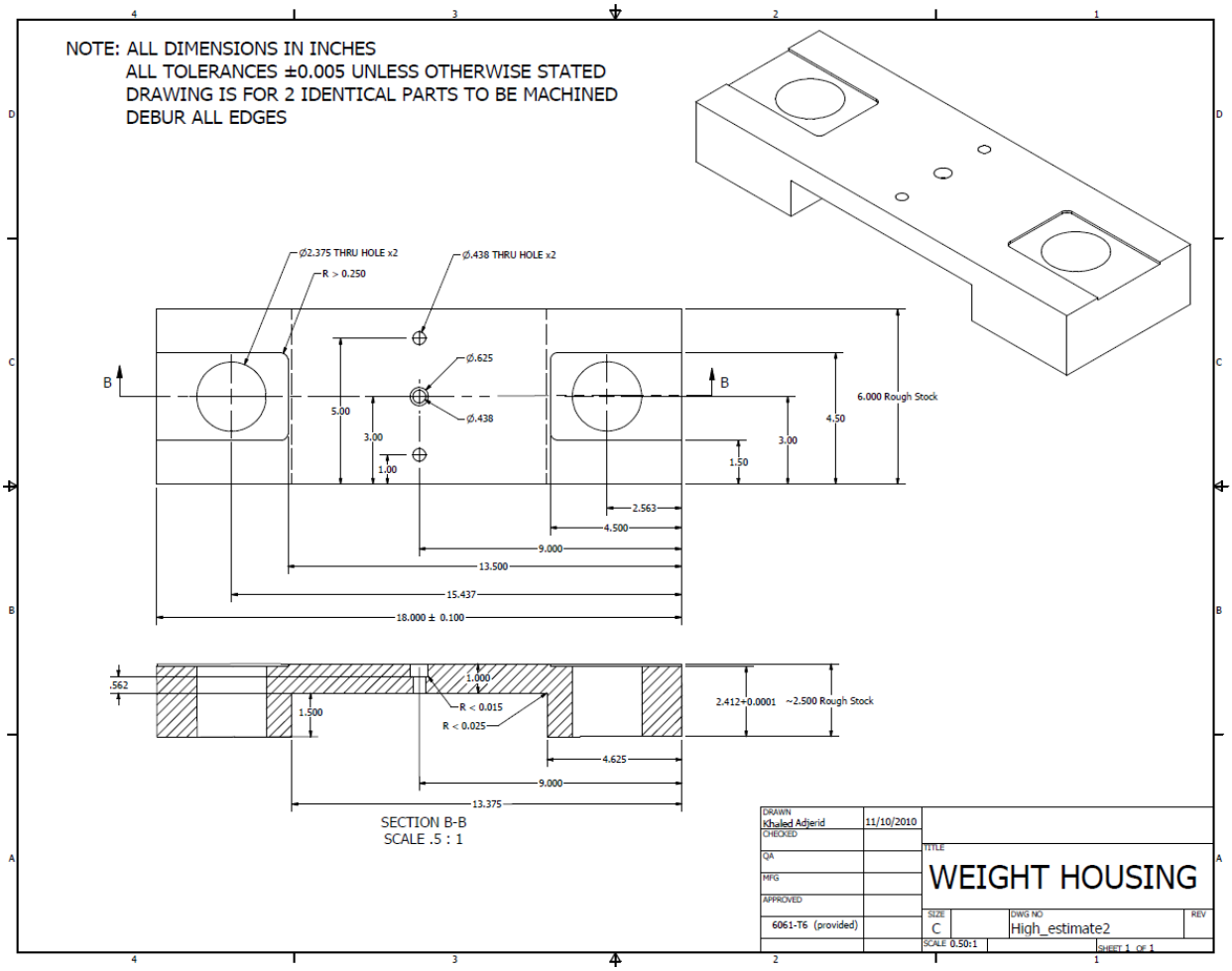

Figure A-1: Engineering CAD sketch for upper and lower weight braces.

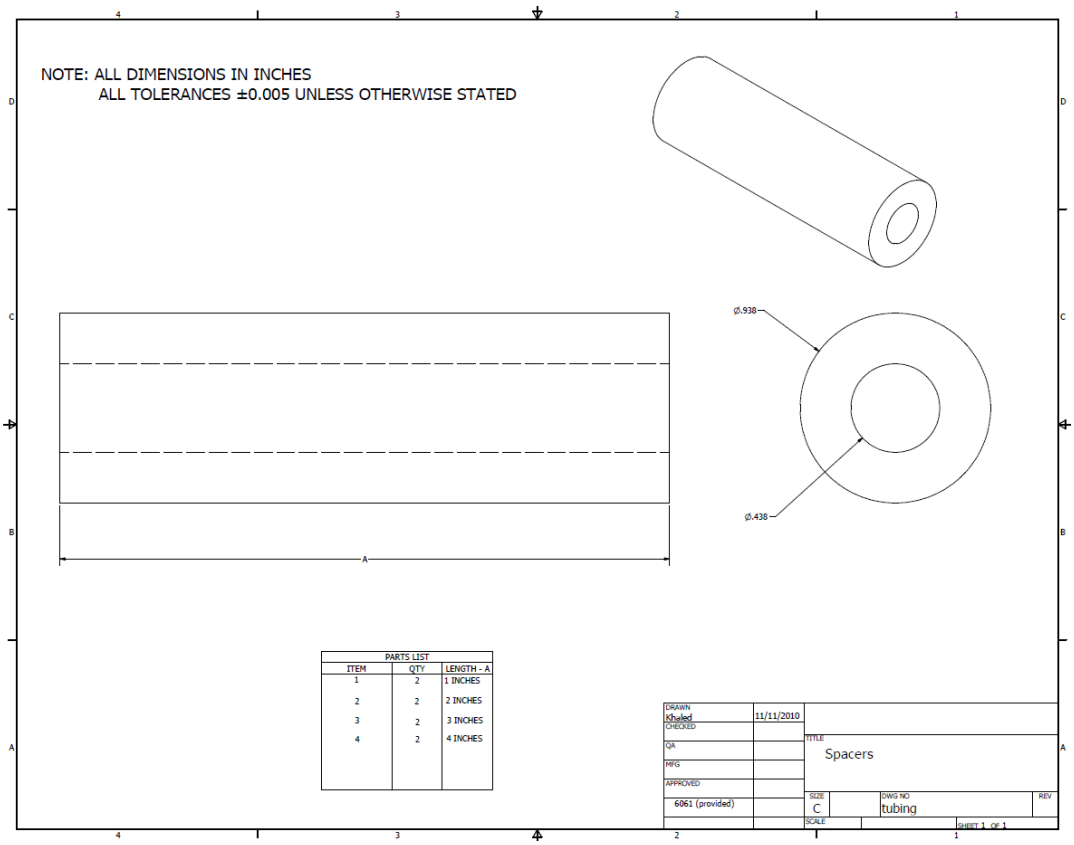

Figure A-2: Engineering CAD sketch for weight spacers.

Appendix B: FEMM Sketches

This appendix shows the detailed FEMM model sketches for the three mounts tested in this study. Included are the model, the mesh grids and the flux density models.

Note: because FEMM software models are modeled axially, only the original form of the model is shown

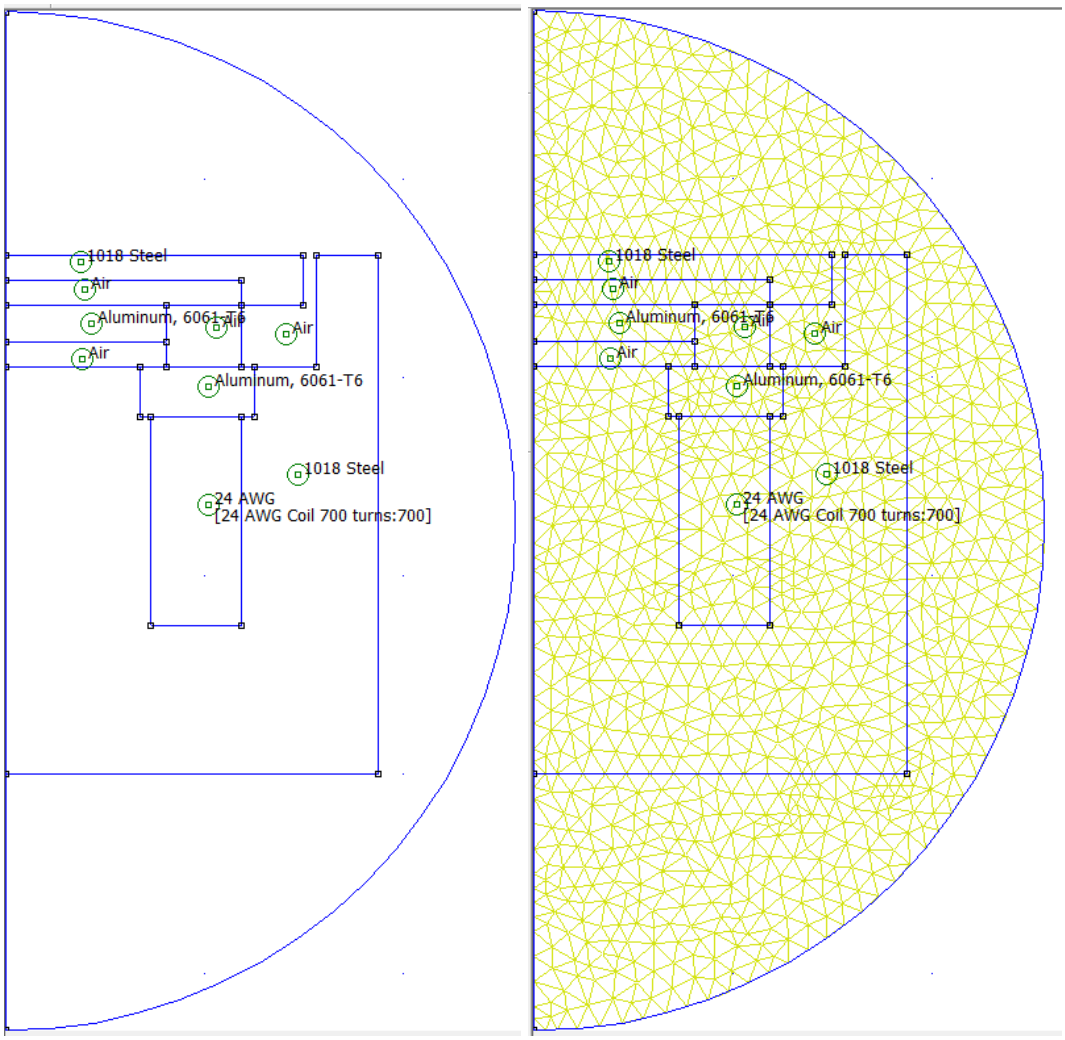

Figure B-1: STE mount FEMM model and mesh-grid.

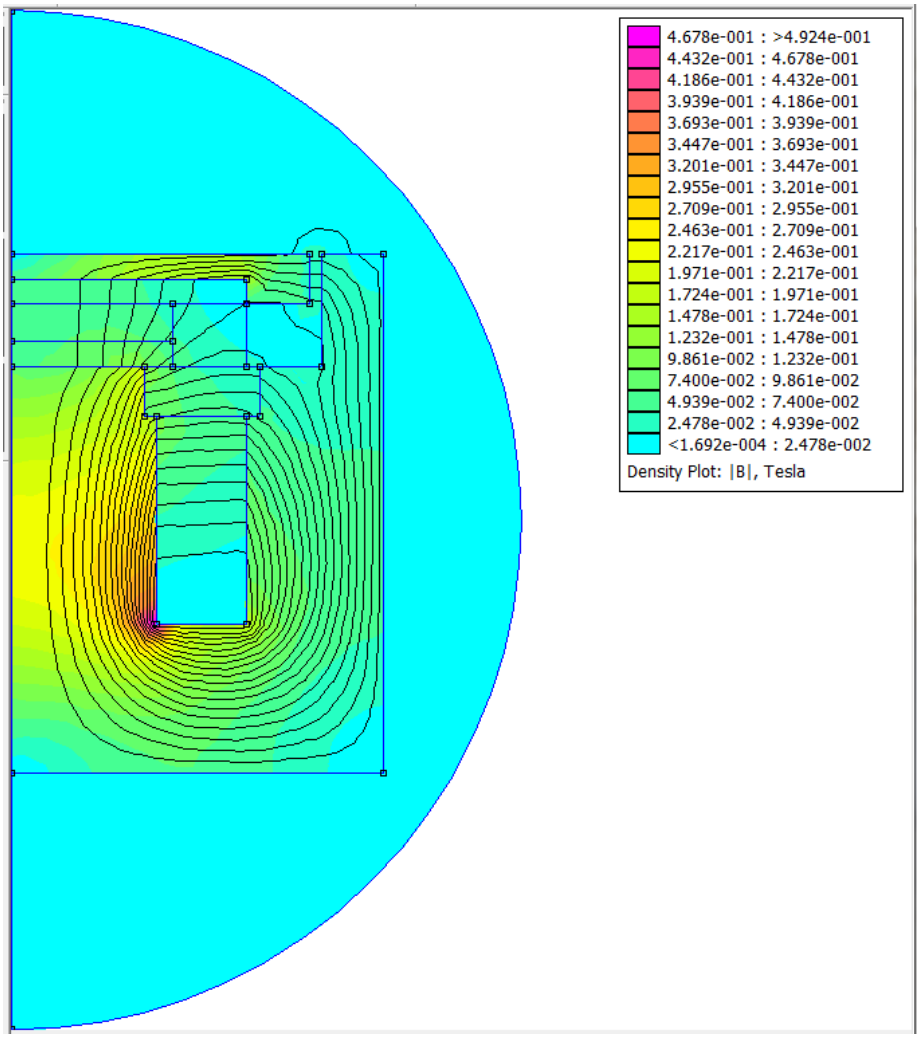

Figure B-2: STE mount FEMM flux density plot.

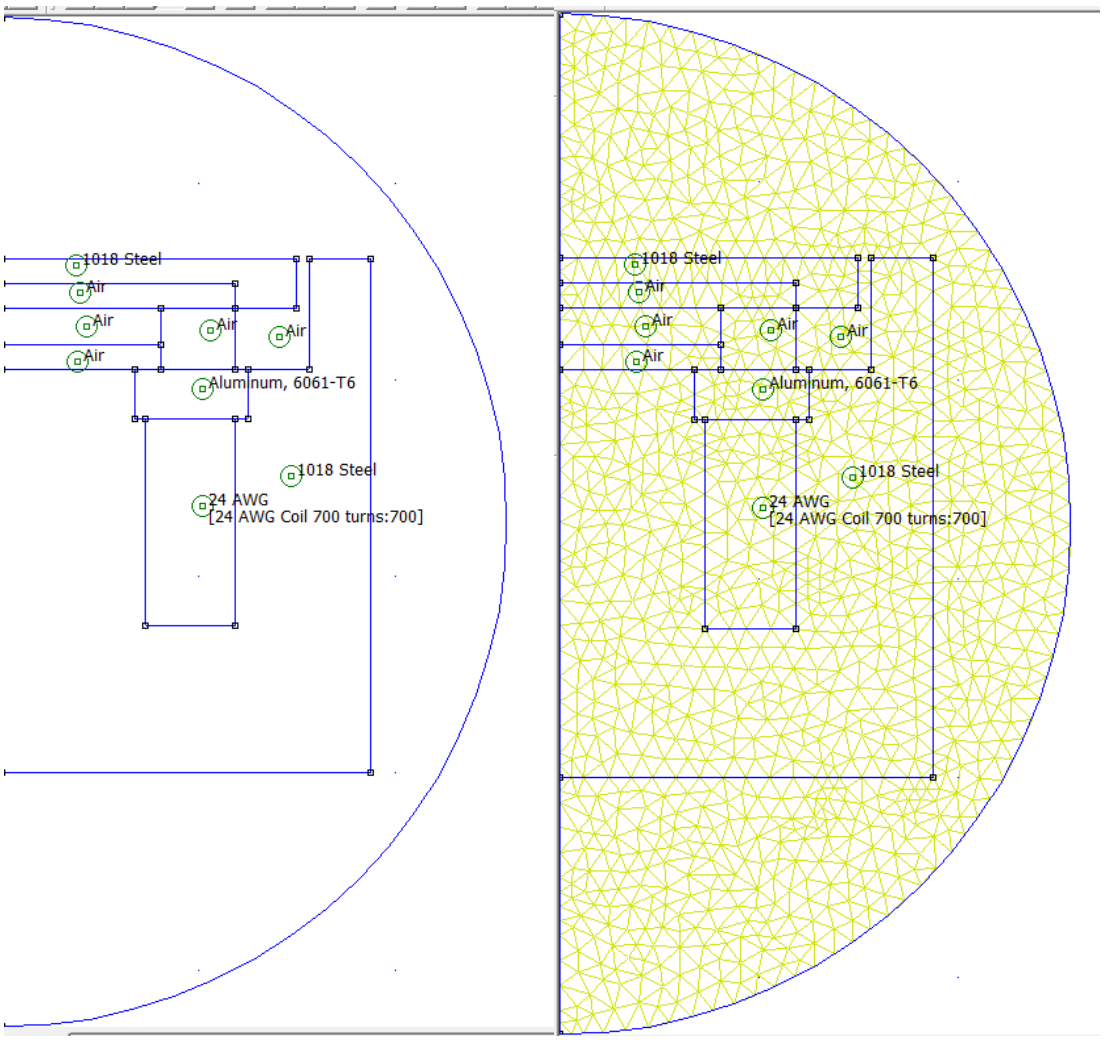

Figure B-3 : RUB mount FEMM model and mesh-grid.

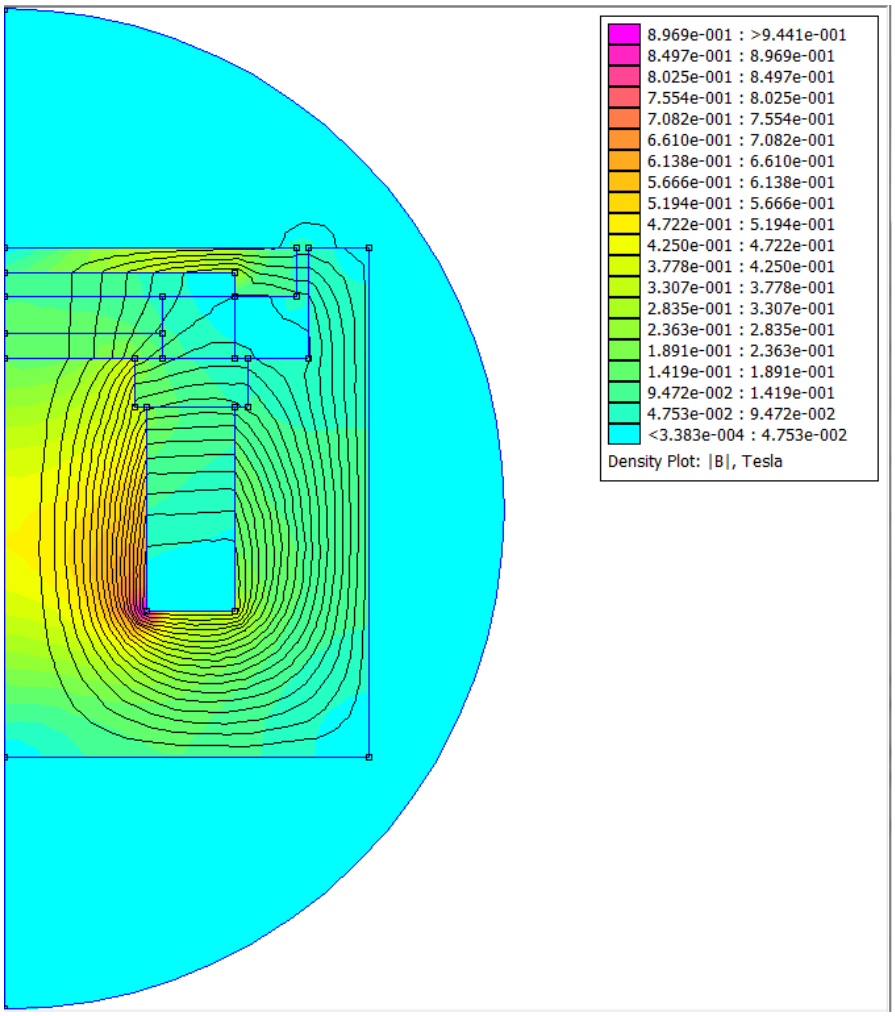

Figure B-4: RUB mount FEMM flux density plot.

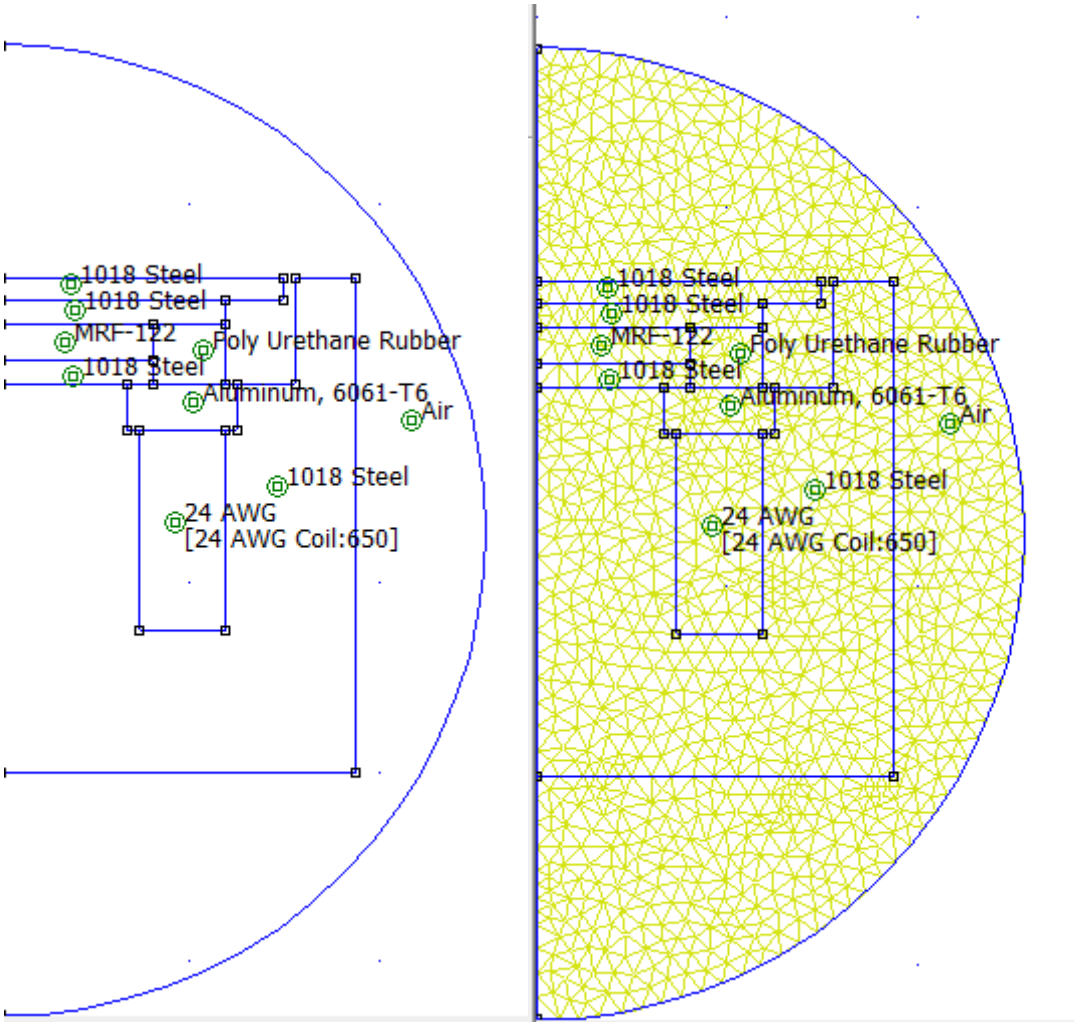

Figure B-5: MRF-122 Mount FEMM model and mesh-grid .

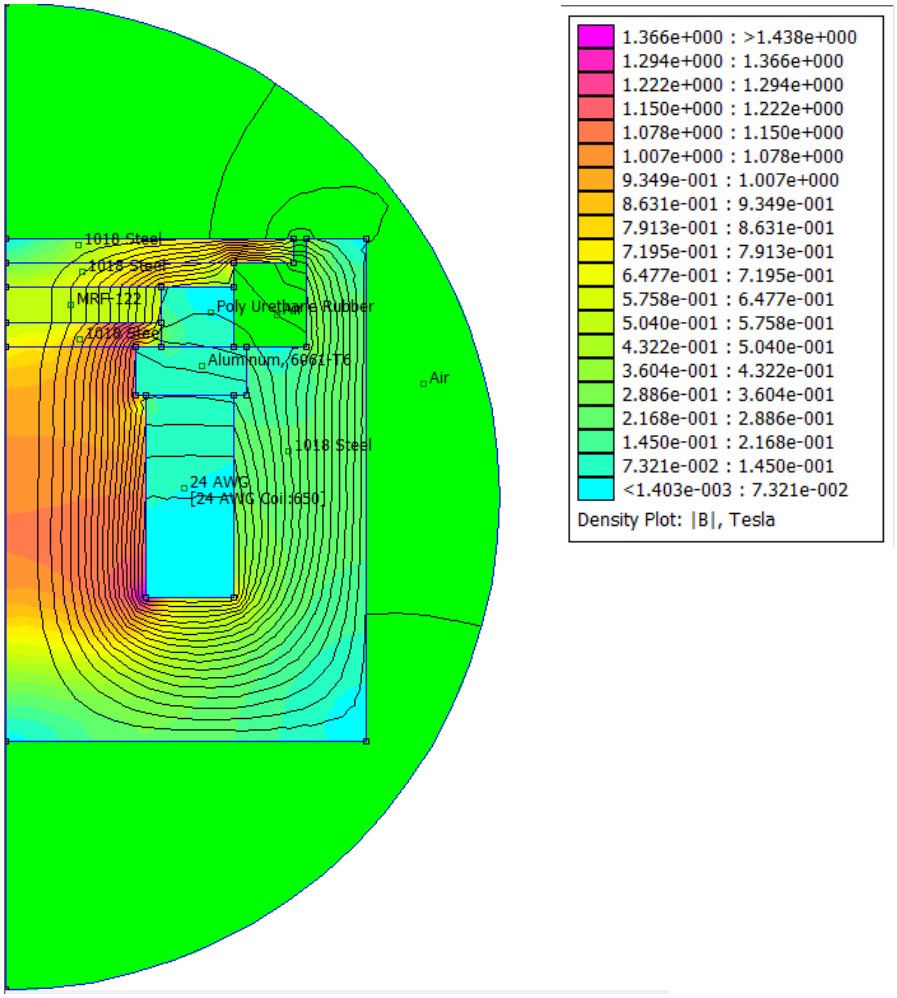

Figure B-6: MRF-122 Mount FEMM flux density model.

Appendix C: Dynamic Test Results

This section provides all of the experimental results from the dynamic test analysis. Due to their extensiveness, they were not presented in the main portion of the study.

Table C-1: Peak resonance values (Hz) for MRF mount by current level.

Current Level amp	R1	R2	R3	R4	R5	Ave	Ave (minusR2)
0	14.04	14.34	13.63	14.44	14.24	14.138	14.0875
0.2	14.24	14.44	13.73	14.65	14.24	14.26	14.215
0.4	14.34	14.65	13.63	14.75	14.75	14.424	14.3675
0.6	14.44	14.85	14.14	15.06	14.75	14.648	14.5975
0.8	14.65	15.06	14.14	15.06	15.16	14.814	14.7525
1	14.95	15.16	14.04	15.16	15.16	14.894	14.8275
1.2	15.06	15.16	14.24	15.56	15.56	15.116	15.105
1.4	15.56	15.56	14.34	15.56	15.56	15.316	15.255
1.6	15.56	15.87	14.75	15.56	15.36	15.42	15.3075
1.8	15.77	14.55	15.06	15.56	15.46	15.28	15.4625
2	15.87	15.16	15.06	15.77	15.87	15.546	15.6425

Table C-2: Peak magnitude values for MRF mount by current level

Current Level amp	R1	R2	R3	R4	R5	Ave	Ave (minusR2)
0	6.5686	5.953	7.418	7.284	7.014	**6.84752**	**7.07115**
0.2	6.268	5.961	8.05	8.776	7.6212	**7.0541**	**7.622**
0.4	9.106	8.93	6.552	6.311	6.435	**7.4668**	**7.101**
0.6	9.348	12.48	7.221	7.332	7.635	**8.8032**	**7.884**
0.8	9.194	13.34	7.003	7.183	8.727	**9.0894**	**8.02675**
1	8.455	9.904	6.564	6.321	6.689	**7.5866**	**7.00725**
1.2	8.731	8.22	7.398	7.562	7.644	**7.911**	**7.83375**
1.4	6.853	8.22	7.033	6.245	9.922	**7.6546**	**7.51325**
1.6	7.031	6.961	7.963	8.108	7.837	**7.58**	**7.73475**
1.8	7.023	6.377	7.503	8.383	7.282	**7.3136**	**7.54775**
2	8.058	8.152	7.937	8.808	5.811	**7.7532**	**7.6535**

Table C-3: Peak Magnitude and Resonance Values for RUB mount.

	R1	R2	R3	R4	R5	Ave	Std Dev.
wn	19.08	19.08	19.15	19.16	19.08	19.11	0.041231
Mag	20.89	21.22	20.96	26.93	21.5	22.3	2.599375

Table C-4: Peak Magnitude and Resonance Values for STE mount.

	R1	R2	R3	R4	R5	Ave	Std Dev.
wn	17.1	17.58	17.09	17.09	17.1	17.215	0.243379
Mag	4.62	4.718	4.702	4.938	5.073	4.85775	0.179407